ENHANCED METHANE HYDRATE FORMATION USING PROMOTERS FOR NATURAL GAS STORAGE AND TRANSPORTATION APPLICATION

Katipot Inkong

A Dissertation Submitted in Partial Fulfilment of the Requirements
for the Degree of Doctor of Philosophy
The Petroleum and Petrochemical College, Chulalongkorn University
in Academic Partnership with
The University of Michigan, The University of Oklahoma,
and Case Western Reserve University
2025

Thesis Title:	Enhanced Methane Hydrate Formation Using Promoters for Natural Gas Storage and Transportation Application
By:	Katipot Inkong
Program:	Petrochemical Technology
Thesis Advisors:	Prof. Pramoch Rangsunvigit
	Assoc. Prof. Praveen Linga
	Dr. Santi Kulprathipanja

Accepted by The Petroleum and Petrochemical College, Chulalongkorn University, in partial fulfilment of the requirements for the Degree of Doctor of Philosophy.

……. College Dean
(Prof. Pramoch Rangsunvigit)

Thesis Committee:

.....	.....
(Prof. Adrian Evan Flood)	(Prof. Pramoch Rangsunvigit)
.....	.....
(Assoc. Prof. Praveen Linga)	(Dr. Santi Kulprathipanja)
.....	.....
(Prof. Apanee Luengnaruemitchai)	(Prof. Boonyarach Kitiyanan)

.....
(Dr. Tanate Danuthai)

ABSTRACT

5681002063: Petrochemical Technology Program
Katipot Inkong: Enhanced Methane Hydrate Formation Using Promoters for Natural Gas Storage and Transportation Application
Thesis Advisors: Prof. Pramoch Rangsunvigit, Assoc. Prof. Praveen Linga, and Dr. Santi Kulprathipanja 168 pp.
Keywords: Solidified natural gas/ Hydrate formation/ Hydrate promoter/ Bio-based surfactant/ Tetrahydrofuran/Sodium dodecyl sulfate/ Hollow silica

Solidified natural gas (SNG) is an alternative technology for natural gas storage and transportation in the clathrate hydrate formed. It has higher volumetric energy storage with the ease to handle not to mention its safety. Effects of different hydrate promoters, including methyl ester sulfonate (MES), tetrahydrofuran (THF), hollow silica (HS), and sodium dodecyl sulfate (SDS), on the methane hydrate formation was investigated. All experiments were performed in an unstirred tank reactor at desired experimental conditions. The results indicated that all promoters significant enhanced the hydrate formation both kinetics and methane uptake compared with pure water. The increase in the MES concentration decreased the induction time and increased the hydrate formation rate, which was the result from the decrease in the surface tension between gas and liquid phase. The methane uptake increased with the increase in the MES concentration. The presence of THF shifted the hydrate phase equilibrium curve to the higher temperature and lower pressure. The results showed that the increase in the experimental temperature increased the methane uptake due to the effective heat distribution to the surrounding, while the hydrate formation kinetics decreased due to the decrease in the driving force. The decrease in the pressure did not affect the methane uptake but the hydrate formation kinetics decreased. There was synergism between THF with MES in the hydrate formation kinetics at the higher temperatures. Moreover, the presence of HS improved the surface contact area to enhance the hydrate formation at moderate conditions. The presence of SDS facilitated the hydrate formation, including induction time and hydrate formation rates, at moderate conditions.

บทคัดย่อ

คติพจน์ อินคง: การปรับปรุงการเกิดมีเทนไฮเดรตโดยการใช้ตัวเร่งสำหรับการประยุกต์ใช้ในการกักเก็บและการขนส่งแก๊สธรรมชาติ (Enhanced Methane Hydrate Formation by Using Promoters for Natural Gas Storage and Transportation Application) อ. ที่ปรึกษา: ศ. ดร. ปราโมช รังสรรค์วิจิตร และ รศ. ดร. ปราวีน ลินกา ดร. สันติ กุลประทีปัญญา 168 หน้า

การกักเก็บแก๊สในรูปของแข็ง (solidified natural gas) เป็นการกักเก็บแก๊สธรรมชาติในรูปของแก๊สไฮเดรต โดยวิธีการดังกล่าวเป็นทางเลือกอีกวิธีที่กำลังได้รับความสนใจ เนื่องจากมีค่าพลังงานต่อหนึ่งปริมาณที่สูง ง่ายในการจัดการ อีกทั้งยังเป็นวิธีที่มีความปลอดภัย อย่างไรก็ตามในกระบวนการแก๊สไฮเดรตนั้นใช้เวลานาน และต้องผ่านกระบวนการเกิดที่อุณหภูมิต่ำและความดันสูง ในงานวิจัยนี้มุ่งในการลดข้อด้อยของกระบวนการดังกล่าว โดยศึกษาผลของการเติมตัวเร่งการเกิดแก๊สไฮเดรต (hydrate promoter) ได้แก่ เมทิลเอสเทอร์ซัลโฟเนต (methyl ester sulfonate, MES), เตตระไฮโดรฟูแรน (tetrahydrofuran, THF), ซิลิกาแบบกลวง (hollow silica) และโซเดียมโดเดซิลซัตเฟต (sodium dodecyl sulfate, SDS) โดยการทดลองศึกษาในสภาวะที่ไม่มีการกวนและอุณหภูมิคงที่ ผลการทดลองแสดงให้เห็นอย่างมีนัยสำคัญว่าการเติมตัวเร่งการเกิดแก๊สไฮเดรตทุกชนิดที่ใช้ในการศึกษานั้นสามารถยกระดับการเกิดแก๊สไฮเดรตให้ดีขึ้นเมื่อเปรียบเทียบกับไม่มีการเติมตัวเร่ง ณ สภาวะที่เดียวกัน การเพิ่มความเข้มข้น MES ช่วยลดเวลาการเกิดแก๊สไฮเดรตและเพิ่มอัตราการแก๊สไฮเดรตให้สูงขึ้น การเติม MES จะทำหน้าที่ลดแรงตึงผิวระหว่างวัฏภาคของแก๊สและสารละลายทำให้เพิ่มการละลายของแก๊สในน้ำได้มากขึ้น ในขณะเดียวกันการเพิ่มความเข้มข้น MES จะเพิ่มปริมาณแก๊สที่ถูกในรูปแก๊สไฮเดรตให้เพิ่มขึ้น สำหรับการเติม THF จะเลื่อนสมดุลวัฏภาคของระบบไปที่อุณหภิมที่สูงขึ้นและความดันต่ำลง โดยการทดลองพบว่าการเพิ่มอุณหภูมิการเกิดแก๊สไฮเดรตเพิ่มปริมาณแก๊สที่ถูกกักเก็บ แต่ในขณะที่อัตราการเกิดแก๊สไฮเดรตลดลง สำหรับการลดความดันในการเกิดแก๊สไฮเดรตไม่มีผลต่อปริมาณแก๊สที่ถูกกักเก็บ แต่จะส่งผลให้อัตราการเกิดแก๊สไฮเดรตลง สำหรับเติมสารละลายผสมระหว่าง THF และ MES เพิ่มอัตราการเกิดแก๊สไฮเดรตที่อุณหภูมิสูงโดยไม่ส่งผลต่อปริมาณของแก๊สที่ถูกกักเก็บในรูปแก๊สไฮเดรต การเติมซิลิกาแบบกลวง (HS) เพิ่มความสามารถในการเกิดแก๊สไฮเดรตที่แรงขับเคลื่อนต่ำ โดยการเพิ่มพื้นที่สัมผัสของสองวัฏภาคและการเติม SDS ช่วยปรับปรุงอัตราการแก๊สไฮเดตรให้สูงขึ้น

GRAPHICAL ABSTRACT

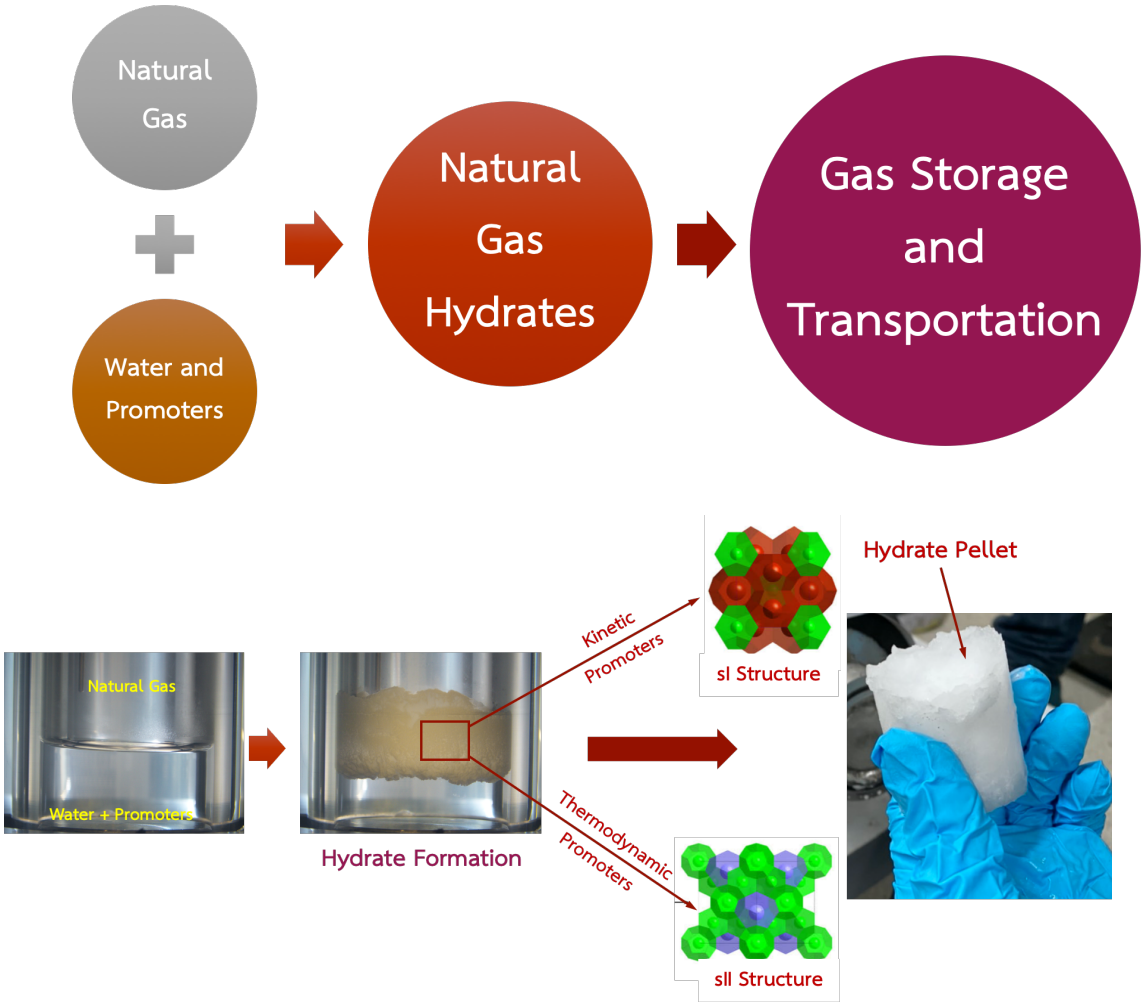

ACKNOWELEDGEMENTS

First and foremost, I would like to express the deepest gratitude to my advisor, Prof. Pramoch Rangsunvigit, and co-advisor, Dr. Santi Kulprathipanja, for the continuous support of my Ph.D study, for providing me a lot of opportunities to think and work, and for his helpful suggestions. They also provided me unflinching encouragement, patience and support in various ways throughout my graduate thesis. Moreover, I would like to thank Mrs. Apinya Kulprathipanja for her kindness when I stayed at USA.

I also would like to express the gratitude my co-advisor, Assoc. Prof. Praveen Linga, for providing me to great opportunity to learn and study about the gas hydrate technology for 4 months at National University of Singapore (NUS), and also providing me with the valuable comments and his support. Moreover, I would like to thank Dr. Hari Prakash who is my mentor helped and gave me a good advice in my research and my publications.

Apart from my advisor and co-advisor, I would like to thank my committees: Prof. Adrian Evan Flood, Prof. Boonyarach Kitiyanun, Prof. Apanee Luengnarumitchai, and Dr. Tanate Danuthai for kindly serving on my thesis committee. Their suggestions are certainly important and helpful for completion of this thesis.

I would like to thank the entire faculty and staff at The Petroleum and Petrochemical College, Chulalongkorn University for their kind assistance and cooperation.

I would like to express my sincere gratitude to thank my family for showing me the joy of intellectual pursuit ever since I was a child for standing by me and for understanding every single part of my mind.

Finally, I would like to thank The Royal Golden Jubilee Ph.D. Program (2.P.CU/58/J.1), Thailand Research Fund; Grant for International Research Integration: Chula Research Scholar, Ratchadaphiseksomphot Endowment Fund, Chulalongkorn University, Thailand; Thailand Energy Conservation Fund, Energy Policy and Planning Office Ministry of Energy for their financial support throughout this research.

TABLE OF CONTENTS

LIST OF TABLES

LIST OF FIGURES

FIGURE **PAGE**

FIGURE **PAGE**

FIGURE **PAGE**

FIGURE **PAGE**

FIGURE **PAGE**

FIGURE **PAGE**

CHAPTER I
INTRODUCTION

Based on the report of annual energy outlook (2019) by EIA, natural gas demand grows 7% per year from 2018 to 2020, which is higher than the 4% per year average growth rate from 2005 to 2015 (EIA, 2019). This is, in part, due to natural gas is the cleanest fossil fuel due to reduction of carbon dioxide during the combustion and friendly environment (Demirbas, 2010b; Rios *et al.*, 2013; Zhang *et al.*, 2010). The storage and transportation of natural gas have become a critical part in responding to the natural gas demand growth. The method for natural gas storage and transportation effectiveness are required. Conventional storage methods for natural gas storage and transportation include compressed natural gas (CNG), liquefied natural gas (LNG), and absorbed natural gas (ANG) (Sapag *et al.*, 2010). CNG is operated by compressing natural gas about 20 to 25 MPa for storage in thick wall and heavy tanks. However, CNG provides the volumetric energy storage density of about one-third of gasoline. For LNG, natural gas must be converted to the liquid form for transportation over a long distance or storage in a massive scale. However, this method requires an expensive cooling system to maintain the temperature below about 191 K (Wang *et al.*, 2010; Zakaria and George, 2011). ANG uses the porous medium to trap natural gas inside a space cavity (Lozano-Castelló *et al.*, 2002; Sapag *et al.*, 2010). The storage capacity of ANG relies on the types of porous material. However, the price of porous is too high. Moreover, the limitation of a designed storage cylinder tank is of concern (Veluswamy *et al.*, 2018). Recently, researchers proposed a new method for natural gas storage and transportation in the solid form called “solidified natural gas” or “SNG”. Natural gas is stored in the clathrate hydrates or hydrate form. This technology has several advantages including high volumetric energy storage capacity, ease to handle and recover the stored gas, and cost-effective compared with the conventional method.

Clathrate hydrates or natural gas hydrates are ice-like crystalline compounds and non-stoichiometric compounds, which form when gas molecules such as methane, ethane, and carbon dioxide are encapsulated inside the cage of water molecule formed by physical interaction (hydrogen bonds) (Sloan and Koh, 2008).

The hydrogen-bonded water molecules can generate the polyhedron cavity. Generally, gas hydrates have three well-known crystal structures - structure I (sI) composed of 46 water molecules, structure II (sII) composed of 136 water molecules, and structure H (sH) composed of 34 water molecules. The structure of hydrates predominantly depends on the size of guest gas molecule and the hydrate formation condition. In nature, natural gas hydrates are found in the permafrost region, and they are stable under high pressure and low temperature (Demirbas, 2010a). Recently, gas hydrates have received much attention not only as a new natural energy resource but also as a new means of natural gas storage and transportation. One volume of hydrates can store about 150-180 volumes of natural gas at STP (Saw *et al.*, 2014). This property makes the hydrates a good candidate for natural gas storage and transportation. However, a slow formation rate, low methane uptake, and stability of natural gas hydrates have been considered problems hindering the hydrate technology in the industrial applications (Partoon and Javanmardi, 2013).

Many researchers proposed the hydrate promoters for solving the limitations of hydrate technology. Surfactants are considered as the kinetic promoter that reduces the surface tension of gas-liquid interface, resulting in increase in the gas molecules solubility. Ganji *et al.* (2007) found that all surfactants increased the hydrate formation rate and gas storage. Additionally, they found the sodium dodecyl sulfate (SDS), an anionic surfactant, exhibited the maximum effect on the formation rate and the stability of the hydrates. Also, many reports substantiated the roles of anionic surfactants in promoting gas hydrate formation effectively (Mandal and Laik, 2008; Okutani *et al.*, 2008; Zhang *et al.*, 2007b). Lin *et al.* (2004) showed that the formation rates of methane hydrates could be enhanced with the maximum storage capacity of 170V/V at 650 ppm SDS. Recently, bio-based surfactants have also been reported as hydrate promoters. Wang *et al.* (2012) found that lignosulfonate biosurfactant, a by-product from paper industry, enhanced both the rate of methane formation and the storage capacity. Moreover, Chaturvedi *et al.* (2018) found that a novel synthesized surfactant from castor oil enhanced the rate of formation, reduced induction time, and increased the gas storage capacity.

Moreover, the presence of porous media, like activated carbon or zeolite, was shown to promote gas storage capacity and hydrate formation rate by provided

higher gas-water contact area (Cha *et al.*, 1988; Siangsai *et al.*, 2015; Zhong *et al.*, 2013). Among porous material, hollow silica (HS) is more attractive than others because of its unique properties such as low density, high pore volume, high porosity, and high specific area (Chen *et al.*, 2013). Prasad *et al.* (2014) reported that the methane hydrate formation in HS matrix at moderate pressure showed the same hydrate yield with pure water system. Chari *et al.* (2015) showed that the methane uptake and hydrate yield in HS were higher than silica sand, and the stirring did not influence on both hydrate yield and the hydrate formation kinetics. Veluswamy *et al.* (2016b) reported that using HS to water ratio beyond 1:6 enhanced the formation kinetics of methane hydrate and methane uptake.

To shift the hydrate formation condition to the higher temperature and lower/moderate pressure, the thermodynamic promoter was chosen. Tetrahydrofuran (THF) was reported as an effective thermodynamic promoter to stabilize the hydrate by shifting phase equilibrium to higher temperature and lower pressures (Florusse *et al.*, 2004; Seo *et al.*, 2001). THF forms sII hydrates by itself without the guest gas molecule by the large cages of sII structure are preferably occupied by THF, while smaller cages are empty (Kumar *et al.*, 2016; Sloan and Koh, 2008). THF has been reported that it enhanced both the methane uptake and hydrate stability. Veluswamy *et al.* (2016c) reported that the presence of 5.6 mol% THF at 7 MPa and 283.2 K predominantly increased the kinetics of methane hydrate formation and enhanced methane uptake about 11.6 times compared with the pure methane at 9.5 MPa and 272.2 K. Also, Veluswamy *et al.* (2016a) investigated the mixed methane-THF at the experimental pressure of 7.2 MPa and different temperatures, 283.2, 288.2 and 293.2 K, and found that the final gas uptake was similar at all temperatures. Kumar *et al.* (2019) studied the hydrate stability and found that the mixed methane-THF hydrate pellet showcased extreme stability for two months.

In order to apply the hydrate technology for gas storage and transportation applications, this work aims to improve the hydrate formation kinetics, gas hydrate storage capacity, and hydrate stability. THF, SDS, methyl ester sulfonate (MES), and HS were used to investigate their effects on the methane hydrate formation and dissociation kinetics.

CHAPTER II
THEORETICAL BACKGROUND AND LITERATURE REVIEW

2.1 Natural Gas

Natural gas is generally considered a non-renewable fossil fuel. It is believed that natural gas was formed from the remains of tiny sea animals and plants, buried by the layers of sediment that turn to rock 200 - 400 million years ago. Over the years, the layers of sedimentary rock became a thousand feet of thickness, causing the energy-rich plant and animal remains to enormous pressure, and transforming their constituent compounds into a mixture of alkanes. Natural gas is formed in deep underground, usually in areas around coal and oil. It is composed mostly of methane, but also contained other chemical species, such as butane and propane. Natural gas might also contain non-hydrocarbon compounds, such as water vapor, carbon dioxide, and hydrogen sulfide. It is one of the most widely used forms of energy in recent years. Natural gas is a cleaner-burning fuel than gasoline and diesel. However, it also contains active and inert compounds, such as sulfur, nitrogen, and carbon dioxide (Sapag *et al.*, 2010). The composition of natural gas is shown in Figure 2.1.

Natural gas can be used in many ways. It is used to generate electricity for households and industries. It is a raw material to produce chemicals, fertilizer, hydrogen and used as a fuel for heating in industries. It is also an alternative fuel for transportation because natural gas is more environmentally friendly than conventional fuel like gasoline and diesel. The International Energy Outlook 2016 (EIA, 2016) shows the trend of natural gas consumption of the world from 2012 to 2040 that increases from 120 trillion cubic feet to 203 cubic feet, Figure 2.2. By energy source, natural gas accounts for the largest increase in world primary energy consumption. Abundant natural gas resources and robust production contribute to the strong competitive position of natural gas among other resources.

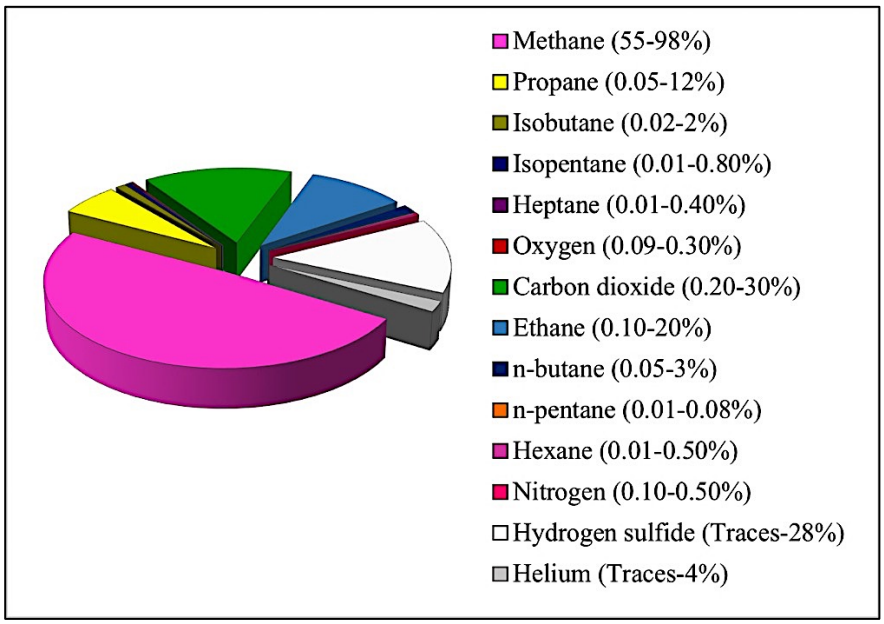

Figure 2.1 Principal constitutes of natural gas (in percentage) (Sapag *et al.*, 2010).

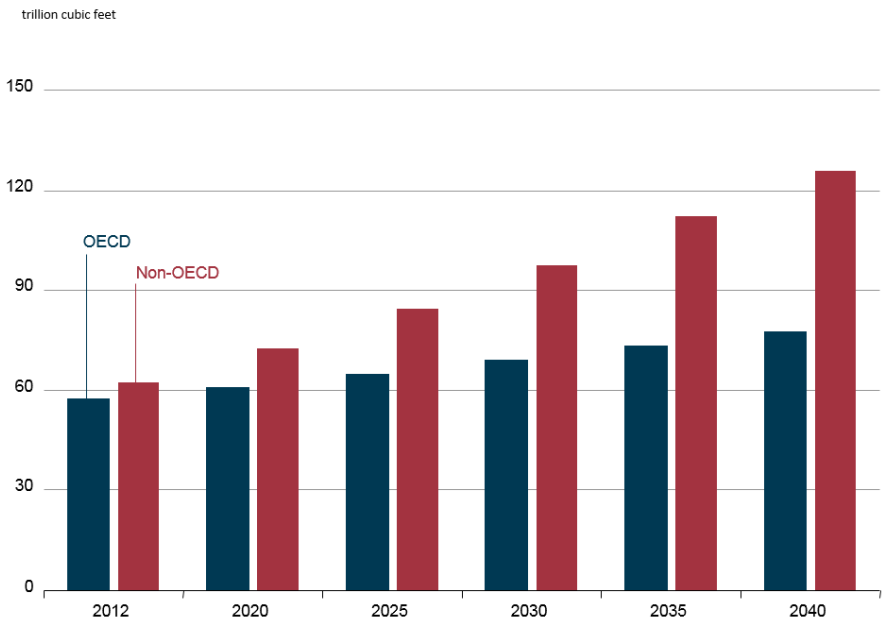

Figure 2.2 World natural gas consumption, 2012-2040 (EIA, 2016).

Table 2.1 Properties of natural gas, gasoline and diesel (modified from Sapag *et al.* (2010))

Property	Natural Gas	Gasoline	Diesel
Flammability Limits (volume % in air)	5-15	1.4-7.6	0.6-5.5
Auto-Ignition Temperature (ºC)	450	300	230
Peak Flame Temperature (ºC)	1,884	1,977	2,054

Natural gas is used across all sectors, in varying amounts, including in industrial, residential, electricity generation, commercial, and transportation sectors (Demirbas, 2010b).

2.2 Natural Gas Storage

The storage of natural gas is required for supplying and transportation to other locations that expects to meets demand of consumers. There are three technologies to store natural gas.

2.2.1 Compressed Natural Gas (CNG)

Natural gas has been used as a transportation fuel in the form of CNG for many years. Natural gas compression is often done at a refueling station using industrial compressors and storage tanks. The CNG flows through a fuel line from the compression tanks into a regulator and from there, it gets injected into the engine just like gasoline (Curran *et al.*, 2014). CNG is produced by compressing the conventional natural gas (which is mainly composed of methane) to less than 1% of the volume it occupies at standard atmospheric pressure that brings its energy density to about 26% of that of gasoline. It is stored and distributed in a rigid container at a pressure of 2,900-3,600 psi, usually in cylindrical shapes metallic cylinder. The

octane number of natural gas is ranging from 120 to 130. Due to this high value of octane number, CNG has a higher knock resistance than gasoline which enables the use of higher compression ratio and thus higher engine efficiency (Khan *et al.*, 2015).

CNG has been commercialized worldwide, but there are some drawbacks from its high operating pressure

1. The storage tanks are limited space and heavy weight due to bulky high-pressure cylinders (about 1 kg per liter for steel tank).

2. The high pressure system requires complex compressors, which consume high energy that is high capital cost for fuel supply compressors.

3. It is perceived as dangerous as it is associated with the high-pressure systems like cylinder corrosion and possibility of explosive release of compressed gas.

2.2.2 Liquefied Natural Gas (LNG)

LNG is a way of transporting natural gas long distances when pipelines are not an option-across oceans. Producing LNG involves compressing and cooling natural gas to around -162 ºC. That process converts the gas to a liquid and cuts its volume to 1/600 time of the original, making it possible to ship the LNG in special tankers. Once it gets to its destination, the LNG can be unloaded at a receiving terminal and regasified-turned back into a gas.

For heavy-duty vehicle applications, cryogenically cooling natural gas to LNG (liquefied natural gas) at -162 ºC and atmospheric pressure (145 psi) increases the density but adds substantially to the cost (Khan *et al.*, 2015). The volumetric energy density of LNG is about 66 percent of total gasoline. The advantage of LNG is that it offers an energy density comparable to petrol and diesel fuels, extending range, and reducing refueling frequency (Khamehchi *et al.*, 2013).

The drawbacks for LNG storage are from large tanks. LNG transportation (usually a 70 m diameter tank, 45 m high, which can hold 100,000 m^3) requires large and expensive infrastructure. Long term storage is also difficult for LNG, as significant losses occur due to warming up and boiling off too fast (Bimbo *et al.*, 2015) because the LNG increases inevitably the temperature within the tank, the pressure rises and could result in a dangerous situation. Moreover, the filling of

the tank must be performed by an expert on cryogenic liquids handling (Sapag *et al.*, 2010)

2.2.3 Adsorbed Natural Gas (ANG)

ANG stores natural gas in porous medium as adsorbents at standard temperature and pressure. It is the process that the gas molecules adhere to the pore and surface of porous medium. Porous medium requires low costs and high gas storage capacities like activated carbon. Therefore, addition of porous medium in gas storage can improve volume of natural gas in the same container at the same pressure and temperature.

The cost of ANG is cheaper than CNG and LNG because it neither needs compression to high pressure nor refrigeration methods nor requires less energy. ANG also has higher storage capacity in equivalent volumes than others storage technologies.

Over the next 20 years, the role of natural gas in global energy consumption will increase substantially. The speed of the transition to natural gas will be driven by environmental constraints, increased demand, and new technologies. A potential source of natural gas lies in the enormous worldwide gas hydrate reserves. However, these deposits can cause problems and safety concerns relating to drilling, production of oil and gas, and building or operation of pipelines. Naturally occurring gas hydrates are normally found at the seafloor or in shallow sediments where the pressures and temperatures are conducive to hydrate formation (Demirbas, 2010b).

2.3 Natural Gas Hydrates

Natural gas hydrates, primary composed of methane, are non-stoichiometric, crystalline substances formed by water and light natural gases. In the molecules of hydrates, gas molecules are entrapped in the water lattice formed by hydrogen bonds. The lattice is composed of cavities of various sizes that are occupied by the gas molecules, and the gas molecules are bound in the lattice through weak van der Waals forces. Given favorable condition of high pressure and low temperature in

addition to the availability of free methane and water, gas hydrates can form and remain stable (Englezos, 1993; Sloan and Koh, 2008). Such conditions can exist in ocean-bottom sediments at water depths below 500 m (Kvenvolden, 1993). Methane is the dominant component among other hydrocarbon gases in sediments, so that the terms "methane hydrates" and "gas hydrates" are often used interchangeably, and refer to the methane–water crystalline structure called a clathrate (Demirbas, 2010a).

Recently, natural gas hydrate technology has drawn much attention as a new technology in many processes such as gas separation process, gas storage, and transportation. During hydrate formation, the liquid water is presented in terms of "metastable liquid". Metastable liquid means liquid, at equilibrium, will exist as hydrates. Gas hydrates are classified by the size of guest molecules in three general structures (Demirbas, 2010a).

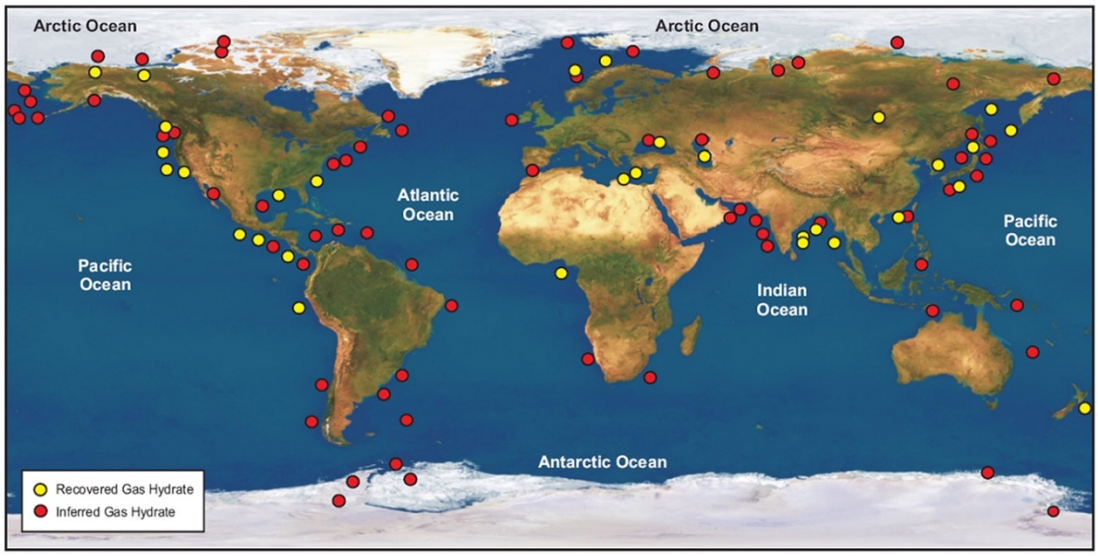

Figure 2.3 Location of sampled and inferred gas-hydrate occurrences in oceanic sediments of outer continental margins and permafrost regions (modified from Kvenvolden (1993).

In fact, numerous field studies have shown that gas hydrates is widespread in permafrost regions and beneath the sea in sediments of outer continental margins (Figure 2.3). Natural gas hydrates have the potential to provide an enormous resource

of natural gas from the world's oceans and the polar regions. Figure 2.4 shows phase diagram of methane hydrate stability zone at different depth-temperature. As seen from the figure, the hydrate deposits themselves may be several hundred meters thick. The resource contained in marine methane hydrate deposits is significantly larger and occurs in many more countries than do Arctic hydrates (Allison, 2008).

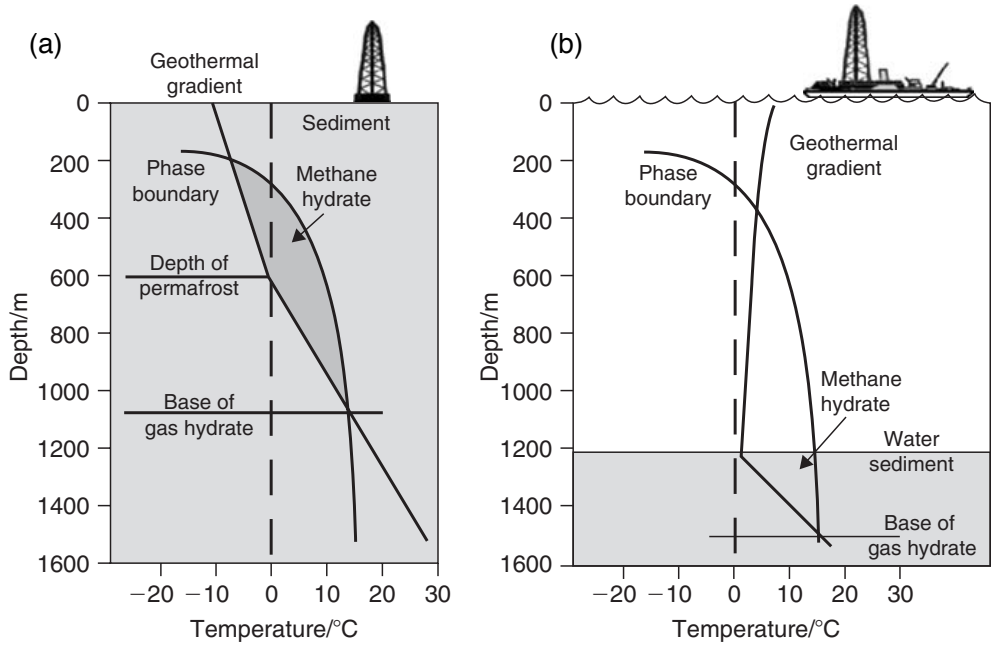

Figure 2.4 Phase diagram of methane hydrate stability zone at different depth-temperature: (a) permafrost and (b) oceanic environment (Allison, 2008).

The global estimates of the methane hydrate resource vary considerably, from 1×10^{15} to 5×10^{15} m^3 at STP to 21×10^{15} m^3. This is significantly larger than the estimate of global conventional natural gas resources of 44×10^{13} m^3 (Kvenvolden, 1999). The methane hydrate estimates are for gas in-place. Actual production would be only a percentage of this volume. However, the potentially producible volume could still be larger than with conventional natural gas resources (Allison, 2008). This volume of natural gas contained in the world's gas hydrate accumulations is generally accepted to greatly exceed that of known gas reserves (Collett, 2002). However, according to the recent National Research Council (United States) report on methane hydrates, there are no fundamental technological hurdles to recover energy from these

natural deposits, although more research needs to be performed to determine the environmental impact of such exploration (Koh *et al.*, 2011).

2.4 Gas Hydrate Structures

Gas hydrate consists of three general structure types. Depending on the size of the guest molecule, natural gas hydrates can consist of any combination of three crystal structures, which are Structure I (sI), Structure II (sII) and Structure H (sH) as shown in Figure 2.5. When pure liquid water freezes, it crystallizes with hexagonal symmetry, but when it "freezes" as a hydrocarbon hydrate it does so with cubic symmetry for sI and sII, reverting to hexagonal symmetry for sH.

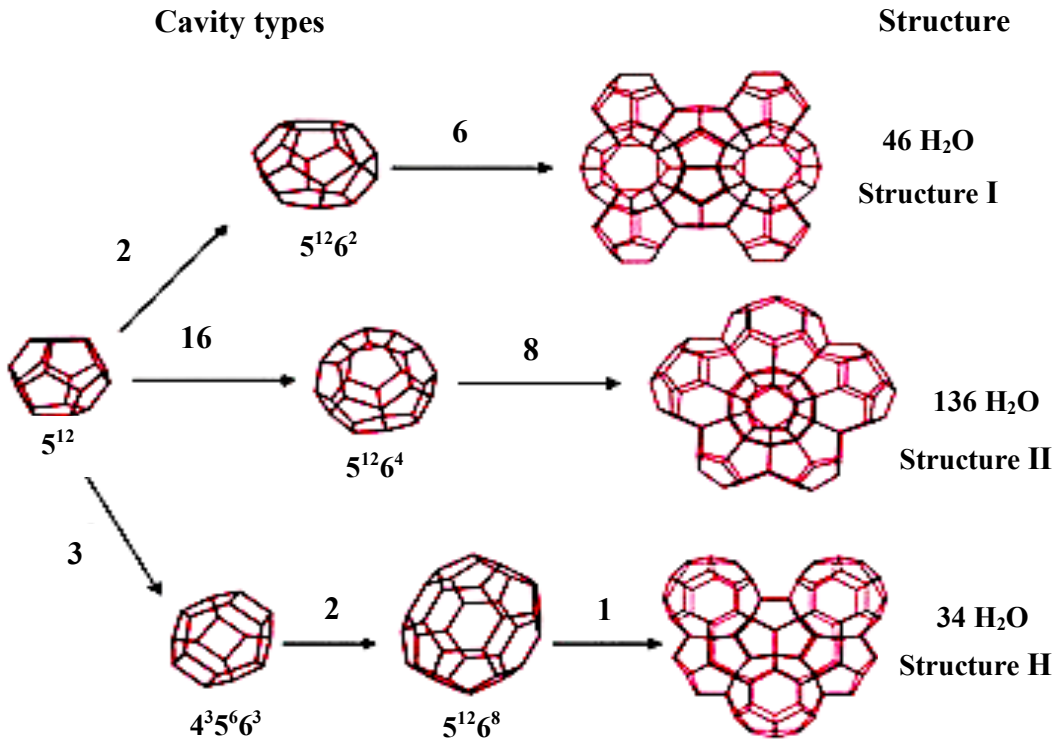

Figure 2.5 Structure types of gas hydrates (Perrin *et al.*, 2013).

Table 2.2 Geometry of hydrate unit cells and cavities (modified from Sloan and Koh (2008))

T	I		II		H		
Crystal system	Cubic		Cubic		Hexagonal		
Number of H_2O molecules	46		136		34		
Cavity	Small	Large	Small	Large	Small	Medium	Large
Description	5^{12}	$5^{12}6^2$	5^{12}	$5^{12}6^4$	5^{12}	$4^35^66^3$	$5^{12}6^8$
Number of cavities/unit cell	2	6	16	8	3	2	1
Avg. cavity radius (Å)	3.95	4.33	3.91	4.73	3.94	4.04	5.79
Variation in radius (%)	3.4	14.4	5.5	1.73	4.0	8.5	15.1
Coordination number	20	24	20	28	20	20	36

2.4.1 Structure I (sI)

Structure I is the structure with the simplest hydrate structure and has a cubical shape. It consists of two types of cavities such as dodecahedron and tetrakaidecahedron. The dodecahedron is a 12-sided polyhedron where each face is a pentagon twelve edge 5^{12}, which is the smallest of the cavities. It contains 20 molecules of water with 30 hydrogen bonds, and has a radius of 3.95 Å. At normal temperature and pressure, the cavities may contain CH_4, N_2, H_2S, H_2, Kr, Ar, and other non-polar gas molecules. Tetrakaidecahedron is a 14-sided polyhedron with 12 pentagonal and two hexagonal side faces, $5^{12}6^2$. This large cavity containing 26 water molecules has a radius of 4.33 Å. The cavities can contain including carbon

dioxide and ethane. Methane can occupy both the small and large cavities, while ethane can only occupy the large (Sloan and Koh, 2008). The unit cell of sI contains 46 molecules of water arranged in lattice around 8 cavities. Of these eight cavities 2 of them are small and 6 of them large (Koh *et al.*, 2011; Sloan and Koh, 2008).

2.4.2 Structure II (sII)

Structure II is more complex than structure I, but still has a cubical shape. It also consists of small and large cavities. The sII hydrate consists of hexsakaidecahedron and dodecahedron. The dodecahedron has exactly the same shape as that of sI, a 12-sided polyhedron where each face is a pentagon twelve edge, 5^{12}. The hexsakaidecahedron is a 16-sided polyhedron with twelve pentagonal side surfaces and four hexagonal side faces, $5^{12}6^4$. The larges cavities of the sII are bigger than the large cavity of sI, and can accommodate larger guest molecules (Koh *et al.*, 2011; Sloan and Koh, 2008). The small cavity of sII has cavity radius slightly less than sI as indicated by Table 2.2. In contrast, sI unit cell has 46 water molecules, while the unit cell of sII has 136 water molecules, arranged in lattice of 24 cavities, 16 small and 8 large. The most common sII hydrate formers are propane and iso-butane, which only occupy the large cavity. sII is the most common structure that formed in oil and the gas industry. This is also the most stable structure (Sloan and Koh, 2008).

2.4.3 Structure H (sH)

The sH hydrated stands for hexagonal, which is the shape of the structure. sH consists of small, medium and large cavity. It occurs much less frequently than the other two, and in terms of stability it lies between sI and sII.

sH requires two types of guest molecules to stabilize the hydrate structure; one help gas that fits into the small and medium cavities, and the structure H former that fits in the large cavities (Ripmeester *et al.*, 1987). The small cavity is still the dodecahedron, while the medium sized cavity is an irregular dodecahedron consisting of 4-square sides, six pentagonal lateral surfaces and three hexagonal sides, $4^3 5^6 6^3$, which has a radius of 4.06 Å. The large cavity is an irregular isocahedron, a 20-sided polyhedron with 12 pentagonal and 8 hexagonal side faces,

$5^{12}6^8$, with a radius of 5.71 Å (Sloan and Koh, 2008). The unit cell of sH consists of 34 water molecules, arranged in 3 small, 2 medium and 1 large cavities.

The sI and sII may be formed in the presence of only one hydrate forming gas only, while structure H requires a help gas such as methane to form the structure. These structure H rarely occurs in natural gas, and this could be the reason why sH occurs less frequently than sI and sII (Carroll, 2014).

2.5 Gas Hydrate Formation Process

Gas hydrate formation is usually described as a crystallization process with nucleation, growth, agglomeration, and breakage. Gas is dissolved in water, and nucleation starts primarily at the gas-water interface where the gas concentration is highest. The formation rate of methane hydrate is governed by a multitude of factors, including pressure, temperature, and gas composition, also called PVT-effects. Also, the rate of hydrate formation is determined by the combined effects of heat and mass transfer. Cooling is required to remove the hydrate heat of formation. Mass transport is required to dissolve the methane gas in liquid water, and to bring the dissolved gas molecules in contact with a growing hydrate crystal. In addition to the above factors, the rate of hydrate formation depends on the nature of crystal growth, also referred to as chemical reaction kinetics. The overall rate of hydrate formation, therefore, depends on PVT-effects, transport-effects, and reaction effects. The hydrate formation process was described by gas absorption, primary and secondary nucleation, growth, agglomeration, and breakage (Sloan and Koh, 2008).

Figure 2.6 shows the process of hydrate nucleation and growth, considering the gas consumption versus time trace in the agitated system, operated at constant pressure and temperature The induction time is marked as 1 and includes the time taken for the hydrate crystal to form. The induction time is defined in practice as the time elapsed until the appearance of a detectable volume of hydrate phase or equal to the consumption of a detectable number of moles of hydrate former gas. The induction time is often also termed the hydrate nucleation or lag time.

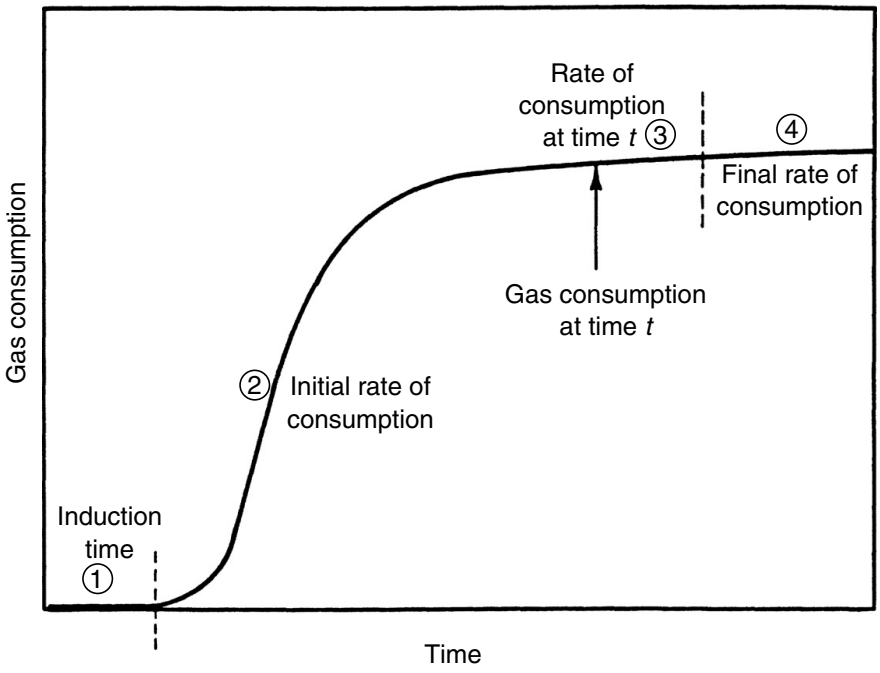

Figure 2.6 Gas consumption versus time for hydrate formation (Sloan and Koh, 2008).

During the induction period, the temperature and pressure conditions are within the hydrate stable region. However, the hydrate does not form within this period because of the metastability, which is the ability of a non-equilibrium state to persist for a long period of time. The growth period in region 2 indicates a very rapid hydrate growth occurs. During the growth period, gas is being concentrated in the hydrate cages-hydrated gas molecules are more densely packed than those in the vapor. As the water is consumed by hydrate formation, the slope of the gas consumption trace eventually decreases with time (Points 3-4) (Sloan and Koh, 2008).

2.6 Dissociation of Gas Hydrates

The dissociation of hydrates is an endothermic reaction. The production of natural gas from hydrates in sediment or permafrost is done by dissociation of the

hydrates by changing the thermodynamic conditions in the system. The dissociation reaction is:

$$CH_4 \cdot 6H_2O(s) \rightarrow CH_4\,(g) + 6H_2O\,(l) \qquad (2.1)$$

There are three methods to dissociate gas hydrates: thermal stimulation depressurization and inhibitor injection (Demirbas, 2010a).

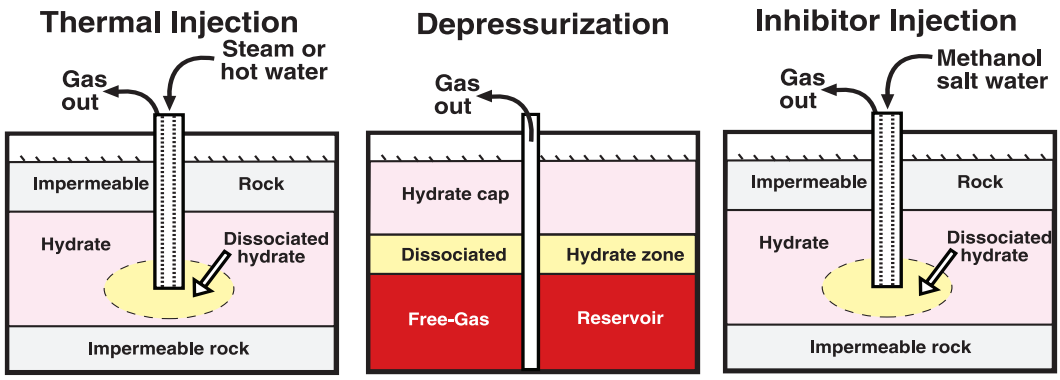

Figure 2.7 Schematic of proposed gas hydrate production techniques (Collett, 2002).

2.6.1 Thermal Stimulation

Thermal stimulation is the process with the addition of heat to raise the temperature of system to higher than the hydrates dissociation temperature via injection of steam, hot water or heated liquid to the system. The entire gas released by thermal stimulation is due to the hydrate dissociation and thermal expansion of gas in the crystallizer so the thermal expansion needs to be accounted to approach actual gas released from the hydrates dissociation (Babu *et al.*, 2013). Nam *et al.* (2008) studied decomposition of methane hydrates by thermal stimulation at a constant pressure of 3.5 MPa and driving force 4°C in silica sand. The results showed that this method can achieve 95 to 98% of methane recovery.

2.6.2 Depressurization

Depressurization is the process that decreases the pressure in the system to the free gas zone, where the hydrates are unstable, and it will decompose to gas and

water. Haligva *et al.* (2010) investigated the decomposition of hydrates by depressurization in different volume of silica sand. They found that the required amount of heat to dissociate hydrates in smaller hydrates was less than the larger hydrates. When the bed size of silica sand decreased, the rate of gas recovery increased meaning the duration of methane recovery was shorter. Xiong *et al.* (2012) indicated that depressurization in porous medium can divide into three stages: free gas release at first, rapid hydrate dissociation, and slow hydrate dissociation. They also concluded that the lowering of dissociation pressure increased the dissociation rate. There are three important factors for depressurization: kinetics of dissociation, heat transfer and flow of fluids (Demirbas, 2010a).

2.6.3 Inhibitor Injection

Inhibitor injection is the process that uses the antifreeze or chemical inhibitors such as glycol, methanol to shift the hydrates equilibrium, where the hydrates are no longer stable in that conditions.

The actual dissociation temperature of gas hydrates may be higher than the temperature of hydrates phase equilibrium because of self-preservation. Self-preservation is the condition, when the ice shield forms around gas hydrates. Dissociation of gas hydrates takes place after the ice shield melts. Hence, it can decrease the dissociation rate of gas hydrates or increase the stability of hydrates (Demirbas, 2010a).

2.7 Hydrate-based Technologies

The enormous reserve of methane gas in the hydrate state is considered as the future energy source. The global estimate of the methane hydrate resource is significantly larger than the estimate of global conventional natural gas resources (Kvenvolden, 1999; Milkov, 2004). Besides, the ability of gas hydrates to contain 150-180 volumes of gas/volume of hydrate makes them to be considered as a potential for natural gas storage and transport Sun *et al.* (2003). Storage of CO_2 in natural gas hydrate reservoirs and at the same time releasing the hydrocarbon gas

trapped in the hydrate state could be considered as double opportunities (Kvamme *et al.*, 2007).

2.7.1 Separation of Gas Mixtures

The component that forms hydrates more easily will be enriched in the hydrate phase. Based on this principle, it is considered possible to separate gas mixtures through forming hydrates. Hydrate-based separation concepts have been proposed for many fields: (1) recovering global warming gases, such as hydrofluorocarbon from air, sulfur hexafluoride (SF_6) from nitrogen, and CO_2 and H_2S from flue gas; (2) recovering organic contaminants from gaseous or aqueous mixtures; (3) recovering hydrogen from hydrogen-containing light hydrocarbon gas mixtures; (4) recovering methane from low-concentration coal mine methane; and (5) separation of methane and ethane, which is required in natural gas, oil processing, and ethylene production. The hydrate-based gas separation is more effective and has many advantages over conventional separation methods, such as cryogenic fractionation, selective adsorption, gas absorption, and membrane process (Sun *et al.*, 2011).

2.7.2 Carbon Dioxide Sequestration

Carbon sequestration is defined as the removal of greenhouse gases from industrial or utility plant streams and their long-term storage in such a way that they cannot interact with the climate system. CO_2 and water can form a stable hydrate when pressure and temperature fall within the hydrate formation region. Since CO_2-containing hydrates are considerably more stable thermodynamically than methane hydrates, it is a possible way to replace the original hydrate bound hydrocarbons by CO_2 (Giavarini *et al.*, 2007). Two goals can be accomplished at the same time: safe storage of carbon dioxide in the hydrate reservoirs, and in situ release of hydrocarbon gas. The hydrates and the matrix mineral surfaces are separated by liquid-containing channels, which will serve as escape routes for released natural gas, as well as distribution channels for injected CO_2 (Kvamme *et al.*, 2007).

2.7.3 Natural Gas Storage

According to the highly concentrated gas in the hydrate form, for example, 1 m^3 of methane hydrate contained 170 m^3 of methane gas at STP (Sun *et al*., 2003). The storage of natural gas is appealing for industrial utilization because of not only its high storage capacity, but also its high safety. Gas hydrates can be stored at 15 °C under atmospheric pressure for 15 days, retaining almost all the gas (Gudmundsson *et al.*, 1994). Methane hydrates remain metastable at 0.1 MPa and temperatures slightly below 0 °C for a certain of time (Stern *et al.*, 2001). That is the increase in storage stability of methane hydrates above 240 K is likely related to the formation of the ice. With high energy density, gas hydrates can be used in storage and transportation of natural gas, which has certain advantages over highly compressed or liquefied gas at higher temperatures and lower pressures.

In comparison with other natural gas storage and transportation methods, such as liquefied transportation, a substantial cost saving (18% - 24%) is expected for the transport of natural gas in the hydrate form (Javanmardi *et al.*, 2005). The natural gas hydrate (NGH) method avoids the capital cost investment for the infrastructure constructions of the LNG method, which is an important point for the transportation of stranded gas. Therefore, especially for the stranded gas, the NGH method can be considered as an alternative for transportation of natural gas.

However, industrial applications of hydrate storage processes are hindered by some problems, such as slow formation rates, unreacted interstitial water as a large percentage of the hydrate mass, reliability of hydrate storage capacity, and economy of process scale-up (Mandal and Laik, 2008). To solve these problems, two approaches including mechanical and chemical means are generally adopted, which are similar to those methods used in hydrate-based gas separation processes. The mechanical method includes stirring (Iwasaki *et al.*, 2005), spraying of liquid in continuous gas phase (Fukumoto *et al.*, 2001), bubbling of gas in continuous liquid phase (Luo *et al.*, 2007), and microbubbling (Takahashi, 2002).

To store gas in the form of hydrates, the crucial issues such as slow formation rates, unreacted interstitial water as a large percentage of the hydrate mass, reliability of hydrate storage capacity, hydrate stability must be improved. There are many researchers studied and investigated on gas hydrate formation and dissociation

by using hydrate promoter including chemical promoters.

2.8 Hydrate Promoters

The drawbacks of gas hydrates include slow formation rate of natural gas hydrates, which has been considered to be a critical problem hindering the industrial application of gas hydrates for storage and transportation of natural gas. To overcome this problem, additives as promoter are often used (Roosta *et al.*, 2013).

2.8.1 Surfactant

The key effect of surfactant is that it reduces the gas-liquid interface surface tension, so that the diffusion resistance between two phases is reduced and the gas molecule solubility is increased, as a consequence, better mass transfer effects is gained. However, the promotion mechanism of surfactants is not very clear yet.

Lin *et al.* (2004) investigated the effects of anionic surfactant sodium dodecyl sulfate (SDS) on the formation/dissociation kinetic behaviors of methane hydrate. They conducted the experiment at 276.4 K and pressurizing methane gas up to 6.6 MPa. The results showed that the presence of SDS could enhance the formation process of methane hydrates. Tests over a SDS concentration range from 0 to 2000 ppm performed on gas storage capacity manifested that a maximum storage capacity of 170 standard volume of methane per volume of hydrate (170 V/V) could be achieved at 650 ppm. The hydrate samples for dissociation experiments with the presence of SDS were uniformly formed at this SDS concentration. Hydrate dissociation rates that the presence of SDS increased the dissociation rates.

The effects of different surfactants on methane hydrate formation rate and storage capacity has been studied by Ganji *et al.* (2007). SDS and linear alkyl benzene sulfonate (LABS), anionic surfactant, cetyl trimethyl ammonium bromide (CTAB), cationic surfactants, and ethoxylated nonylphenol (ENP), nonionic surfactant were used. The experiment was conducted by pressurizing with

methane gas up to 8.3 MPa at 298.2 K. The results showed that the methane hydrate formation rate was increased with the presence of surfactants compared to pure water. In addition, for all hydrate samples at each constant temperature, the maximum dissociation rate occurred at the beginning of dissociation stages and then the rate decreased. As a result, they indicated that among the surfactants tested, SDS was the best one for utilizing methane hydrates for storage and transportation of gas with the maximum promotion effect on hydrate dissociation rate while the stability of hydrate formed was satisfactory at 268.2 K.

Okutani *et al.* (2008) investigated the effects of the alkyl chain length of surfactant on the formation of a methane hydrate in a quiescent methane/liquid-water system. The surfactants used in the present study were SDS, sodium tetradecyl sulfate (STS) and sodium hexadecyl sulfate (SHS). The experiment was conducted by pressurizing with methane gas up to 3.9 MPa at 273 K. The results showed that the three surfactants caused the same change in the hydrate-formation behavior. Hydrate layers grew on the chamber wall above the level of the aqueous phase, while dendritic hydrate crystals bristled downward from the surface of the aqueous phase. The hydrate-layer growth on the chamber wall accounts for the major portion of the total hydrate formation inside the chamber. SDS is very effective for increasing both the rate of hydrate formation and the final water-to-hydrate conversion ratio, if its concentration ~ 1000 ppm or above. However, equivalent promotion was available with STS at a much lower concentration ~ 100 ppm. SHS having the longest alkyl chains and the lowest solubility was less effective in increasing the rate of the hydrate formation, compared to SDS and STS.

Zhang *et al.* (2007a) investigated the effect of SDS solubility in liquid water at temperatures ranging from 270 to 282 K by using high-pressure reactor. The result presented that the SDS solubility under high-pressure for methane hydrate-forming was equivalent to the SDS solubility under atmospheric pressure at investigation temperature. Moreover, the SDS Kraft point under methane hydrate forming conditions did not change. The promotion on gas hydrate nucleation in the presence of SDS below Kraft point was not caused by SDS micellization but possibly

caused by reducing the energy barrier to generate the nucleation by adsorbing on the hydrate nuclei.

Recently, many research fields focused on the using bio-based materials to decrease the risk of the environment and humans impacts. So that, many researchers in hydrate technology found and developed the new surfactants, which were produced from bio-based resource (De *et al.*, 2015).

Rogers *et al.* (2003) investigated five biosurfactant categories by-product of microbial activity, including hydroxylated and cross-linked fatty acids, polysaccharide-lipid complexes or polymers, glycolipids, lipoproteins-lipopeptides, and phospholipids, in seabed on the methane hydrate formation. They found that all biosurfactants had a profound effect on gas hydrate formation rate and induction time. The formation rate predominantly increased from 96% to 288% and the induction times significantly decreased from 20% to 71% relative to the system without biosurfactant.

Wang *et al.* (2012) used the lignosulfonate biosurfactant as the hydrate promoter to promote methane hydrates. Lignosulfonate biosurfactant was byproduct from paper industry. The presence of lignosulfonates biosurfactant reduced the hydrate nucleation time and enhanced both the rate of methane formation and the storage capacity. The presence of small concentration of lignosulfonates biosurfactant, 0.5 wt%, significantly increased the storage capacity of methane hydrate to 170 V/V. Moreover, the recyclability of the lignosulfonates biosurfactant provided that the induction time, rate of formation and storage capacity are about the same with the fresh solution.

Recently, Chaturvedi *et al.* (2018) synthesized a novel surfactant from castor oil and used as a gas hydrate promoter. They found that the increasing concentration of the novel surfactant decreased the interfacial surface tension and induction time, whereas, the rate of hydrate formation and gas storage capacity increased with increasing the novel surfactant concentration. The optimum concentration of 9000 ppm gave the storage capacity of 96% of the theoretical maximum value (172 V/V) and the induction time of 12 min.

2.8.2 Tetrahydrofuran (THF)

THF is a chemical hydrate promoter, which remarkably reduces the required hydrate formation pressure and increase the required temperature to form gas hydrates due to its effect on the thermodynamics equilibrium of gas hydrates.

Seo *et al.* (2001) investigated the effect of different thermodynamic promoters on the mixed-CH_4 hydrate phase equilibrium. They used four chemicals including acetone, THF, 1,4-dioxane, and propylene oxide to change hydrate phase equilibrium of pure methane hydrate to mixed methane hydrate. The result showed that the equilibrium temperature of the methane and THF mixed hydrated appeared to be the highest among the tested promoters, and THF was proven to be the strongest to stabilizing methane hydrates. Moreover, they found that the increase in THF concentration increased both hydrate stability and equilibrium dissociation temperature.

Lee *et al.* (2005) studied the mole fraction of THF for tuning the hydrate formation for hydrogen storage. They investigated the THF hydrogen hydrate formation by using Raman and NMR spectroscopy. The results showed that the full loading of hydrogen in the small cavities of sII structure would have a storage capacity of 2.1 wt% H_2. In order to increase the hydrogen content in the hydrate structure, the hydrogen guest must enter in the large cages of sII structure. Interestingly, with the decrease in the THF concentration down to 0.15 mol% THF, the mole ratio of H_2/THF increased up to 23 times for 0.15 mol% THF. It indicated that the large cages must contain hydrogen. Moreover, the eutectic concentration of THF hydrates was at 1.0 mol% THF. However, the result confirmed that at the low concentration of THF (below 1.0 mol%), the hydrogen gas did not occupy in the large cages of sII, and only THF formed the hydrates in this occupancy. Also, Anderson *et al.* (2007) demonstrated the phase relation and binary clathrate hydrate formation in the system of THF-H_2-H_2O. The result confirmed the formation of sII binary THF-H_2 hydrates with stoichiometric THF-to-water ratio of 1:17.

Prasad *et al.* (2009) observed the mixed THF-CH_4 hydrates by using Micro-Raman spectroscopy. Mixed gas hydrates were synthesized with different THF concentrations from 1.46 to 5.88 mol% under the methane atmosphere. The result indicated that THF molecules occupied the large cages of sII hydrates in all

cases. They stated that the formation of sII hydrates occupied the unfilled cages (small cages) by CH_4 for THF concentration ranging from 2.95 to 5.88 mol%. At the same time, the Raman spectral indicated that mixed gas hydrates at 1.46 mol% of THF was non-uniform and the hydrate structure transformed from sII to sI due to the hydrate melting. The mixed methane-THF hydrate formation in the molecular level was prevailed by the report of Kumar *et al.* (2016). Kumar *et al.* (2016) used microdifferential scanning calorimeter (HP μ-DSC) to investigate the mechanism of during formation of mixed THF-CH_4 hydrates in the sII region of mixed methane-THF hydrate phase equilibrium curve. They found that the heat flow change was detected in two steps during mixed methane-THF hydrate formation. It can imply that the mixed methane-THF hydrate formation constituted of two steps of mixed methane-THF hydrate formation. First, THF was incorporated in the large cages of sII structure, later methane was encapsulated in the small caged of sII structure. This result corresponded with the report of Kumar *et al.* (2019). Kumar *et al.* (2019) investigated the real time mixed methane-THF hydrate formation mechanism by using *in-situ* Raman spectroscopy. During the real time mixed methane-THF hydrate formation mechanism, THF occupied the large cages of sII hydrates, while the small cages of sII structure was occupied by methane gas.

Lee *et al.* (2012) studied the phase equilibrium of THF-CH_4, THF-CO_2, CH_4-CO_2, and THF-CH_4-CO_2 hydrates. The Raman measurements of the CH_4-CO_2 hydrates indicated that the population of CH_4 molecules in the small 5^{12} cages of the sI hydrate framework was higher than that in the large $5^{12}6^2$ cages, while the CO_2 molecules preferentially occupied the large $5^{12}6^2$ cages. In the case of THF-CH_4-CO_2 hydrates, the CH_4 and CO_2 molecules were encaged only in the small 5^{12} cages of the sII hydrate framework, whereas the large $5^{12}6^4$ cages were fully occupied by THF molecules at the stoichiometric concentration of 5.56 mol %. The comparison of dissociation pressure of THF-CH_4 and THF-CO_2 hydrates with the THF concentration of 5.56 mol% is shown in Figure 2.8.

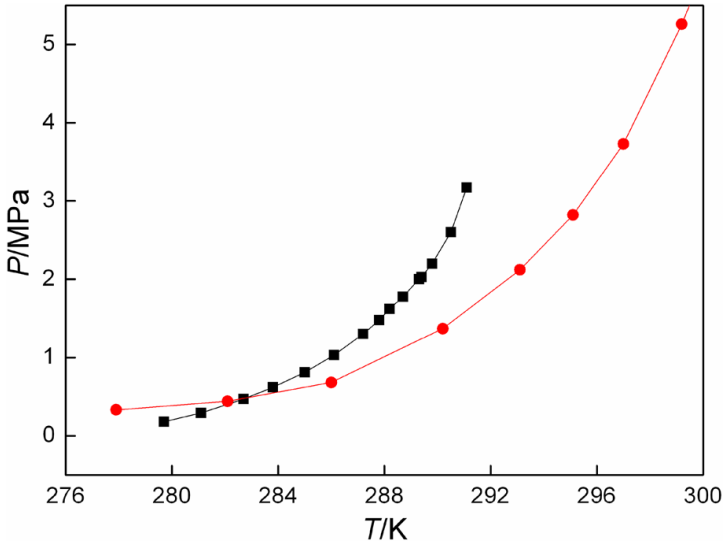

Figure 2.8 Comparison of dissociation pressure of THF-CH_4 (●) and THF-CO_2 (■) hydrates with the THF concentration of 5.56 mol% (Lee *et al.*, 2012).

Sharma *et al.* (2014) reported the formation kinetics of methane hydrates in aqueous solution of THF at concentration of 6.03 mol% and different pressures of the range of 0.88-8.21 MPa in a stirred reactor. There was 90% of methane consumption for the hydrate formation in THF/CH_4/water system occurred significantly faster than CH_4/water system. It was observed that the increase in the initial pressure decreased the induction time of mixed THF-CH_4 hydrates. The overall hydrate yield in the mixed hydrates—the small cages and large cages of sII were occupied by methane and THF molecules, respectively— was always more than pure methane hydrate in structure I. In addition, the significant amount of methane release occurred from the mixed hydrates at temperature higher than the ice melting temperature. They noted that the mixed hydrates system could be used as a medium to store and transport the methane gas.

Veluswamy and Linga (2013) studied the kinetics of mixed THF-H_2 hydrate formation for hydrogen storage in a stirred tank reactor. THF concentration was varied between 1 mol% and 5 mol%. The results clearly demonstrated that, in the dissolution phase, the increase in the driving force pressure resulted in an increase in gas uptake until saturation for all concentrations of THF promoter.

Moreover, the increase in the concentrations of THF from 2.4 mol% to 5 mol% resulted in decreasing the gas uptake. However, the increase in the driving force had little effect on the reduction of induction time even at high promoter (THF) concentration. In addition, for any THF concentration, the rate of hydrate formation increased with the increase in driving force pressure. Hydrate growth increased with the increase in the driving force for hydrogen/THF hydrates at all THF concentrations. Moreover, they also stated that the faster induction times, the higher rate of hydrate formation and higher gas consumption were desirable for a successful demonstration of the clathrate process for hydrogen storage.

Veluswamy *et al.* (2016c) investigated the effects of 5.56 mole% THF as a thermodynamic promoter on the mixed methane THF hydrate formation at 283.3 K and 7 MPa. This condition was in the sII region of mixed methane-THF hydrate formation equilibrium curve. They found that adding 5.56 mole% THF at 283.2 K and 7 MPa increased the rate of hydrate formation, and the methane uptake increased 11.66 time compared to pure methane at 9.5 MPa and 272.K. Moreover, the enhanced rate of hydrate formation and methane uptake was the result from the hydrate crystal channels. The presence of hydrate crystal channels facilitated the migration of solution from the bulk liquid to in the upward direction by the capillary action, the methane easily converted to mixed hydrates. Therefore, the presence of promoter like THF mixed with methane in the process of hydrate formation can enhance both thermodynamic and kinetic performance, which abled to the development of a low cost and energy efficient of solid natural gas technology via clathrate hydrates for natural gas storage.

Moreover, Veluswamy *et al.* (2016a) studied the effects of temperature on the mixed methane-THF hydrate formation. They used 5.56 mol% THF as the hydrate promoter and varied different temperature (283.2 K, 288.2 K, and 293.2 K) and 7.2 MPa. At the chosen experimental temperatures and pressure, it is possible to form sII hydrates only and there exists no chance for the formation of pure sI methane hydrates. The report showed that no significant difference of gas uptake in different temperature (283.2 K, 288.2 K, and 293.2 K). This result also showed that increasing the temperature come up with decreasing of the rate of formation; however, they used SDS as a co-promoter to enhance the methane hydrate

formation kinetics at the higher temperature of 293.2 K.

2.8.3 Hollow Silica

Hollow silica is silica grains, which have inner void. It has attractive unique properties such as permeable surface, large cavity, low density, high pore volume, high porosity, high specific area and good thermal insulation (Chen *et al*., 2013).

Prasad *et al.* (2014) studied gas hydrate formation in hollow silica matrix. The hydrates in pure water system formed at a high pressure, and the hydrate yield depended on driving force (pressure) of the system, while the hydrates in the hollow silica system formed at a moderate pressure (4-5 MPa) and gave higher hydrate yield. The result shows that the hydrate yield in the hollow silica increased rapidly at the moderate pressure but slowly increased at the high pressure, which was different from the pure water system. The hydrate yield was higher because of the effect of physicsorption and methane hydrate formation. The hollow silica improved contact surface area between gas and water molecules to form hydrates, and another reason was the silica surfaces had lower polarity than water molecules so the methane hydrates formed easier on silica surfaces.

Chari *et al.* (2015) observed the methane hydrate formation in two different types of silica compared with pure methane. They investigated effects of stirring and non-stirring reactor. Pure silica, solid silica, and hollow silica were used as a porous media in stirred reactors. The methane hydrate formation was found to be the minimum in solid silica and maximum in hollow silica. For non-stirred reactor systems, the hydrate formation in pure silica and solid silica were almost negligible compared to hollow silica as well as the kinetics and hydrate yield. Therefore, type of silica played an important role in hydrate formation. Furthermore, the fast hydrate formation, kinetics and high hydrate yield of hollow silica in non-stirred reactor decreased the energy and cost of synthesis the hydrate efficiently. Thus, the hollow silica could be considered as an advantage for storage and transportation of methane gas hydrate.

Veluswamy *et al.* (2016b) investigated the mechanism of methane hydrate formation in the presence of hollow silica at 8 MPa and 278.2 K. Moreover,

they studied the effect of hollow silica to water ratio on the methane hydrate formation/dissociation morphology. The result showed that all ratio of silica to water improved both rate of hydrate formation and methane uptake. They believed that water molecules transported to the interface from the hollow silica bed through network of capillary channels formed can enhance the hydrate formation when the presence of hollow silica. Moreover, they found that the ratio of hollow silica-to-water ratio at 1:6 is the critical ratio to promote hydrate formation. Beyond a critical hollow silica-to-water ratio, the hydrates preferentially crystallized on the top of the bed by drawing water from the interstitial pores, whereas below this ratio the hydrate formation occurred within the bed between inter-particular spaces of hollow silica.

CHAPTER III
EXPERIMENTAL

3.1 Objectives

The objective of this research are as follows:

1. To study the effect of bio-based surfactants, methyl ester sulfonate (MES), on the methane hydrate formation and dissociation.

2. To study the effect of temperature and pressure on the methane hydrate formation and dissociation with presence of THF.

3. To enhance the methane hydrate formation at the higher temperature and lower pressure by using the mixing of THF and porous media, hollow silica (HS).

3.2 Materials

High purity methane gas (99.99% purity) was purchased form Linde Public Company, Thailand. Tetrahydrofuran (THF, AR grade 99.99 %) was obtained from Lab-Scan, Thailand. The hollow silica power (HSC, 99 %), a mean diameter of 30-70 μm, was obtained from Nanoshel, India. Sodium dodecyl sulfate (SDS, 99.9% purity) was purchased from Aldrich, Germany. Methyl ester sulfonate (MES, 99.7%) supported by Lion Cooperation, Japan. Deionized water (DI) was used for hydrate formation.

3.3 Experimental Section

3.3.1 Apparatus

The methane hydrate formation and dissociation apparatus was set in Figure 3.1a. The apparatus consisted of 180 cm^3 high-pressure stainless steel crystallizer (CR) and 100 cm^3 supply vessel (R) immersed in a cooling bath. The external refrigerator (Model RC-20, Daeyang, Korea) circulated the mixed glycol and water to controlled temperature in a cooling bath. The pressure transmitter (PT)

(Cole-Pamer®, Singapore) with a range of 0 - 21 MPa and 0.13 % global error was used to measure the pressure in the system. Three K-type thermocouples with ±1.0 K accuracy were located at the gas phases, the interface between two phases and in the solution represented by T1, T2 and T3 respectively as showed in Figure 3.1b. A data logger (AI210, Wisco Industrial Instruments, Thailand) was connected to a computer to record the data during the experiment. All experiments were carried out in the quiescent condition with a fixed amount gas and solution in the closed system.

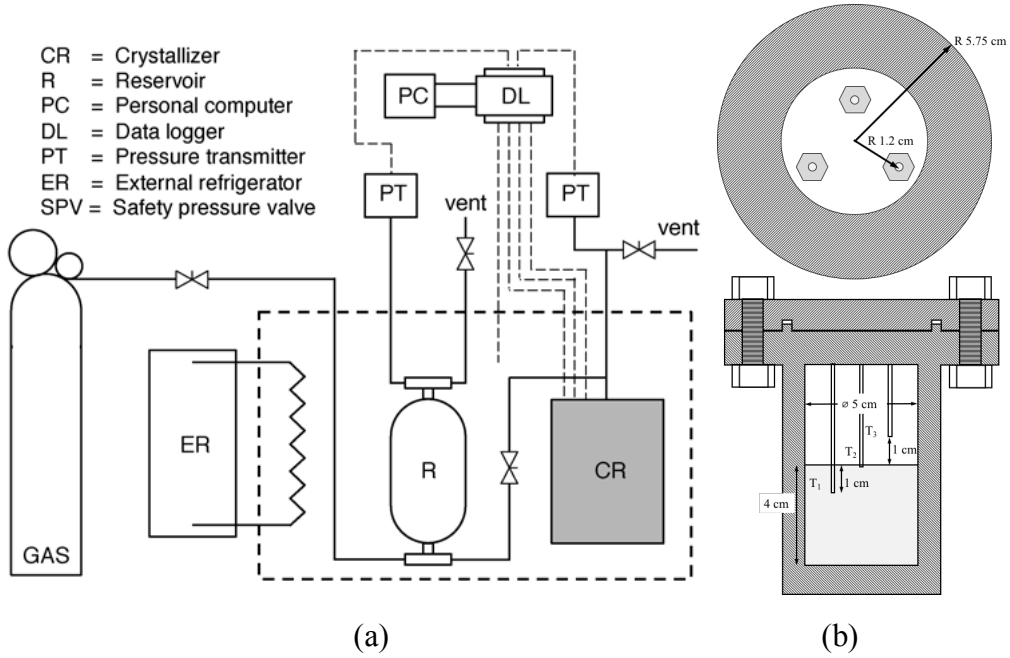

Figure 3.1 Schematic of experimental apparatus (a) and cross-section of a crystallizer (b). Modifiled from Siangsai *et al.* (2015).

3.3.2 Hydrate Formation Experiment

The solution of 90 cm^3 was placed into the crystallizer. In order to eliminate the air in the system in the crystallizer was pressurized to 0.5 MPa by methane gas and depressurized to atmospheric pressure twice. The experimental temperatures were set at desired temperature. Methane gas was introduced into the crystallizer at desired pressure . The data was recorded every 10 s after methane gas was introduced into crystallizer by the data logger. During the hydrate formation, the pressure in the crystallizer dropped due to the hydrate formation. The experiment

continued until there was no further pressure drop at least 1 h. The pressure and temperature data were used to calculate the moles of methane consumed by equation 3.1;

$$\Delta n_{H,\downarrow} = n_{H,0} - n_{H,t} = \left(\frac{PV}{zRT}\right)_{G,0} - \left(\frac{PV}{zRT}\right)_{G,t} \quad (3.1)$$

where $\Delta n_{H,\downarrow}$ is the moles of gas consumed for the hydrate formation at the end of experiment. $n_{H,0}$ is the moles of hydrates at the start of experiment. $n_{H,t}$ is the moles of the hydrates at time *t*. Subscripts *G,0* and *G,t* represent the gas phase at the start of the experiment and time *t*, respectively. *P* and *T* are the pressure and temperature in the system. *V* is the volume of gas phase in the crystallizer, *R* is the universal gas constant, and *z* is the compressibility factor calculated by Pitzer's correlation (Smith *et al.*, 2005).

3.3.3. Hydrate Dissociation Experiment

The hydrates were dissociated by increasing the temperature from the formation temperature at the same heating rate for all experiments to 308 K. The hydrate dissociates when the temperature in the crystallizer crosses the equilibrium phase boundary. The moles of methane released from the hydrate at any time during the hydrate dissociation can be calculated by

$$\Delta n_{H,\uparrow} = n_{H,t} - n_{H,0} = \left(\frac{PV}{zRT}\right)_{G,t} - \left(\frac{PV}{zRT}\right)_{G,0} \quad (3.2)$$

when $\Delta n_{H,\uparrow}$ represents the moles of gas released from the hydrates. The methane recovery is calculated by equation 3.3 as a function of time for any dissociation experiment (Haligva *et al.*, 2010; Linga *et al.*, 2007).

$$\%\text{methane recovery} = \frac{(\Delta n_{H,\uparrow})}{(\Delta n_{H,\downarrow})} \times 100 \quad (3.3)$$

where $\Delta n_{H,\downarrow}$ is the moles of gas consumed for the hydrate formation at the end of experiment.

CHAPTER IV
INVESTIGATION ON THE KINETICS OF METHANE HYDRATE FORMATION IN THE PRESENCE OF METHYL ESTER SULFONATE

4.1 Abstract

The kinetics of methane hydrate formation in the presence of methyl ester sulfonate (MES), a bio-based anionic surfactant, was evaluated in an unstirred reactor. MES concentration was varied from 1 mM to 8 mM (0.029 wt% to 0.232 wt%) and its effect on the kinetics of the methane hydrate formation was observed at 277.2 K and 8 MPa. MES drastically improved the kinetics of methane hydrate formation and methane consumption compared to pure water. The increase in the MES concentration dramatically decreased the induction time as well. In addition, the morphology of methane hydrate formation with the MES concentrations was presented. Hydrate nucleation was observed at the interphase of gas/liquid phase followed by the hydrate growth in the upward direction into the gas phase and downward direction into the liquid phase, respectively. Dissociation characteristics and methane recovery were not significantly different from different MES concentrations.

Keywords: Gas hydrates, Promoter, Bio-based surfactant, Methyl ester sulfonate, Solidified natural gas, Morphology

4.2 Introduction

Natural gas hydrates or clathrate hydrates are crystalline solid structures formed by the hydrogen bonding between the water molecules and small gas molecules like methane which is encapsulated inside the cavities of the water molecules under specific operating conditions (lower temperature and high pressure). The hydrogen-bonded water molecules can form the polyhedron cavity as a nomenclature A^xB^y where x and y are the number of A- or B- face that is constructing

the polyhedron. Gas hydrates have three well-known crystal structures - structure I (sI) composed of 46 water molecules (six($5^{12}6^2$) two(5^{12})), structure II (sII) composed of 136 water molecules (eight($5^{12}6^4$)·sixteen(5^{12})), and structure H (sH) composed of 34 water molecules (one($5^{12}6^8$)·two($4^35^66^3$)·three(5^{12})). The structure formed predominantly depends on the size of guest gas molecule (Sloan and Koh, 2008).

Natural gas hydrates are widely distributed in marine sediments and permafrost regions. DOE (US Department of Energy) estimate of the global methane hydrate resource is 20,000 trillion cubic meters, or about 700,000 Tcf (Lou Capitanio *et al.*, 2017; Makogon, 2010; Makogon *et al.*, 2007; Yang *et al.*, 2019).Natural gas hydrates are considered a significant resource for the supply of natural gas in the future (Boswell and Collett, 2011; Demirbas *et al.*, 2016; EIA, 2016). One volume of solid methane hydrate can store about 150-180 volume methane gas at standard temperature and pressure (Sloan Jr, 2003). This characteristic feature of natural gas hydrates is favorable not only for recovering the methane gas from the gas hydrate reserves but also instills considerable interest for using the hydrate technology for transporting and storing natural gas in large quantities (Hao *et al.*, 2008). Gas storage and transportation through hydrate technology is a feasible and most cost-effective option in the small scale and medium distance operations than conventional methods (Chong *et al.*, 2016; Gudmundsson *et al.*, 1994; Li *et al.*, 2016). However, the hydrate-based natural gas storage technology has not yet been commercialized due to slow growth kinetics and low methane uptake (Lang *et al.*, 2010; Veluswamy *et al.*, 2018).

Experimental research has been conducted to improve the kinetics by enhancing the mass transfer between the gas phase and liquid phase during the hydrate formation process. Two approaches have been followed to enhance the contact of gas and liquid either by mechanical methods like stirring or by the application of kinetic additives, e.g. surfactants (Du *et al.*, 2014; Zhang *et al.*, 2007a). However, the former requires significant energy during the formation of the hydrate that is less cost-effective (Shi *et al.*, 2017).

Surfactants have been reported to promote gas hydrate formation effectively due to the solubility enhancement by reducing the interfacial surface tension between the aqueous and gas phases (Ganji *et al.*, 2007; Kumar *et al.*, 2015; Lin *et al.*, 2004; Veluswamy *et al.*, 2015a; Veluswamy *et al.*, 2015b; Wang *et al.*, 2015a; Zhong and

Rogers, 2000). Ganji *et al.* (2007) investigated the effect of different surfactants on methane hydrate formation. They found that anionic surfactants especially sodium dodecyl sulfate (SDS) exhibited the maximum promotion effect on the formation rate and the stability of the hydrates. Okutani *et al.* (2008) studied the effects of alkyl chain length of surfactant on the methane hydrate formation. They reported that a surfactant with a long alkyl chain length was less effective in improving the hydrate formation rate due to the low gas solubility. Effects of SDS on the methane hydrate formation were investigated by Lin *et al.* (2004). Their experimental results showed that the formation rates of methane hydrates could be enhanced with SDS and the SDS concentration of 650 ppm showed the maximum storage capacity of 170V/V. In addition, effects of SDS concentration on the hydrate formation rate was further studied by Zhang *et al.* (2007a), who reported that the formation in the presence of 770 ppm SDS took place faster than 260 ppm SDS.

However, most surfactants studied to improve hydrate formation kinetics are predominantly synthetic surfactants. These surfactants have degradability concerns and sometimes lead to the risk to the environment and humans. Thus, the idea to use bio-based materials came into existence (De *et al.*, 2015). Amino acids have been reported to be alternative promoters to enhance the rate of hydrate formation. Liu *et al.* (2015) reported the kinetic promotion of methane hydrate formation in the presence of different amino acids. They reported that 0.5wt% of l-leucine amino acid was the best promoter for methane hydrate formation. Bhattacharjee *et al.* (2016) reported that the presence of l-histidine significantly enhanced methane hydrate growth kinetics compared to pure water for both experimental and molecular simulation, and the final gas uptake with 1 wt % l-histidine was found to be comparable to that with 1 wt % SDS. Veluswamy *et al.* (2017) examined the effects of three amino acids–tryptophan, histidine, and arginine–on the kinetics of methane hydrate formation. Among the three amino acids studied, tryptophan was the best kinetic promotion for methane hydrate formation in both stirred and unstirred reactor configurations. Beside amino acids, bio-based surfactants have also been reported as the hydrate promoter. The bio-based surfactants are developed from oil like coconut oil, jatropha oil, castor oil, palm oil, and other vegetable resources (Babu *et al.*, 2015; Kumar *et al.*, 2017). These surfactants are candidates to replace the synthetic surfactants in terms of performance

and economic feasibility. In addition, these surfactants have low toxicity and are environmentally friendly. Rogers *et al.* (2003) investigated biosurfactant by-product of microbial activity in seabed on the methane hydrate formation. They found that biosurfactants increased rates of formation from 96% to 288% and decreased induction times from 20% to 71% relative to the system without biosurfactant. Wang *et al.* (2012) found that lignosulfonate biosurfactant produced form paper industry can be used as a promoter on the methane hydrate formation. Lignosulfonates enhanced both the rate of methane formation and the storage capacity by increasing the storage capacity of methane hydrate to 170 V/V when adding 0.5 wt% lignosulfonate. Recently, Chaturvedi *et al.* (2018) synthesized a novel surfactant from castor oil and used as a gas hydrate promoter. They found that using the novel surfactant enhanced the rate of formation, reduced induction time and increased the gas storage capacity. The storage capacity of 96% of the theoretical maximum value (172 V/V) and the induction time of 12 min were obtained for the system with 9000 ppm concentration of the novel surfactant.

From the environmental point of view, using a bio-based surfactant with methane hydrate formation is desirable. However, there are very few literatures available. Therefore, this research presents the performance of methyl ester sulfonate (MES), which is produced from palm oil and is a biodegradable surfactant(Balson *et al.*, 1995; Tobori and Kakui, 2019), as a hydrate promoter for methane hydrate formation. Detailed kinetics of methane hydrate formation and dissociation with MES surfactant will be reported. In addition, for the first time, morphology of methane hydrates in the presence of different MES concentrations during the formation and dissociation experiments will be investigated.

4.3 Experimental

4.3.1 Materials

Ultra-high purity methane (99.99 %) supplied by Linde Public Company, Thailand was used for hydrate formation with distilled deionized water. Methyl ester sulfonate (MES, 99.7%) surfactant was provided by Lion Cooperation, Japan.

4.3.2 Experimental Apparatus for the Hydrate Formation Kinetic Experiment

Figure 4.1 presents the schematic diagram of the gas hydrate experimental setup containing an isothermal/isobaric crystallizer. The hydrates are formed in the high-pressure stainless-steel crystallizer (CR) that can withstand a 20-MPa rating and internal volume of 180 cm^3 shown in Figure 4.1(right side). The supply gas or a reservoir (R) with a volume of 100 cm^3 was connected with the hydrate crystallizer. The crystallizer and reservoir were immersed in the temperature-controlled mixed glycol/water bath. The temperature in the mixed glycol/water bath was controlled by an external refrigerator (Model RC-20, Daeyang, Korea) with an accuracy of ± 1K. The pressure transmitters (Cole Parmer®, model 68073-68074, Singapore) with the range of 0-21 MPa and 0.13 % global error were used to measure the pressure. The temperature in the crystallizer was measured by four K-type thermocouples, located at different positions, as seen in Figure 4.1(right side). The pressure and temperature during experiments was recorded by data logger (AI210, Wisco Industrial Instruments, Thailand) that was connected to a personal computer. All experiments were carried out in the quiescent condition with a fixed amount gas and water in the closed system.

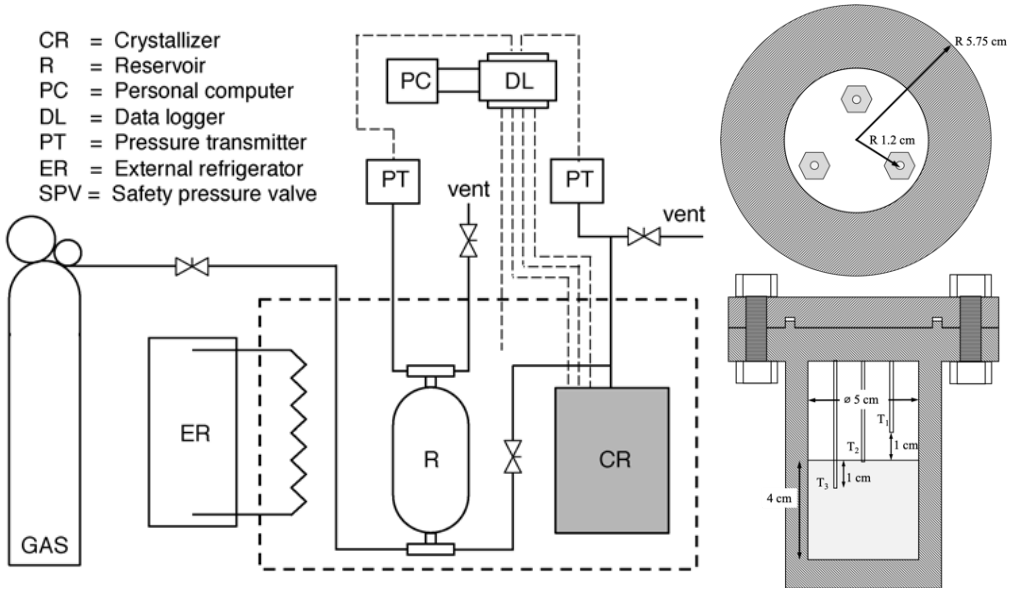

Figure 4.1 Schematic of experimental apparatus (left side) and cross-section of a crystallizer (right side). Modified from Siangsai *et al.* (2015).

4.3.3 Experimental Apparatus for the Morphology of Hydrate Formation and Dissociation

A detailed description of the experimental apparatus is available in the study by Veluswamy *et al.* (2016a); Veluswamy *et al.* (2016b). The crystallizer column is made from transparent sapphire supported by two stainless steel lids. The crystallizer column has an inner diameter of 30 mm, height of 80 mm, and was designed to withstand 10 MPa pressure. The temperature and pressure in the reactor were measured by an Omega constantan thermocouple with 0.1 K error and Rosemount pressure transmitter with 0.1% error in the range of 0−20 MPa, respectively. The temperature in the water bath was controlled by Polyscience SD15R circulator. Temperature and pressure during the hydrate formation and dissociation were recorded every 20 s by using a data acquisition system supplied by National Instruments. The images of hydrate formation and dissociation were captured every 20 s by using Stereoscopic zoom microscope SMZ1000 from Nikon coupled with Nikon Digital Sight (DS-Fi1) camera and Optika Pro HDMI camera.

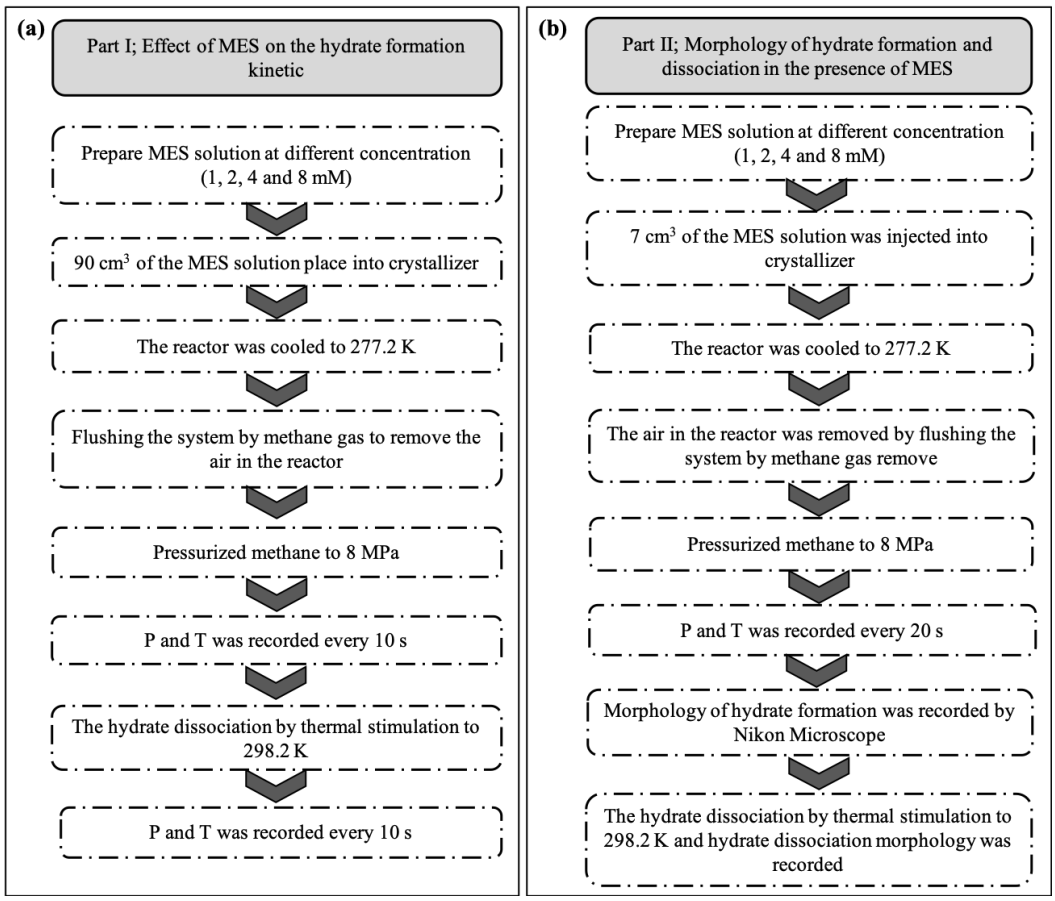

Figure 4.2 Experimental procedure (a) for the kinetic study and (b) for the morphology study.

4.3.4 Hydrate Formation

Experimental procedures for kinetic and morphology studies are provided as in Figure 4.2a and 4.2b respectively. MES concentrations - 1, 2, 4 and 8 mM (0.029, 0.058, 0.116 and 0.232 wt%) were prepared for both kinetic investigation and morphology studies. As seen from Figure 4.2, the procedure is similar for both studies except for the sample volumes. 90 cm^3 of the solution was added into the crystallizer for kinetic study whereas 7 cm^3 of the solution was taken into the transparent sapphire crystallizer for all morphological experiments. The crystallizer was pressurized to 0.5 MPa by methane gas and depressurized to atmospheric pressure twice to ensure no more air remains in the system. The methane gas was then introduced to the hydrate crystallizer at the desired experimental condition. The experimental condition is set at 8 MPa and 277.2 K. The pressure and temperature data

were recorded every 10 s for the kinetic study and 20 s for the morphology study by the data loggers. During the hydrate formation, the pressure in the crystallizer decreased due to the conversion of methane gas to methane hydrates. As the pressure in the crystallizer decreased, the temperature in the system increased since the reaction is exothermic in nature. The experiment was continued until there was no further pressure drop observed for at least 1 h (stable pressure data recorded during this time). The pressure and temperature data were used to calculate the moles of methane consumed by equation 4.1 (Babu *et al.*, 2013; Veluswamy and Linga, 2013);

$$\Delta n_{H,\downarrow} = n_{H,0} - n_{H,t} = \left(\frac{PV}{zRT}\right)_{G,0} - \left(\frac{PV}{zRT}\right)_{G,t} \quad (4.1)$$

where $\Delta n_{H,\downarrow}$ is the number of moles of gas consumed for hydrate formation at the end of experiment. $n_{H,0}$ is the number of moles of gas at time zero and $n_{H,t}$ is the number of moles of the gas at time *t*. Subscripts of *G,0* and *G,t* represent the gas phase at time zero and time *t*, respectively. *P* and *T* are the pressure and temperature in the system, *V* is the volume of gas phase in the crystallizer, *R* is the universal gas constant and *z* is the compressibility factor calculated by Pitzer's correlation (Smith *et al.*, 2005). Hydrate yield is defined as the percentage conversion of water to hydrates with equation 4.2 (Veluswamy and Linga, 2013);

$$\text{Hydrate yield (\%)} = \frac{\Delta n_{H,\downarrow} \times \text{Hydration number}}{n_{H_2O}} \times 100 \quad (4.2)$$

where n_{H_2O} is the number of moles of water in the system. The hydration number is the number of water molecules required per gas molecule to form the hydrate structure. For sI hydrate structure formed in our experiments, this value is considered as 5.75 (Mech *et al.*, 2016; Sloan and Koh, 2008). The normalized initial hydrate formation rate (NR_t) for the first t minutes from the start of hydrate nucleation was calculated by equation 4.3 (Pandey *et al.*, 2018; Veluswamy *et al.*, 2016a; Veluswamy and Linga, 2013).

$$NR_t = \frac{R_t}{V_{water}} \tag{4.3}$$

where V_{water} is the volume of water (m^3) taken in the reactor, and R_t is the rate of hydrate growth (mmol/min) calculated by fitting the average gas uptake due to hydrate growth at each experimental condition versus time for the first t minutes after the induction time or first hydrate nucleation, using the least squares method. The time period of t minutes that gave the best fit was selected for rate quantification based on the hydrate gas uptake profiles for all experiments.

4.3.4 Hydrate Dissociation

After the completion of methane hydrate formation experiment, the methane hydrate was dissociated by thermal stimulation. The temperature was increased from the experimental temperature of 277.2 K to the desired dissociation temperature (298.2 K). The start of the temperature rise was considered as time zero for the hydrate dissociation experiments. When the temperature in the crystallizer crosses the hydrate phase equilibrium, the methane hydrate starts to dissociate and continues to dissociate till it reaches set dissociation temperature of 298.2 K. Equilibrium pressure of methane hydrate at 298.2 K is 44.2 MPa (Gayet *et al.*, 2005). Thus, at the dissociation temperature (298.2 K), all hydrates formed are completely dissociated. The gas released from the hydrates during the dissociation was measured by the pressure transducer. The experiments were stopped when the pressure was constant at the set dissociation temperature. At any given time, the total moles of gas in the system equal to the moles of gas at time zero. The moles of methane released from the hydrate at any time during the hydrate dissociation were calculated by equation 4.4. This equation is the negative of the equation 1 detailed above as initially there were fewer moles of gas, and with the progress in dissociation number of moles of gas increased till the completion.

$$\Delta n_{H,\uparrow} = n_{H,t} - n_{H,0} = \left(\frac{PV}{zRT}\right)_{G,t} - \left(\frac{PV}{zRT}\right)_{G,0} \tag{4.4}$$

The percentage of methane recovery is calculated by Equation 4.5 (Babu *et al.*, 2013; Linga *et al.*, 2009)

$$\%\text{methane recovery} = \frac{(\Delta n_{H,\uparrow})}{(\Delta n_{H,\downarrow})_{End}} \times 100 \tag{4.5}$$

where $\Delta n_{H,\uparrow}$ is the number of moles of released gas from hydrates during the hydrate dissociation at any given time. $(\Delta n_{H,\downarrow})_{End}$ is the number of moles of gas consumption for hydrate formation at the end of experiments.

4.4 Results and Discussion

First, the experiments were performed using only water without any surfactant in order to understand the effect of water on the kinetics of methane hydrate formation (akin to a control experiment). The methane hydrates were formed and dissociated as mentioned in the procedure outlined earlier. The hydrate formation experiment in fresh water was performed at 277.2 K and 8 MPa. After this, experiments in the presence of 1 to 8 mM MES surfactant solution was subjected to the methane hydrate formation and dissociation. This range of MES concentration was chosen as it covers above and below its critical micelle concentration (CMC), which is 4 mM (Roberts *et al.*, 2008). Each experiment was performed at least three times to ensure the repeatability of observed results. Table 4.1 comprehensively summarizes the experimental observations for all experiments conducted with water and different concentrations of MES solution. This table also includes the induction time, hydrate yield and total gas uptake achieved at the end of the experiment.

Table 4.1. Hydrate formation experimental conditions at 277.2 K and 8 MPa

No. Exp	*Induction Time (min)	% Hydrate Yield	Methane Consumption (mole CH_4/H_2O)	**Rate of Hydrate Formation (mol of methane/min/m^3 of water)
		1 mM MES		
B-1	161.33	68.46	0.1191	50.53 (R^2 = 0.93)
B-2	139.38	71.70	0.1247	53.33 (R^2 = 0.96)
B-3	133.50	60.21	0.1047	51.50 (R^2 = 0.95)
		2 mM MES		
C-1	90.83	70.17	0.1220	56.50 (R^2 = 0.96)
C-2	83.83	74.99	0.1304	61.33 (R^2 = 0.95)
C-3	92.17	74.81	0.1301	55.33 (R^2 = 0.97)
		4 mM MES		
D-1	51.17	75.06	0.1305	71.33 (R^2 = 0.96)
D-2	41.67	75.57	0.1314	70.00 (R^2 = 0.98)
D-3	68.33	80.86	0.1406	74.50 (R^2 = 0.96)
		8 mM MES		
D-1	40.17	84.63	0.1472	89.50 (R^2 = 0.97)
D-2	35.50	85.20	0.1482	93.33 (R^2 = 0.96)
D-3	47.00	84.38	0.1467	85.44 (R^2 = 0.98)

Note: No hydrate formation 48 hr after starting experiment for three experiments (A1-A3) of pure water

* Induction time is taken for fist hydrate nucleation.

** Rate of hydrate formation calculated for 10 min from induction time

As seen from Table 4.1, the pure water system does not show any evidence of hydrate formation at this condition after 48 h. All experiments were performed at 8 MPa and 277.2 K, thus a pressure driving force about 4.2 MPa (Nakamura *et al.*, 2003) exists at the experimental condition. Though there is no significant gas uptake during

the formation experiment, it is plausible that hydrates could form on the interface of gas-solution like a thin film which prevents the methane gas diffusion to the liquid phase for further hydrate growth (Fandiño and Ruffine, 2014).

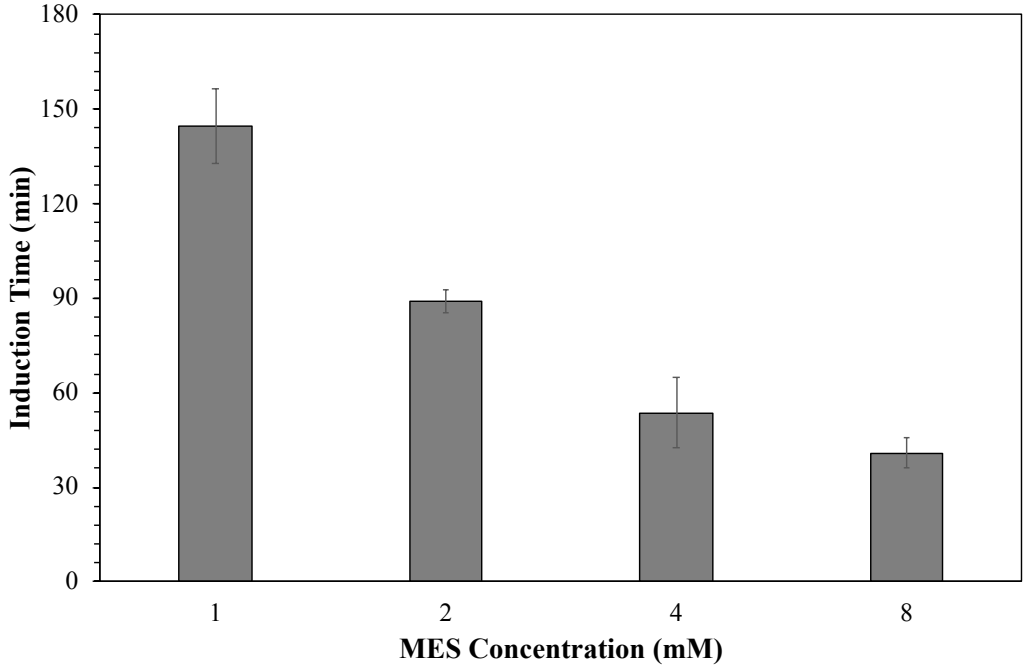

Figure 4.3 Effect of MES concentration on induction time at 277.2 K and 8 MPa.

It can be observed from Table 4.1 that the presence of MES enhances the hydrate formation. The induction time for methane hydrate formation is an important parameter for applying the hydrate technology in gas storage and transportation application. Induction time is the time where the first hydrate nucleus forms and indicated by a sudden increase in methane uptake and a spike of temperature in the first step. For natural gas storage and transportation applications, a short induction time is essential. The effect of MES concentration on the induction time is shown in Figure 4.3. It can be clearly seen from Figure 4.3 that the presence of MES improves the first hydrate nucleation compared with the pure water system. This could be attributed to the presence of surfactant decreases the interfacial tension between gas and liquid phases as resulted in the methane gas ease to diffuse into the solution and easily convert to the hydrate nucleation (Wang *et al.*, 2015a). Moreover, it can be observed that the induction time decreases with the increase in the MES concentration which

corresponds to the decrease in the surface tension with the increase in the surfactant concentration until it reaches its CMC. The induction time shows the similar trend reported in the literature with the presence of different surfactants (Chaturvedi *et al.*, 2018; Ganji *et al.*, 2007; Kakati *et al.*, 2016; keshavarz Moraveji *et al.*, 2017; Wang *et al.*, 2015a). Furthermore, the induction time does not lower significantly when the MES concentration is higher than the CMC. This could be attributed that the increase in surfactant concentration above CMC did not affect the surface tension between the gas and liquid phase. As such, the induction time of the hydrate formation above CMC is similar to the induction at CMC. The result in this work corresponds with the report of Zhong and Rogers (2000) who reported that there was a decrease in the induction time observed with the increase in the SDS concentration during the hydrate formation until the CMC of SDS. However, when SDS concentration was above the CMC, it did not lead to further decrease in the induction time.

The gas hydrate formation kinetics is also considered as an important factor for gas storage and transport applications (Sun *et al.*, 2003; Zhong and Rogers, 2000). Figure 4.4 presents the comparative NR_{10} at different MES concentrations. It can be clearly observed that the presence of MES improves the hydrate formation kinetics. Du *et al.* (2014) reported that the kinetics of hydrate formation was enhanced in the presence of anionic surfactant because of the promotion of methane hydrate nucleation via heterogeneous nucleation from the surfactant crystals (foreign particles). The energy barrier to form the hydrate nucleation was also believed to reduce and promote the hydrate formation by adsorption of the surfactant on the hydrate nuclei Zhang *et al.* (2007a). Moreover, NR_{10} increases with the increase in the concentration of MES. Although there is only a slight increase in NR_{10} (11.45%) when the MES concentration increases from 1 to 2 mM, the increase in the NR_{10} is more pronounced when the concentration is changed from 1 to 4 and 8 mM, respectively.

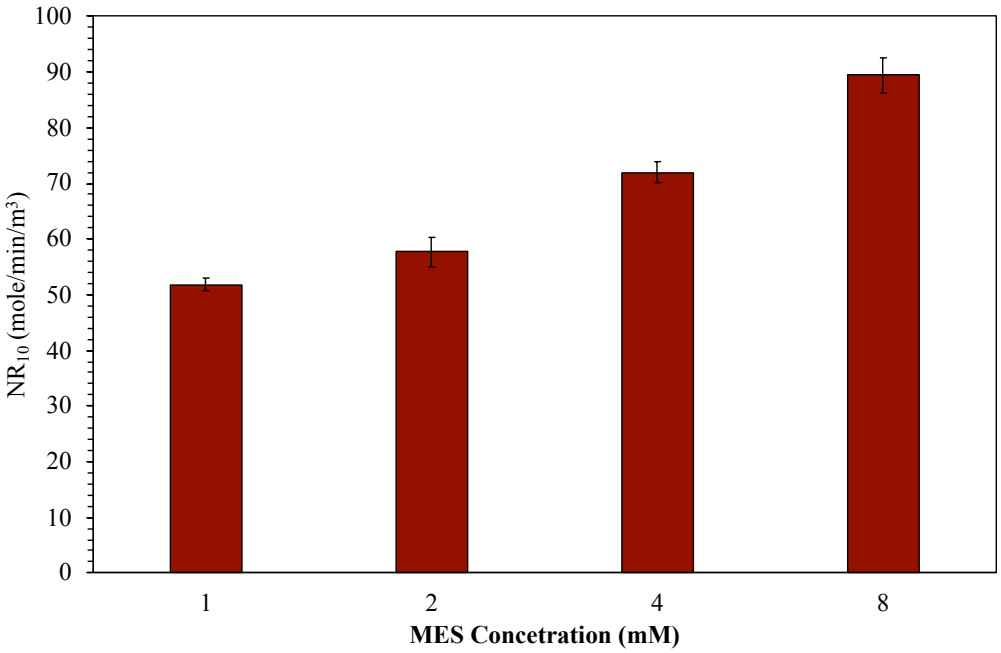

Figure 4.4 Effect of MES concentration on NR_{10} at 277.2 K and 8 MPa.

The gas uptakes during methane hydrate formation along with temperature profiles for the experiment conducted in 1 and 8 mM MES solution are shown in Figure 4.5. The methane uptakes and temperature profiles in 2 and 4 mM MES solution was presented in Figure S4.1 in Supporting Information. It can be seen from Figure 4.5 that there are several temperature spikes indicating the occurrence of new nucleation. The several temperature spikes are a result of the multiple hydrate nucleation as reported by Mekala *et al.* (2014); Veluswamy *et al.* (2016c) and Yang *et al.* (2016). The first hydrate nucleation shows the highest increase in the temperature as the result from the free energy required to overcome the activation barrier of initiate nucleation is the highest (Khurana *et al.*, 2017). Additionally, it can be seen that the temperature spikes in each step after first hydrate nucleation corresponds to the increase in the gas uptake (slope change in the gas uptake). Thus, it can be deduced that the multiple nucleation increases methane uptake and changes the methane uptake rate as well. After that, the methane gas is consumed to grow the hydrates until reaching the plateau inferring that no more gas is allowed to form the hydrate with free water.

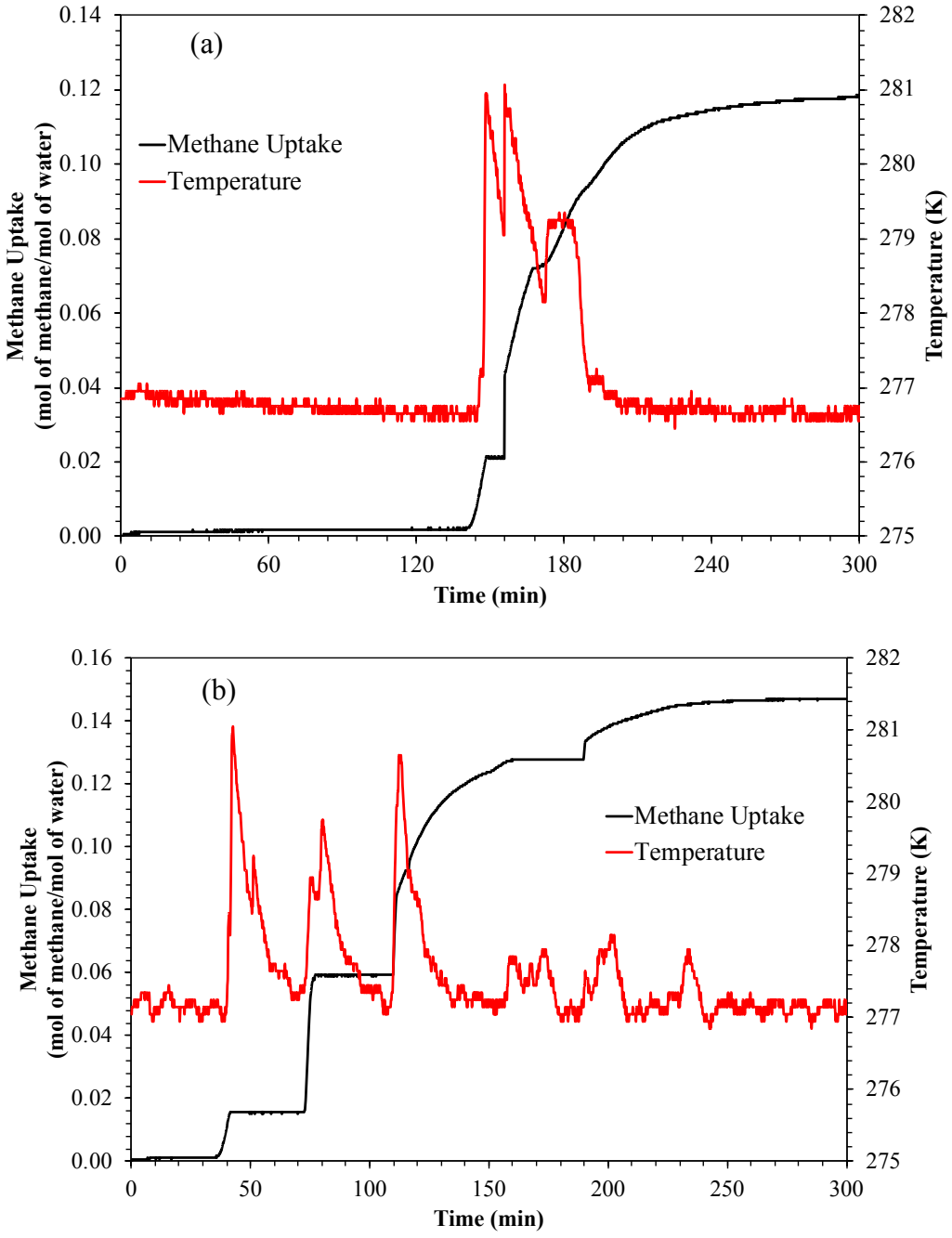

Figure 4.5 Methane uptake and temperature profiles in the presence of (a) 1 mM MES (Exp B-2 in Table 4.1) and (b) 8 mM MES (Exp E-2 in Table 4.1).

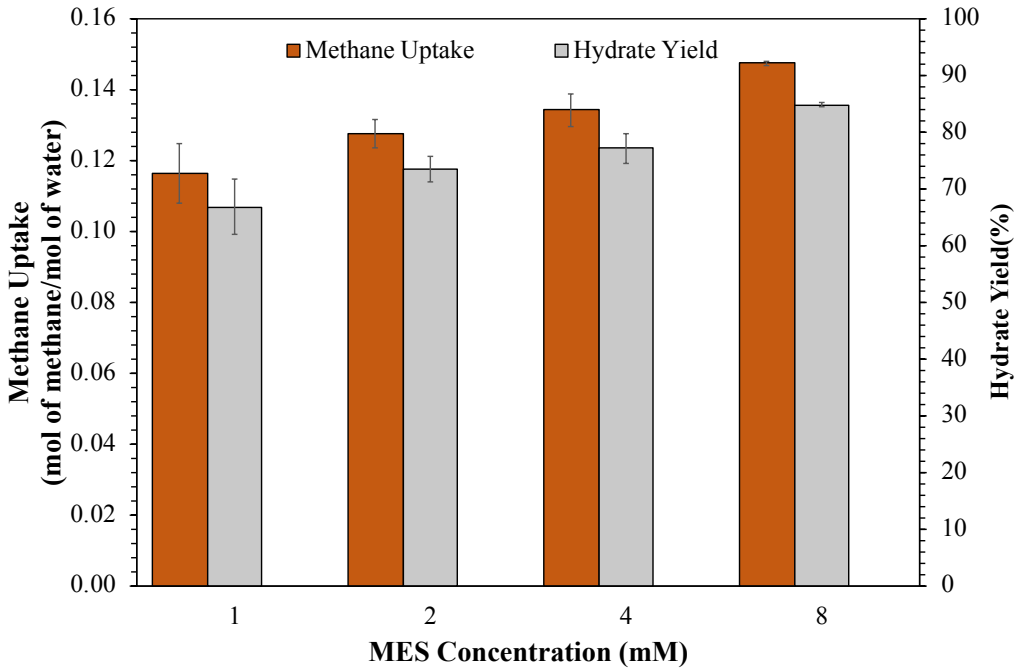

Figure 4.6 Effect of MES concentration on methane uptake and hydrate yield at 277.2 K and 8 MPa.

The methane gas uptake and hydrate yield after the completion of the hydrate formation are shown in Figure 4.6. It can be observed that both gas uptake and hydrate yield significantly increase with the presence of MES regardless of concentration. It can be deduced that the presence of the surfactant decreases the mass transfer between the gas and liquid phases resulting in the hydrate formation. In addition, the methane uptake and hydrate yield slightly increase with the increase in the MES concentration from 1 to 8 mM. However, the increase in the final gas consumption and hydrate yield of the system with the surfactant concentration above CMC, which is 8mM, is negligible. As such, the results are consistent with the study conducted by (Ando *et al.*, 2012) and Lin *et al.* (2004). Ando *et al.* (2012) showed that increasing lithium dodecyl sulfate (LDS) and dodecylbenzene sulfonic acid (DBSA) higher than their CMCs did not affect the average rate of hydrate formation nor the final gas consumption. They concluded that the micelle formation above the CMC neither promoted nor retarded the hydrate formation. This is also the case when SDS was used by Lin *et al.* (2004).

Table 4.2 Summary of methane uptake in the presence of different surfactants in the methane hydrate formation*

System No.	Surfactant	Pressure (MPa)	Temperature (K)	Methane Uptake (mol of gas/mol of water)	Reference
1	SDS	8.3	276.2	0.1438	Ganji *et al.* (2007)
	LABS	8.3	276.2	0.1247	
	CTAB	8.3	276.2	0.1486	
	ENP	8.3	276.2	0.1319	
2	SDS	6.6	276.2	0.1530	Lin *et al.* (2004)
3	SDS	8.0	277.2	0.1520	Siangsai *et al.* (2018)
4	SDS	7.5	276.1	0.0432	Mech *et al.* (2016)
5	DTAC	15.0	274.0	0.0482	Du *et al.* (2014)
	DAH	15.0	274.0	0.1044	
	DN_2Cl	15.0	274.0	0.137	
This work	MES	8.0	277.2	0.1474	

*It should be noted this table presents the maximum methane uptake reported in each of the reference article.

For comparison purpose, the methane uptake from this work along with those from literature using synthetic surfactants are presented in Table 4.2. The table clearly shows that the methane uptake from the hydrate formation at 277.2 K and 8.0 MPa with bio-based surfactant, 8 mM MES, 0.1474 mol of gas/mol of water, is comparable or higher than using the synthetic surfactants. It has been found that under similar or comparable experimental conditions (Ganji *et al.*, 2007; Mech *et al.*, 2016; Siangsai *et al.*, 2018), the methane uptake in the hydrate formed using MES surfactant as the promoter is about the same with the use of SDS.

The decomposition study on methane hydrates was performed in order to understand the dissociation behavior of the stored methane from gas hydrates. Thermal stimulation method was used to study the decomposition by increasing from 277.2 to 298.2 K. After the hydrate formation complete of each experiment, the pressure in the reactor decreases to 6.2-6.7 MPa (from 8 MPa). At 6.2 - 6.5 MP, the equilibrium temperature of the methane/water system was obtained through interpolation of available experimental data provided by Nakamura *et al.* (2003) to be approximately 280 - 282 K. Thus, the hydrates start to dissociate beyond this temperature under the considered experimental conditions. Figure 4.7 shows the typical pressure profiles increasing along with the respective temperature profiles observed during the hydrate dissociation from the hydrates formed in the experiment A-1 (1 mM MES) and experiment C-1 (4 mM MES). For better understanding, the pressure plotted in the figure excludes the initial pressure before the dissociation so the pressure in the profiles starts from zero. In Figure 4.7, the pressure and the temperature profiles of both experiments are observed to be similar for approximately the first 20 min from the start of hydrate dissociation, and the temperature inside the reactor remains below the equilibrium temperature of 280-282 K. The increase in the pressure during the first 20 min after the start of dissociation is the result of the thermal expansion of the gas in the system not the hydrate dissociation. After the temperature gradually increases and crosses the equilibrium temperature, the methane hydrate starts to dissociate. It can be seen from the figure that there is a sharp increase in the pressure profile. This can be correlated to the temperature increase observed in the reactor. From Figures 7a and 7b, the final pressure of experiment C-1 is higher than that of experiment A-1. It can be attributed to the higher methane uptake of experiment C-1 than experiment A-1 (Table 4.1), so that the gas released the hydrates formed from experiment C-1 is higher. The time for the completion of hydrate dissociation is about 120 min. In addition, it can be clearly seen that the pressure and temperature profiles from the two experiments have the same trend. The final methane recovery in the presence MES is higher than 95 %, as shown in Figure S4.2 in Supporting Information. Nevertheless, methane gas still remains dissolved in the solution, and it is not recoverable, as reported by Linga *et al.* (2009). In order to observe the effects of MES on the dissociation kinetics, the normalized gas recovery profiles which take the different

amount of methane in the hydrates into account are presented in Figure S3 in Supporting formation. From Figure S3, it can observe that the dissociation kinetics which observed from the slope of profiled slightly increase with the increase in MES the concentration of MES. This result corresponds with the report of Ganji *et al.* (2007)and Lin *et al.* (2004).

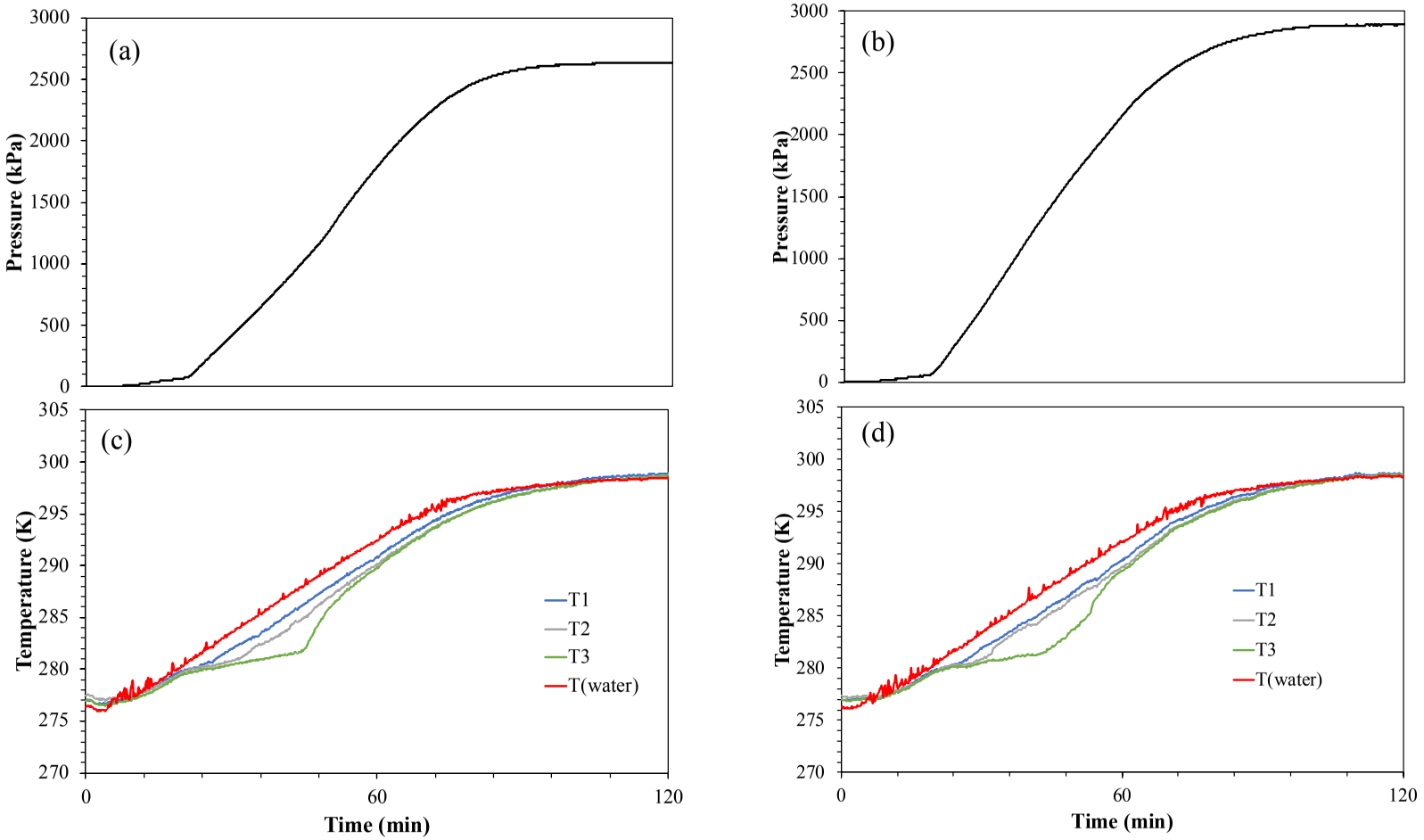

Figure 4.7 Pressure profiles during hydrate dissociation for (a) A-1 and (b) C-1; temperature profiles of the reactor and water during hydrate dissociation for (c) A-1 and (d) C-1. Experiment A-1 and C-1 conducted at 6.7 and 6.2 MPa, respectively.

The morphology during the methane hydration formation with different MES concentrations was also investigated in this work. Each experiment was repeated at least twice to ensure its reproducibility. The induction time, methane uptake achieved at the end of hydrate formation and NR_{10} for morphology experiments using the small-scale reactor column (7 cm^3) are represented in Table S4.1 in Supporting Information. All experiments were conducted at 277.2 K and 8 MPa. The trend of induction time, methane uptake achieved at the end of hydrate formation and NR_{10} in the morphology of hydrate formation experiment corresponds with the experiment of hydrate formation kinetics. However, these values in the morphology study are different from the hydrate formation kinetic experiments due to the difference in the reactor size and the amount of methane gas involved. Only morphology experiments with 2, 4, and 8 mM are presented here. The three concentrations cover those below CMC (2 mM), at CMC (4mM) and above CMC (8 mM) of MES surfactant. The hydrate morphology of 1 mM MES are also presented in Figure S4.3 in Supporting Information.

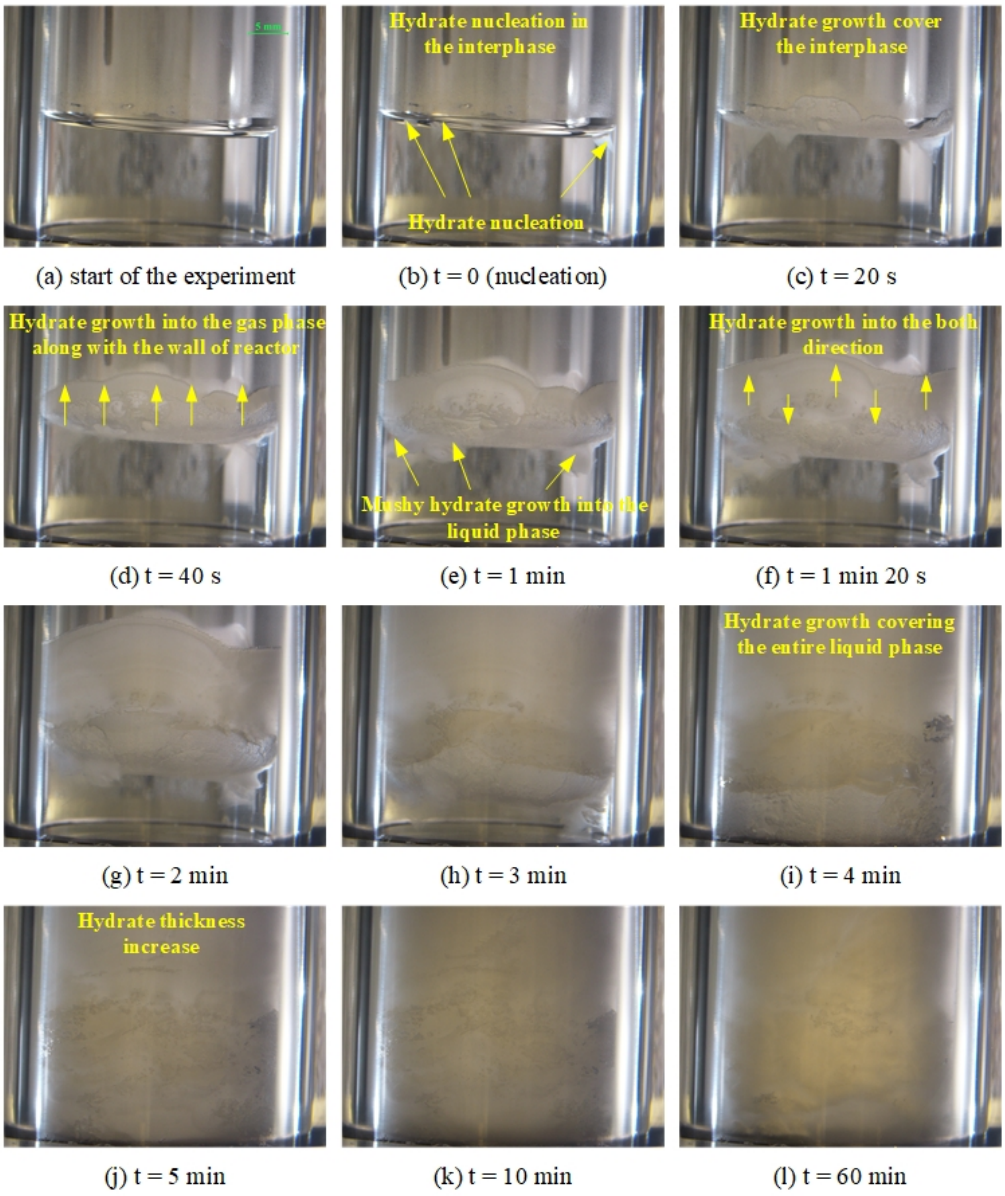

Figure 4.8 (a-l) Morphology at different time lapses during methane hydrate formation in the presence of 2 mM MES at 8.0 MPa and 277.2 K.

Figure 4.8 represents the series of the morphology observations during hydrate nucleation and growth for a system having 2 mM MES conducted at 8 MPa and 277.2 K. Figure 4.8a shows the start of the experiment along with the gas phase and thermocouple, and the interphase between gas and liquid phase is clearly visible. Figure 4.8b presents the hydrate nucleation along with at the gas/liquid interphase. The hydrate nucleation at the interface is commonly observed for the quiescent systems because the gas/liquid interphase offers the high contract area between the gas and

liquid phases. Figure 4.8c (20 s after the start of the experiment) shows hydrate growth covers the gas/liquid interphase along with the wall of the reactor. At 40 s and 1 min after the hydrate nucleation, Figures 4.8d and 4.8e, the cloud of hydrates along the wall of the reactor column can be observed in the direction toward the gas phase. This could be attributed to the surfactant concentration on the wall of the reactor column is higher than the gas-liquid interphase (due to adsorption of surfactant at wall of reactor column) as the result of transformation of the surfactant solution via the porous hydrates by capillary force (Gayet *et al.*, 2005; Zhang *et al.*, 2007b). The gas molecule in the gas phase easily converts available water to hydrate; hence, the hydrates grow along the wall of the reactor column. Approximately 1 min 20 s after the hydrate nucleation (Figure 4.8f), the hydrates grow both upward and downward directions. Distinct separation of the hydrate layers between the bulk solution and the gaseous phase can be seen. Figures 4.8g-4.8i (after 2 - 4 min after the hydrate nucleation) reveal that the hydrates continue to grow along the wall of the reactor both upwardly and downwardly. During the hydrate growth in the upward and downward directions, Figure 4.8g-4.8i (after 2 - 4 min after the start of the hydrate nucleation), the growth of mushy hydrates occurring between the hydrate layers. The figures also demonstrate that the thickness of the hydrate layers increase and grow predominantly in the downward direction and later in the upward direction. These phenomena result in the change from mushy hydrates to dense hydrates (Yoslim *et al.*, 2010). In Figure 4.8j (5 min after the hydrate nucleation), dense hydrates completely envelop the bulk solution, and the separation of hydrates and the mushy hydrate cannot be observed. However, the vein-like formations indicating the thickening of hydrates can be observed. This thickening of hydrates can be observed after 5 min from the hydrate nucleation (Figure 4.8j). There is no significant change in the morphology of the hydrates 10 to 60 min from the hydrate nucleation, Figures 4.8k-8l.

Next, the concentration of MES is changed to its CMC, 4 mM, in the formation carried out at 8.0 MPa and 277.2 K, and the results are in Figure 4.9. Figure 4.9a shows the clear interphase between gas and solution phases. The nucleation at the gas/liquid interphase can be observed in Figure 4.9b, which is similar to the case with 2 mM MES. At 20 s from the hydrate nucleation, as shown in Figure 4.9c, the hydrate grows along the wall of the reactor in the upward direction, and the cloudy hydrate along

with the wall of the reactor column on the gas phase above the bulk hydrate can be observed. The hydrate growth continues in the upward direction along with the wall of the reactor column until 1 min after the hydrate nucleation, as seen in Figures 4.9c-4.9e. At 1 min 20 s after the hydrate nucleation, Figure 4.9f, the hydrate growth is in both directions from the gas/liquid interphase. The hydrates continue to grow along the wall of the reactor both upward and downward directions, Figures 4.9g-4.9h, and completely envelop the bulk solution, around 4 min into the experiment (Figure 4.9i). During the hydrate growth upwardly and downwardly, there is an indication of the porous nature of the formed hydrates unlike the vein-like morphology observed with 2 mM MES. This leads to the appearance of mushy or cloudy hydrates in the bulk solution and middle of bulk hydrate (interphase of the starting experiment). After 5 min from the hydrate nucleation, the thickening of hydrates can be observed in Figure 4.9j. Figure 4.9k (after 10 min of the start of hydrate nucleation) clearly shows that the thickening of the hydrates increases. After 10 min from the start of the hydrate nucleation to the end of the experiment, as shown in Figures 4.9k-4.9l, the hardened hydrate crystals inside the reactor column can be observed with no further significant morphological changes.

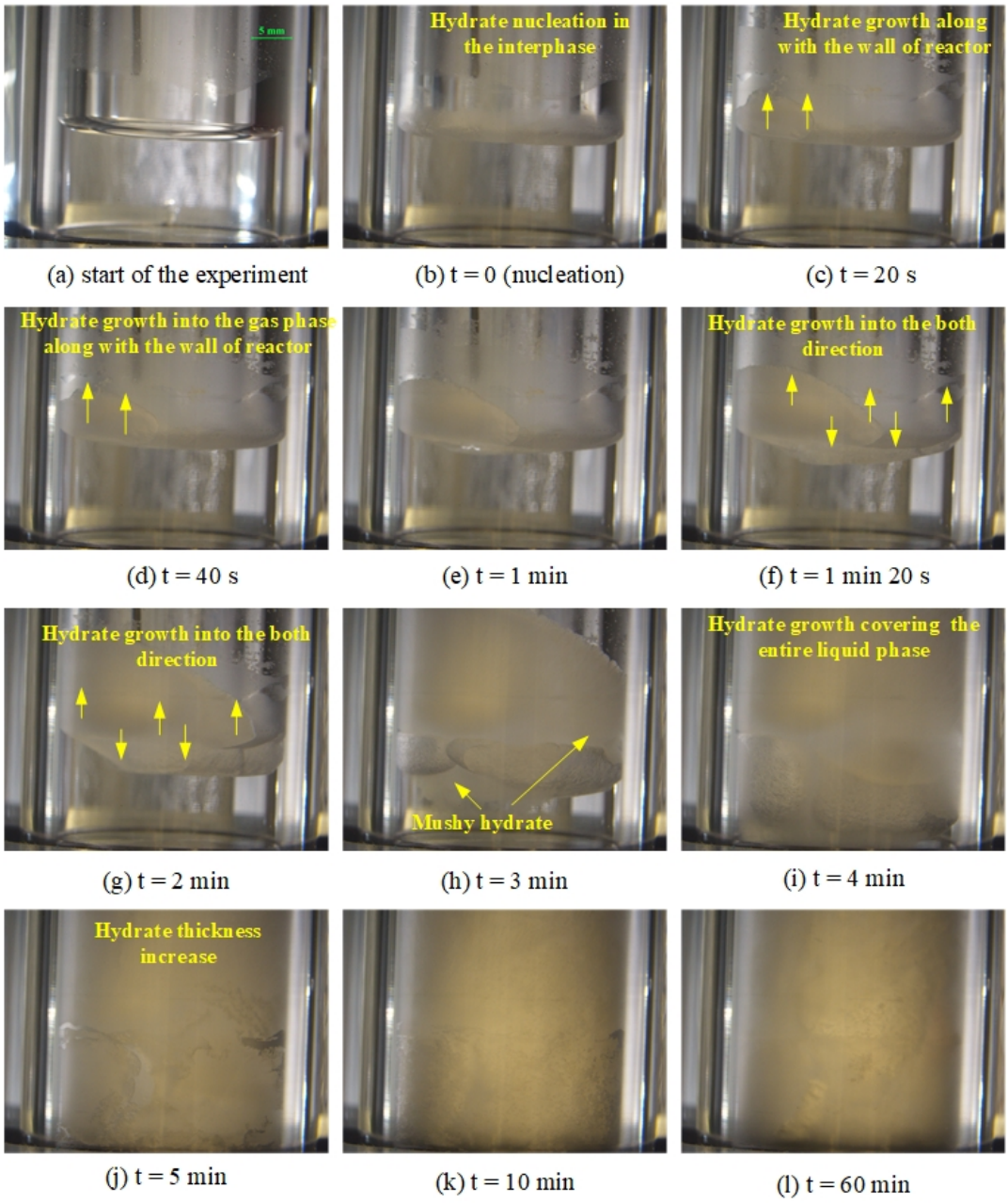

Figure 4.9 (a-l) Morphology at different time lapses during methane hydrate formation in the presence of 4 mM MES at 8.0 MPa and 277.2 K.

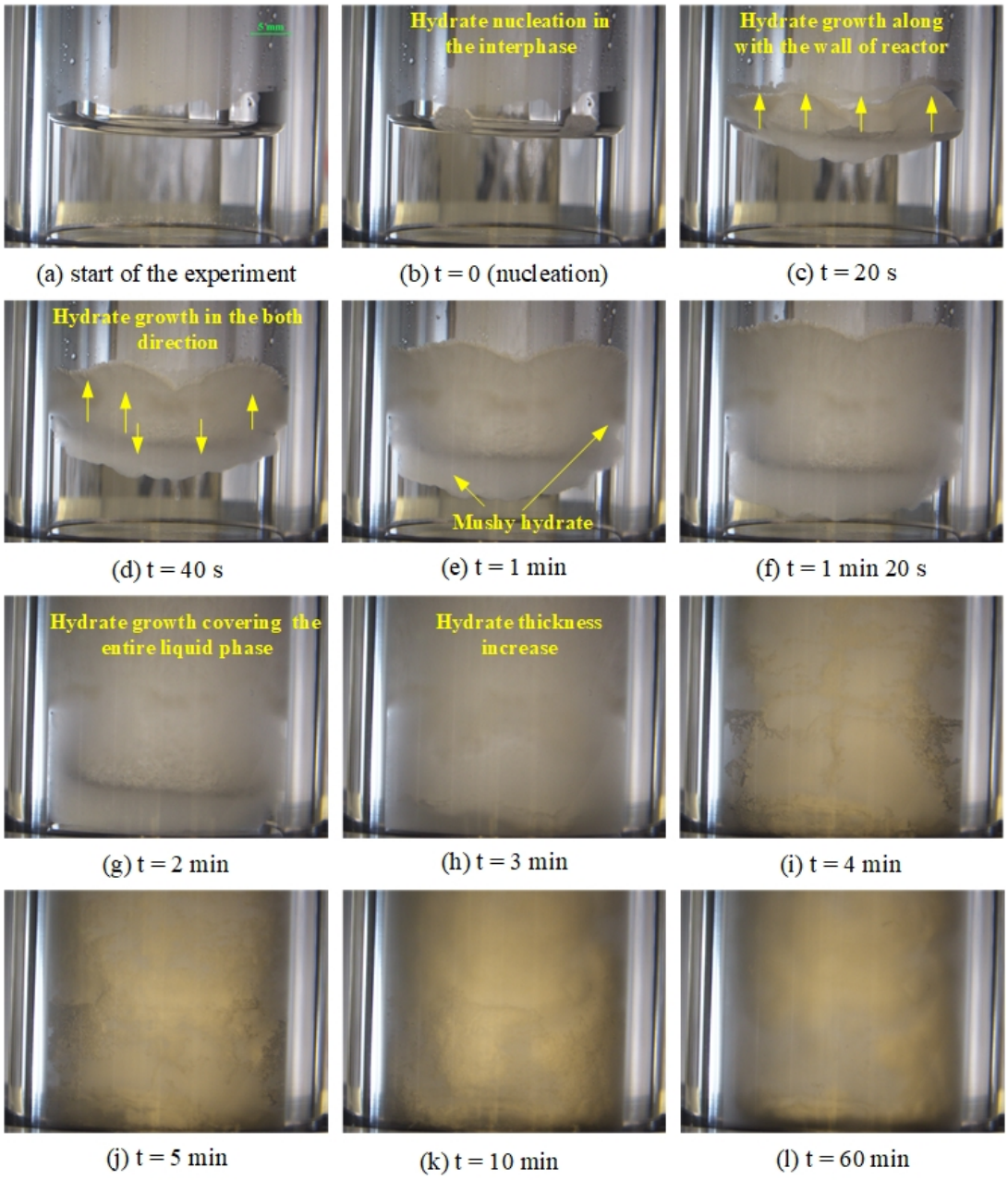

Figure 4.10 (a-l) Morphology at different time lapses during methane hydrate formation in the presence of 8 mM MES at 8.0 MPa and 277.2 K.

The MES concentration is further increased to 8 mM, which is higher than its CMC, at the same temperature and pressure. Figure 4.10 presents the series of morphology observations from the start of the experiment to hydrate nucleation and growth. Figure 4.10a represents the start of the experiment inside the reactor column before the hydrate formation. Figure 4.10b represents the hydrate nucleation which

takes place at the gas/liquid interphase on the wall of the reactor column which is similar to the previous two experiments. After 40 s (Figure 4.10c), the hydrates grow along with the wall of the reactor both upward (gas phase) and downward (bulk solution) directions. Due to the higher concentration of MES, this stage occurs quickly in comparison to the lower concentrations presented above. During the hydrate growth in the downward direction, Figures 4.10d-4.10g, the thickness of bulk hydrates increases in the downward direction and can observe the form of the cloudy hydrates in the downward direction, which similar with the hydrate growth of the system of MES at CMC, 4mM. As hydrate growth proceeds, the bulk solution is completely covered with cloudy hydrates within 2 min from the hydrate nucleation (Figure 4.10 g). Thus, the presence of 8 mM MES resulted in the fastest hydrate formation which corresponds with the results in the kinetic part. At 3 min after the hydrate nucleation, Figure 4.10h, the thickening of hydrates can be observed. At 4 min after hydrate nucleation, the vein-like channels are observed in Figure 11i. There is no significant change in the morphology after 4 min, Figure 4.11i, to 60 min of the hydrate nucleation. Form the Figure 4.8-4.10, the hydrates morphology during the hydrate formation with the presence of 2, 4, and 8 mM shows similar hydrate growth pattern. However, the hydrate formation morphology was studied with repeat runs for all four systems, and the video of the hydrate formation with different concentration has been presented in the Supporting Information VS 4.1-4.4.

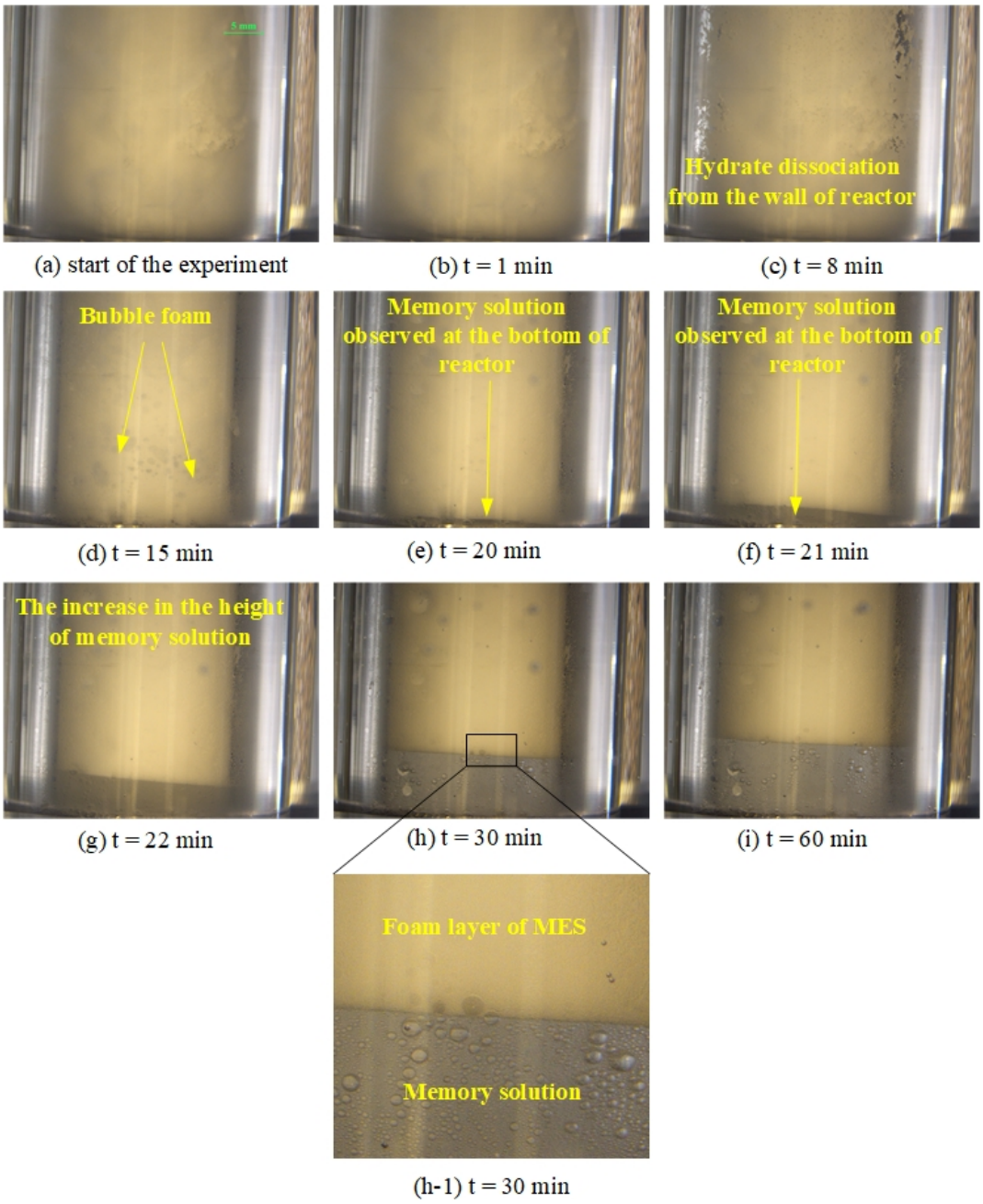

Figure 4.11 (a-i) Morphology at different time of methane hydrate dissociation in the presence of 4 mM MES.

The morphology study of the hydrate dissociation with the presence of different MES concentration shows the same pattern. Therefore, this section will discuss the morphology of hydrates during hydrate dissociation by using the

experiment with 4 mM MES. The hydrate morphology with other MES concentrations are in Supporting Information (Figure S4.5-S4.7). Figure 4.11 represents the series of morphology observations during hydrate dissociation from the hydrates formed with 4 mM. Figure 4.11a shows the morphology of hydrates at the start of hydrate dissociation (as observed at the end of formation experiment). The hydrates are observed to completely cover the reactor column after the completion of hydrate formation. At 8 min after the start of hydrate dissociation (Figure 4.11c), the thick hydrate layer decomposes along the wall of the reactor, which is from the heat transfer from cooling water. As the heat transfers into the reactor causing the temperature inside the reactor to increase, methane in the hydrate cage gradually releases. After 15 min from the start of hydrate dissociation, Figure 4.11d, the morphology largely changes, it can be persisted with the hydrate was dissociated due to it can be observed bubbles foam inside the reactor as results from the recovered gas trapped inside the MES surfactant solution. The thickness of the hydrates in the reactor column gradually decreases indicating that the hydrates gradually decompose. After 20 min from the start of the hydrate dissociation, Figure 4.11e, there is liquid solution at the bottom of the reactor indicating substantial hydrate dissociation. The height of the liquid solution increases steadily over the next 60 min (Figures 4.11f−4.11i) as the dissociation proceeds, and gas bubbles can also be observed inside the aqueous solution, Figures 4.11h-4.11i. To clarify the layer of foam during the hydrate dissociation, Figure 4.11h-1 presents the zoomed area between the foam layer and memory solution. After the completion of the hydrate dissociation, it can also be observed that the entire volume of the reactor column above the solution (two-thirds of the picture) is covered with foam.

Hydrate dissociation by thermal stimulation methods present the bubble foam after the completion of hydrate dissociation. The undesirable property of surfactant for using as the hydrate promoter in the gas storage technology by hydrate technology is the generation of an excessive amount of foam during the hydrate dissociation which has been documented well in literature (Rahimi Mofrad *et al.*, 2016; Wang *et al.*, 2016; Wang *et al.*, 2015b). In order to decrease of foam problem during the hydrate dissociation using MES, the mixture of anionic surfactant and antifoam may be used, as reported by Pandey *et al.* (2018) or the mixture of anionic surfactant and silicon

surfactant may be use, as reported by Bhattacharjee *et al.* (2018). Though MES surfactant inadvertently results in foam formation, it is an anionic bio-based surfactant that can enhance the hydrate formation and has good performance as the conventional SDS surfactant.

4.5 Conclusions

Experiments were performed to study the effects of MES surfactant, a bio-based anionic surfactant, on the methane hydrate formation at 277.2 K and 8 MPa. The concentrations of MES used were 1, 2, 4 and 8 mM for methane hydrate formation and dissociation experiments. The results indicated that the methane hydrate formation with the presence of MES showed the significant improvement of methane hydrate formation rate and methane consumption compared with pure water (no methane hydrate formation for 48 h). The induction decreased with the increase in the MES concentration. The results also revealed that during the hydrate formation in all MES concentrations, the multiple hydrate nucleation events occurred. The methane uptake during the hydrate formation increased with the increase in the MES concentration. Moreover, the hydrate morphology during the hydrate formation of all MES concentrations showed similar growth pattern. Hydrate nucleation started at the interface of gas and liquid, followed by the hydrate growth in the upward direction and then downward direction. Hydrate growth further continued in both directions until the hydrates covered all the reactor column. In order to recover the methane gas from the gas hydrate, hydrate dissociation was performed by thermal stimulation method by increasing the temperature from 277.2 K to 298.2 K. Methane recovery was not significantly different with different MES concentrations. The average of methane recovery was more than 95%. Hydrate morphology during the dissociation showed that the dissociation started from the wall of the reactor column followed by bulk hydrates from the wall to the inside of the reactor until hydrate dissociation was complete.

4.6 Acknowledgements

This work was supported by The Royal Golden Jubilee Ph.D. Program (2.P.CU/58/J.1), Thailand Research Fund; The Petroleum and Petrochemical College (PPC), Chulalongkorn University, Thailand; Center of Excellence on Petrochemical and Materials Technology (PETROMAT), Thailand; Grant for International Research Integration: Chula Research Scholar, Ratchadaphiseksomphot Endowment Fund, Chulalongkorn University, Thailand; Thailand Energy Conservation Fund, Energy Policy and Planning Office Ministry of Energy; Department of Chemical and Biomolecular Engineering, Faculty of Engineering, National University of Singapore (NUS); UOP, A Honeywell Company, USA.

Nomenclature

CTAB	cationic surfactant cetyl trimethyl ammonium bromide
DAH	dodecylamine hydrochloride
DN_2Cl	N-dodecylpropane-1,3-diamine hydrochloride
DTAC	dodecyltrimethylammonium chloride
ENP	ethoxylated nonylphenol
LABS	linear alkyl benzene sulfonate

4.7 Supporting Information

Table S4.1 Hydrate formation experimental conditions at 277.2 K and 8 MP for the morphology of methane hydrate experiment

No. Exp	*Induction Time (h)	% Hydrate Yield	Methane Consumption (mole CH_4/H_2O)	**Rate of Hydrate Formation (mol of methaen/min/m^3 of water)
		1 mM MES		
E-1	11.3	42.44	0.0739	70.00 (R^2 = 0.98)
E-2	10.5	41.40	0.0720	72.85 (R^2 = 0.98)
		2 mM MES		
F-1	8.5	44.28	0.0770	78.85 (R^2 = 0.98)
F-2	9.1	46.00	0.0800	77.14 (R^2 = 0.99)
		4 mM MES		
G-1	7.2	51.75	0.0900	84.13 (R^2 = 0.96)
G-2	6.6	56.35	0.0980	80.00 (R^2 = 0.98)
		8 mM MES		
H-1	6.2	58.65	0.1020	95.65 (R^2 = 0.99)
H-2	6.5	58.94	0.1025	93.78 (R^2 = 0.98)

* Induction time is taken for first hydrate nucleation

** Rate of hydrate formation calculated for10 min from induction time

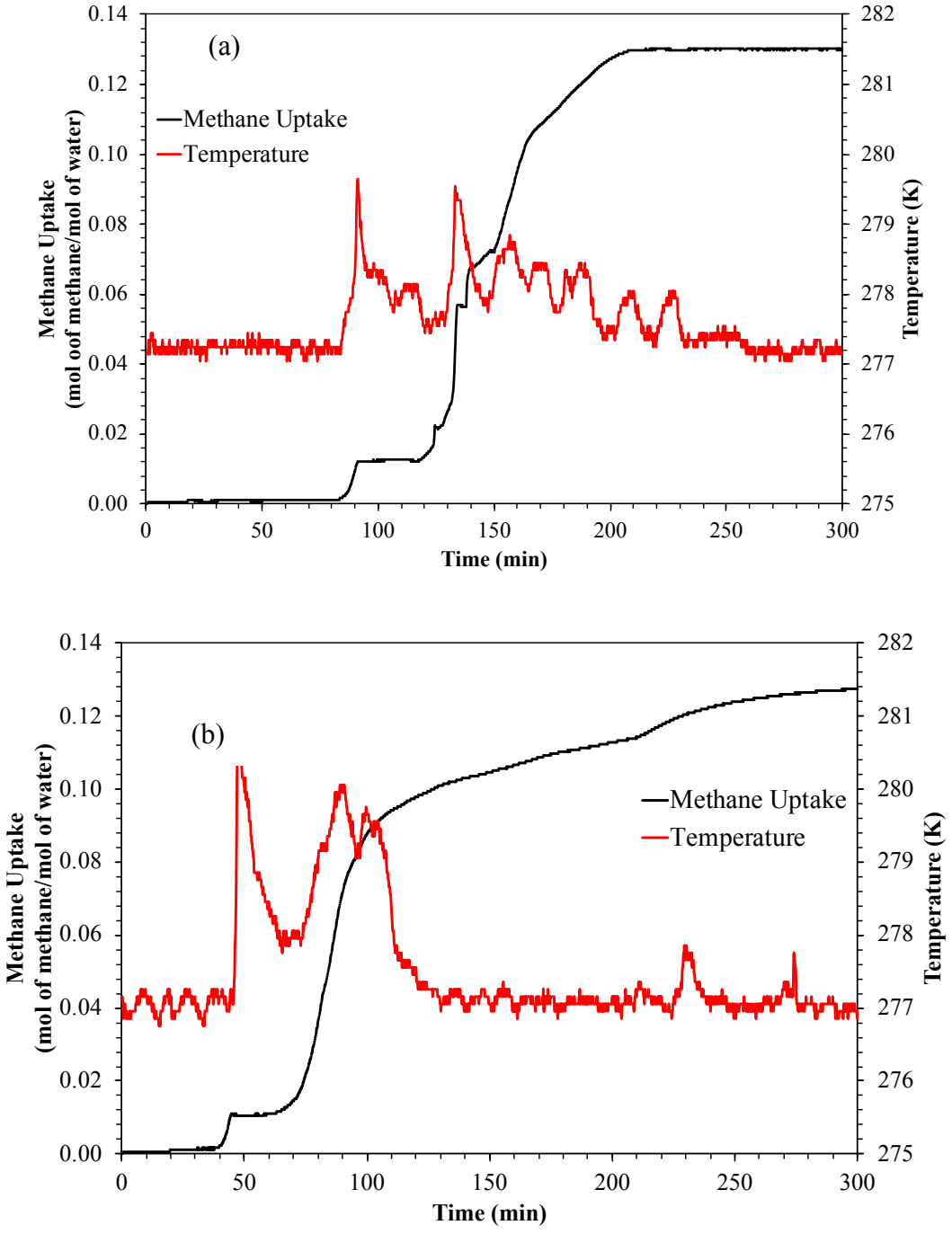

Figure S4.1 Methane uptake and temperature profiles in the presence of (a) 2 mM MES (No. exp C-2 in Table 4.1) and (b) 4 mM MES (No. exp D-2 in Table 4.1).

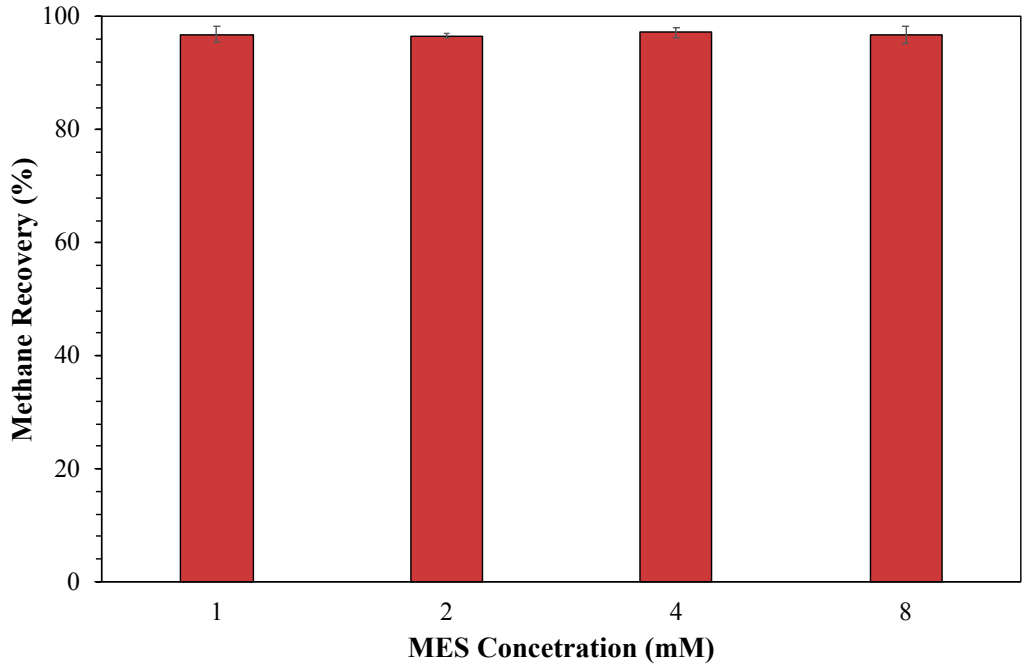

Figure S4.2. Methane recovery during hydrate dissociation at different concentrations of MES.

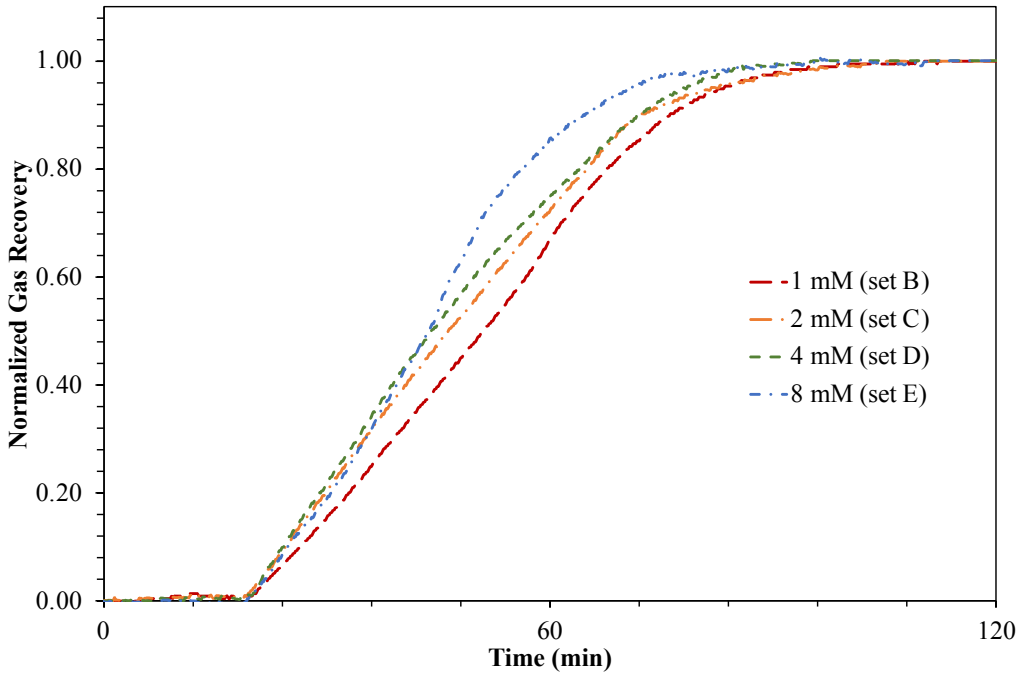

Figure S4.3 Average normalized recovery curves during the hydrate dissociation in the presence of different MES concentrations.

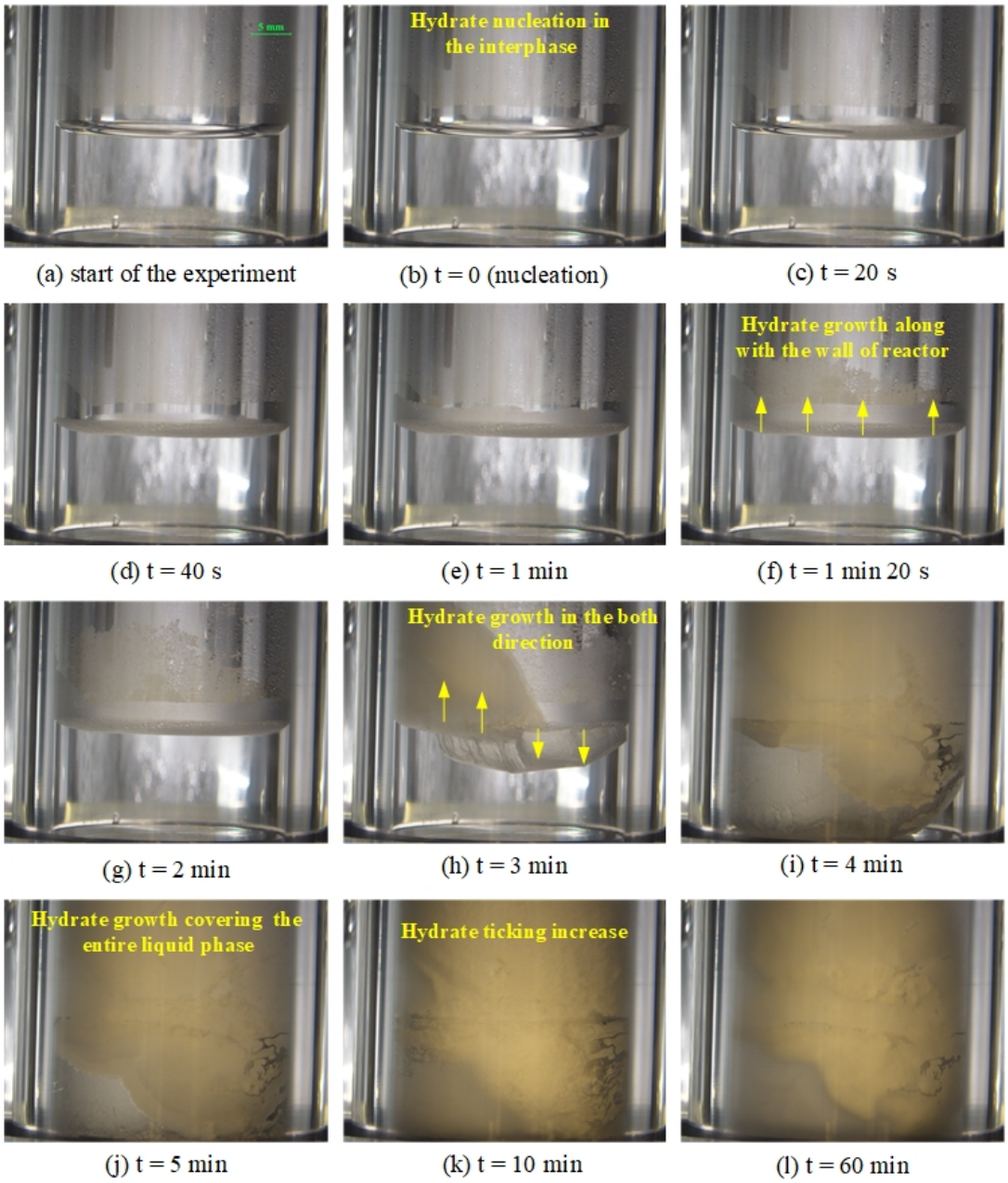

Figure S4.4 (a-l) Morphology images at different time of methane hydrate formation in the presence of 1 mM MES at 8.0 MPa and 277.2 K.

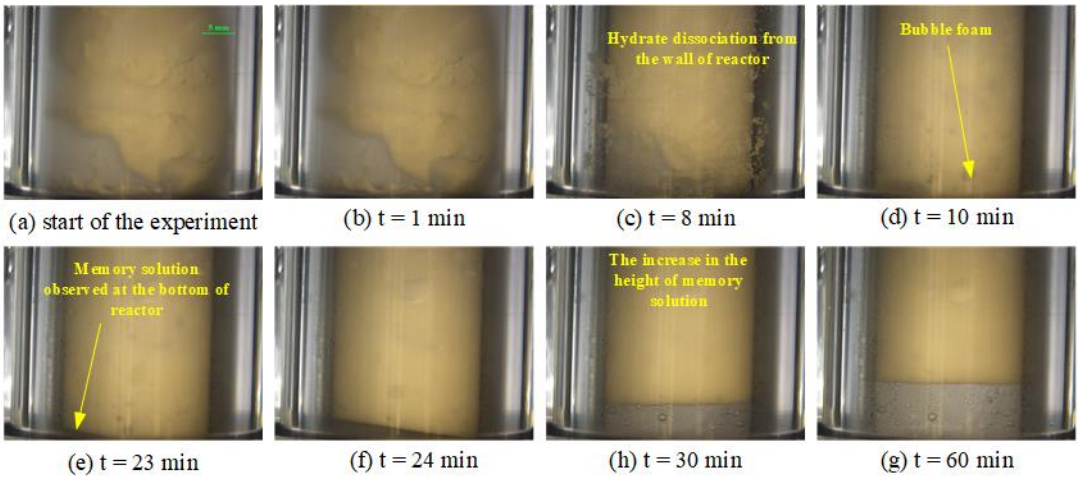

Figure S4.5 (a-i) Morphology images at different time of methane hydrate dissociation in the presence of 1 mM MES.

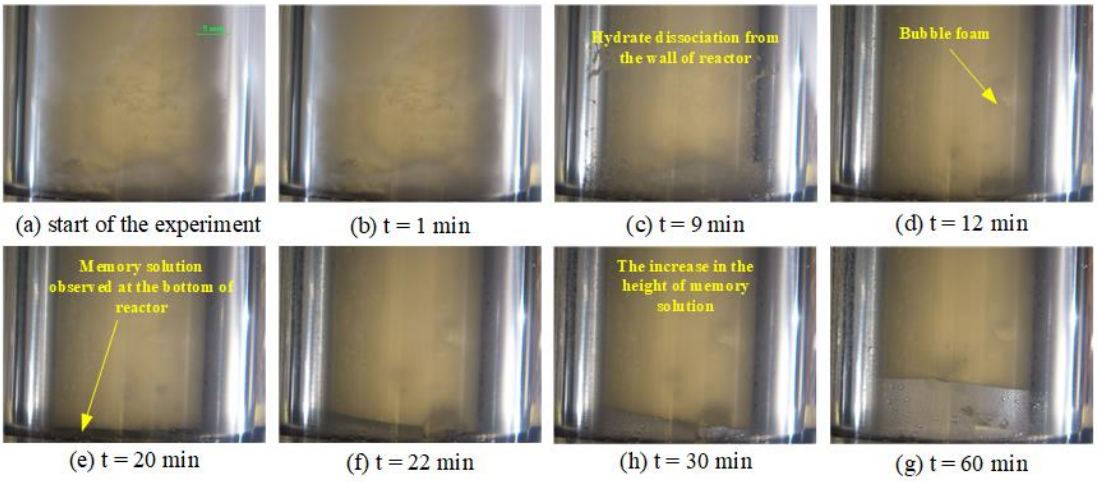

Figure S4. 6 (a-i) Morphology images at different time of methane hydrate dissociation in the presence of 2 mM MES.

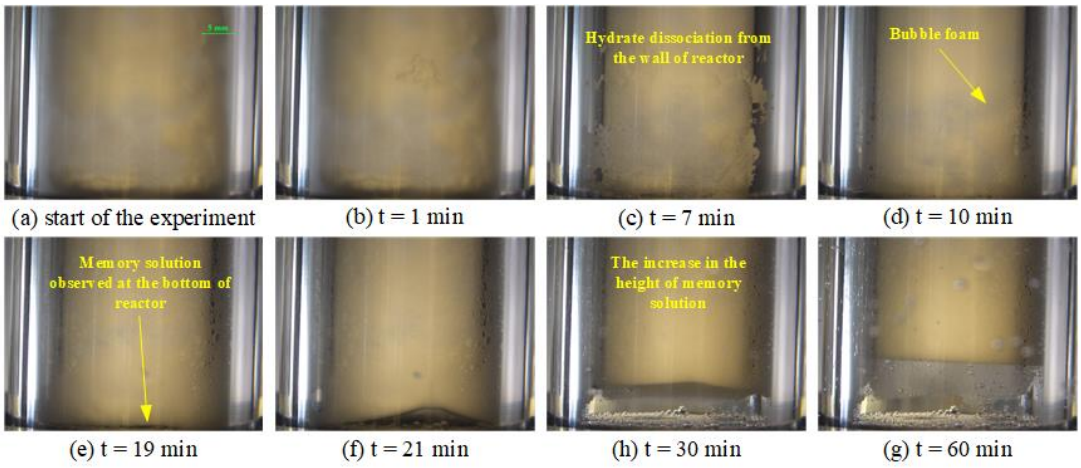

Figure S4.7 (a-i) Morphology images at different time of methane hydrate dissociation in the presence of 8 mM MES.

4.8 References

Ando, N., Kuwabara, Y., and Mori, Y. H. (2012). Surfactant effects on hydrate formation in an unstirred gas/liquid system: An experimental study using methane and micelle-forming surfactants. Chemical Engineering Science, 73, 79-85.

Babu, K., Maurya, N., Mandal, A., and Saxena, V. (2015). Synthesis and characterization of sodium methyl ester sulfonate for chemically-enhanced oil recovery. Brazilian Journal of Chemical Engineering, 32(3), 795-803.

Babu, P., Kumar, R., and Linga, P. (2013). Pre-combustion capture of carbon dioxide in a fixed bed reactor using the clathrate hydrate process. Energy, 50, 364-373.

Balson, T., Berger, H., Brown, D., Domsch, A., Felix, M. S. B., Painter, H. A., Russell, N. J., Steber, J., Ginkel, C. G. v., and White, G. F. (1995). *Biodegradability of Surfactants* (D. R. Karsa and M. R. Porter Eds. 1 ed.): Springer Science+Business Media Dordrecht.

Bhattacharjee, G., Barmecha, V., Kushwaha, O. S., and Kumar, R. (2018). Kinetic promotion of methane hydrate formation by combining anionic and silicone surfactants: Scalability promise of methane storage due to prevention of foam formation. The Journal of Chemical Thermodynamics, 117, 248-255.

Bhattacharjee, G., Choudhary, N., Kumar, A., Chakrabarty, S., and Kumar, R. (2016). Effect of the amino acid l-histidine on methane hydrate growth kinetics. Journal of Natural Gas Science and Engineering, 35, 1453-1462.

Boswell, R., and Collett, T. S. (2011). Current perspectives on gas hydrate resources. Energy & Environmental Science, 4(4), 1206-1215.

Chaturvedi, E., Prasad, N., and Mandal, A. (2018). Enhanced formation of methane hydrate using a novel synthesized anionic surfactant for application in storage and transportation of natural gas. Journal of Natural Gas Science and Engineering, 56, 246-257.

Chong, Z. R., Yang, S. H. B., Babu, P., Linga, P., and Li, X.-S. (2016). Review of natural gas hydrates as an energy resource: Prospects and challenges. Applied Energy, 162, 1633-1652.

De, S., Malik, S., Ghosh, A., Saha, R., and Saha, B. (2015). A review on natural surfactants. RSC Advances, 5(81), 65757-65767.

Demirbas, A., Rehan, M., Al-Sasi, B. O., and Nizami, A.-S. (2016). Evaluation of natural gas hydrates as a future methane source. Petroleum Science and Technology, 34(13), 1204-1210.

Du, J., Li, H., and Wang, L. (2014). Effects of ionic surfactants on methane hydrate formation kinetics in a static system. Advanced Powder Technology, 25(4), 1227-1233.

EIA. (2016). Annual Energy Outlook 2016. 152.

Fandiño, O., and Ruffine, L. (2014). Methane hydrate nucleation and growth from the bulk phase: Further insights into their mechanisms. Fuel, 117, 442-449.

Ganji, H., Manteghian, M., Sadaghiani zadeh, K., Omidkhah, M. R., and Rahimi Mofrad, H. (2007). Effect of different surfactants on methane hydrate formation rate, stability and storage capacity. Fuel, 86(3), 434-441.

Gayet, P., Dicharry, C., Marion, G., Graciaa, A., Lachaise, J., and Nesterov, A. (2005). Experimental determination of methane hydrate dissociation curve up to 55MPa by using a small amount of surfactant as hydrate promoter. Chemical Engineering Science, 60(21), 5751-5758.

Gudmundsson, J. S., Parlaktuna, M., and Khokhar, A. A. (1994). Storage of natural gas as frozen hydrate. SPE Production & Facilities, 9(01), 69-73.

Hao, W., Wang, J., Fan, S., and Hao, W. (2008). Evaluation and analysis method for natural gas hydrate storage and transportation processes. Energy Conversion and Management, 49(10), 2546-2553.

Kakati, H., Mandal, A., and Laik, S. (2016). Effect of SDS/THF on thermodynamic and kinetic properties of formation of hydrate from a mixture of gases (CH4+C2H6+C3H8) for storing gas as hydrate. Journal of Energy Chemistry, 25(3), 409-417.

keshavarz Moraveji, M., Ghaffarkhah, A., and Sadeghi, A. (2017). Effect of three representative surfactants on methane hydrate formation rate and induction time. Egyptian Journal of Petroleum, 26(2), 331-339.

Khurana, M., Yin, Z., and Linga, P. (2017). A review of clathrate hydrate nucleation. ACS Sustainable Chemistry & Engineering, 5(12), 11176-11203.

Kumar, A., Bhattacharjee, G., Kulkarni, B. D., and Kumar, R. (2015). Role of Surfactants in Promoting Gas Hydrate Formation. Industrial & Engineering Chemistry Research, 54(49), 12217-12232.

Kumar, S., Kumar, A., and Mandal, A. (2017). Characterizations of surfactant synthesized from Jatropha oil and its application in enhanced oil recovery. AIChE Journal, 63(7), 2731-2741.

Lang, X., Fan, S., and Wang, Y. (2010). Intensification of methane and hydrogen storage in clathrate hydrate and future prospect. Journal of Natural Gas Chemistry, 19(3), 203-209.

Li, X.-S., Xu, C.-G., Zhang, Y., Ruan, X.-K., Li, G., and Wang, Y. (2016). Investigation into gas production from natural gas hydrate: A review. Applied Energy, 172, 286-322.

Lin, W., Chen, G. J., Sun, C. Y., Guo, X. Q., Wu, Z. K., Liang, M. Y., Chen, L. T., and Yang, L. Y. (2004). Effect of surfactant on the formation and dissociation kinetic behavior of methane hydrate. Chemical Engineering Science, 59(21), 4449-4455.

Linga, P., Haligva, C., Nam, S. C., Ripmeester, J. A., and Englezos, P. (2009). Recovery of methane from hydrate formed in a variable volume bed of silica sand particles. Energy & Fuels, 23(11), 5508-5516.

Liu, Y., Chen, B., Chen, Y., Zhang, S., Guo, W., Cai, Y., Tan, B., and Wang, W. (2015). Methane storage in a hydrated form as promoted by leucines for possible application to natural gas transportation and storage. Energy Technology, 3(8), 815-819.

Lou Capitanio, Jared Ciferno, and Boswell, R. (2017). METHANE HYDRATE SCIENCE AND TECHNOLOGY: A 2017 UPDATE. In (pp. 40).

Makogon, Y. F. (2010). Natural gas hydrates – A promising source of energy. Journal of Natural Gas Science and Engineering, 2(1), 49-59.

Makogon, Y. F., Holditch, S. A., and Makogon, T. Y. (2007). Natural gas-hydrates — A potential energy source for the 21st Century. Journal of Petroleum Science and Engineering, 56(1), 14-31.

Mech, D., Gupta, P., and Sangwai, J. S. (2016). Kinetics of methane hydrate formation in an aqueous solution of thermodynamic promoters (THF and TBAB) with and without kinetic promoter (SDS). Journal of Natural Gas Science and Engineering, 35, 1519-1534.

Mekala, P., Babu, P., Sangwai, J. S., and Linga, P. (2014). Formation and dissociation kinetics of methane hydrates in seawater and silica sand. Energy & Fuels, 28(4), 2708-2716.

Nakamura, T., Makino, T., Sugahara, T., and Ohgaki, K. (2003). Stability boundaries of gas hydrates helped by methane—structure-H hydrates of methylcyclohexane and cis-1,2-dimethylcyclohexane. Chemical Engineering Science, 58(2), 269-273.

Okutani, K., Kuwabara, Y., and Mori, Y. H. (2008). Surfactant effects on hydrate formation in an unstirred gas/liquid system: An experimental study using methane and sodium alkyl sulfates. Chemical Engineering Science, 63(1), 183-194.

Pandey, G., Bhattacharjee, G., Veluswamy, H. P., Kumar, R., Sangwai, J. S., and Linga, P. (2018). Alleviation of foam formation in a surfactant driven gas hydrate system: Insights via a detailed morphological study. ACS Applied Energy Materials, 1(12), 6899-6911.

Rahimi Mofrad, H., Ganji, H., Nazari, K., Kameli, M., Rezaie Rod, A., and Kakavand, M. (2016). Rapid formation of dry natural gas hydrate with high capacity and

low decomposition rate using a new effective promoter. Journal of Petroleum Science and Engineering, 147, 756-759.

Roberts, D. W., Giusti, L., and Forcella, A. (2008). Chemistry of methyl ester sulfonates. Inform (Silver Spring, Md.) (Inform), 19, 2-9.

Rogers, R. E., Kothapalli, C., Lee, M. S., and Woolsey, J. R. (2003). Catalysis of Gas Hydrates by Biosurfactants in Seawater-Saturated Sand/Clay. The Canadian Journal of Chemical Engineering, 81(5), 973-980.

Shi, B.-H., Yang, L., Fan, S.-S., and Lou, X. (2017). An investigation on repeated methane hydrates formation in porous hydrogel particles. Fuel, 194, 395-405.

Siangsai, A., Inkong, K., Kulprathipanja, S., Kitiyanan, B., and Rangsunvigit, P. (2018). Roles of sodium dodecyl sulfate on tetrahydrofuran-assisted methane hydrate formation. Journal of oleo science 67(6), 707-717.

Siangsai, A., Rangsunvigit, P., Kitiyanan, B., Kulprathipanja, S., and Linga, P. (2015). Investigation on the roles of activated carbon particle sizes on methane hydrate formation and dissociation. Chemical Engineering Science, 126, 383-389.

Sloan, E. D., and Koh, C. A. (2008). *Clathrate Hydrates of Natural Gases*. New York: CRC Press.

Sloan Jr, E. D. (2003). Fundamental principles and applications of natural gas hydrates. Nature, 426, 353.

Smith, J. M., Van Ness, H. C., and Abbott, M. M. (2005). *Introduction to Chemical Engineering Thermodynamics*. Singapore: McGraw-Hill.

Sun, Z., Wang, R., Ma, R., Guo, K., and Fan, S. (2003). Natural gas storage in hydrates with the presence of promoters. Energy Conversion and Management, 44(17), 2733-2742.

Tobori, N., and Kakui, T. (2019). Chapter 9 - Methyl Ester Sulfonate. In D. G. Hayes, D. K. Y. Solaiman, and R. D. Ashby (Eds.), *Biobased Surfactants (Second Edition)* (pp. 303-324): AOCS Press.

Veluswamy, H. P., Ang, W. J., Zhao, D., and Linga, P. (2015a). Influence of cationic and non-ionic surfactants on the kinetics of mixed hydrogen/tetrahydrofuran hydrates. Chemical Engineering Science, 132, 186-199.

Veluswamy, H. P., Chen, J. Y., and Linga, P. (2015b). Surfactant effect on the kinetics of mixed hydrogen/propane hydrate formation for hydrogen storage as clathrates. Chemical Engineering Science, 126, 488-499.

Veluswamy, H. P., Hong, Q. W., and Linga, P. (2016a). Morphology study of methane hydrate formation and dissociation in the presence of amino acid. Crystal Growth & Design, 16(10), 5932-5945.

Veluswamy, H. P., Kumar, A., Seo, Y., Lee, J. D., and Linga, P. (2018). A review of solidified natural gas (SNG) technology for gas storage via clathrate hydrates. Applied Energy, 216, 262-285.

Veluswamy, H. P., Lee, P. Y., Premasinghe, K., and Linga, P. (2017). Effect of Biofriendly Amino Acids on the Kinetics of Methane Hydrate Formation and Dissociation. Industrial & Engineering Chemistry Research, 56(21), 6145-6154.

Veluswamy, H. P., and Linga, P. (2013). Macroscopic kinetics of hydrate formation of mixed hydrates of hydrogen/tetrahydrofuran for hydrogen storage. International Journal of Hydrogen Energy, 38(11), 4587-4596.

Veluswamy, H. P., Prasad, P. S. R., and Linga, P. (2016b). Mechanism of methane hydrate formation in the presence of hollow silica. Korean Journal of Chemical Engineering, 33(7), 2050-2062.

Veluswamy, H. P., Wong, A. J. H., Babu, P., Kumar, R., Kulprathipanja, S., Rangsunvigit, P., and Linga, P. (2016c). Rapid methane hydrate formation to develop a cost effective large scale energy storage system. Chemical Engineering Journal, 290, 161-173.

Wang, F., Jia, Z.-Z., Luo, S.-J., Fu, S.-F., Wang, L., Shi, X.-S., Wang, C.-S., and Guo, R.-B. (2015a). Effects of different anionic surfactants on methane hydrate formation. Chemical Engineering Science, 137, 896-903.

Wang, F., Liu, G.-Q., Meng, H.-L., Guo, G., Luo, S.-J., and Guo, R.-B. (2016). Improved Methane Hydrate Formation and Dissociation with Nanosphere-Based Fixed Surfactants As Promoters. ACS Sustainable Chemistry & Engineering, 4(4), 2107-2113.

Wang, F., Luo, S.-J., Fu, S.-F., Jia, Z.-Z., Dai, M., Wang, C.-S., and Guo, R.-B. (2015b). Methane hydrate formation with surfactants fixed on the surface of polystyrene nanospheres. Journal of Materials Chemistry A, 3(16), 8316-8323.

Wang, W., Huang, Z., Chen, H., Tan, Z., Chen, C., and Sun, L. (2012). Methane hydrates with a high capacity and a high formation rate promoted by biosurfactants. Chemical Communications, 48(95), 11638-11640.

Yang, L., Liu, Y., Zhang, H., Xiao, B., Guo, X., Wei, R., Xu, L., Sun, L., Yu, B., Leng, S., and Li, Y. (2019). The status of exploitation techniques of natural gas hydrate. Chinese Journal of Chemical Engineering.

Yang, S. H. B., Babu, P., Chua, S. F. S., and Linga, P. (2016). Carbon dioxide hydrate kinetics in porous media with and without salts. Applied Energy, 162, 1131-1140.

Yoslim, J., Linga, P., and Englezos, P. (2010). Enhanced growth of methane–propane clathrate hydrate crystals with sodium dodecyl sulfate, sodium tetradecyl sulfate, and sodium hexadecyl sulfate surfactants. Journal of Crystal Growth, 313(1), 68-80.

Zhang, J. S., Lee, S., and Lee, J. W. (2007a). Does SDS micellize under methane hydrate-forming conditions below the normal Krafft point? Journal of Colloid and Interface Science, 315(1), 313-318.

Zhang, J. S., Lee, S., and Lee, J. W. (2007b). Kinetics of methane hydrate formation from SDS solution. Industrial & Engineering Chemistry Research, 46(19), 6353-6359.

Zhong, Y., and Rogers, R. E. (2000). Surfactant effects on gas hydrate formation. Chemical Engineering Science, 55(19), 4175-4187.

CHAPTER V
EFFECTS OF TEMPERATURE AND PRESSURE ON THE METHANE HYDRATE FORMATION WITH PRESENCE OF TETRAHYDROFURAN (THF) AS A HYDRATE PROMOTER IN AN UNSTIRRED TANK REACTOR

5.1 Abstract

In this work, the effect of temperature and pressure on the methane hydrate formation and dissociation with the presence of 5.56 mole% THF solution in the quiescent condition is investigated. The experiments were conducted at 8 MPa and at 277.2, 283.2, 288.2 and 293.2 K. The results show that the methane uptake increased with the increase in the experimental temperature due to at the fact that higher experimental temperature showed the multiple hydrate nucleation and effective heat distribution to the surrounding. The experiment at 277.2 K showed the fastest induction time and shortest time to reached 90% of the methane uptake (t_{90}). The highest methane uptake was observed at 293.2 K. Moreover, the effect of experimental over pressure on the methane hydrate formation was investigated by varying the pressure from 8 to 4 MPa at 288.2 K. The result showed that the pressure did not affect the methane uptake but the rate of formation at the higher pressure is higher than at lower pressure. Furthermore, this work reports a synergistic effect of kinetic promotion of methane hydrate formation by coupling THF with methyl ester sulfonate (MES) at 293.2 K. The results showed that the presence of MES improved both induction time and rate of hydrate formation. The dissociation experiment was conducted after the formation by increasing the temperature to 308.2 K. The results showed that up to 98% of methane could be recovered.

Keywords*:* Gas hydrates, Formation, Promoter, Hydrate structure, Tetrahydrofuran, Solidified natural gas

5.2 Introduction

In 2017, based on a report by International Gas Union (IGU), the global gas consumption is estimated to have grown by 3.7% year-over-year, more than double the 1.5% average annual growth rate from 2010 to 2016. The gas consumption growth was largely in line with total global primary energy demand from 2010-2016 and the gas consumption in 2017 grew faster than global energy demand (2.1% year-over-year growth) (IGU, 2018). That is, in part, because of natural gas being cleaner burning and meeting stringent environmental norms (Demirbas, 2010b; Rios *et al.*, 2013; Zhang *et al.*, 2010) The storage and transportation of natural gas is important in the commercial scale. Natural gas conventional storage methods include compressed natural gas or CNG, liquefied natural gas or LNG, and absorbed natural gas or ANG (Sapag *et al.*, 2010). For CNG, natural gas is compressed at a high pressure about 20 to 25 MPa in thick wall and heavy cylindrical tanks. However, the volumetric energy storage density of CNG is about one-third of gasoline. For LNG, natural gas must be converted to the liquid form. LNG is more efficient than CNG as LNG has volumetric energy storage density about two-third of gasoline. However, LNG requires an expensive pressurization and cooling system below the critical temperature of methane, about 191 K (Wang *et al.*, 2010; Zakaria and George, 2011). For ANG, using porous medium as an adsorbent is to used. Therefore, ANG has higher storage capacity in an equivalent volume than other storage technologies. However, ANG requires low cost of adsorbent and the addition of porous medium in gas storage increases the weight of the storage tank (Lozano-Castelló *et al.*, 2002; Sapag *et al.*, 2010). The solidified natural gas or SNG is a technology to store natural gas in the form of clathrate hydrates or gas hydrate (Veluswamy *et al.*, 2018). This technology has several advantages including high volumetric energy storage capacity about 170 m^3 of methane gas in 1 m^3 of hydrate. It is very safe to handle because of non-explosive nature, easy to recover the stored gas, and cost-effective compared with the conventional method like CNG. Moreover, the hydrate technology is receiving wide attention not only for natural gas transportation and storage but also for gas separation (Ricaurte *et al.*, 2014; Sun *et al.*, 2014; Tang *et al.*, 2013), carbon capture and storage (Babu *et al.*, 2013; Babu *et al.*, 2015; Kang and

Lee, 2000; Linga *et al.*, 2007), desalination (Babu *et al.*, 2018; Han *et al.*, 2017; Kang *et al.*, 2014; Yang *et al.*, 2014) etc.

Natural gas hydrates or methane hydrates are solid crystalline compounds and non-stoichiometric compounds, which consisting of methane (CH_4) enclathrated inside three-dimension lattice framework structure formed by hydrogen bonds from water molecules (Englezos, 1993; Sloan and Koh, 2008). There are three structures of gas hydrates, including structure I (sI), structure II (sII), and structure H (sH), the size of the gas molecules and condition determine the hydrate structure (Sloan and Koh, 2008). Gas hydrates were discovered that they accommodate a large amount of natural gas. This property is the key factor for gas hydrate technology in the gas storage (Demirbas, 2010a; Gudmundsson *et al.*, 1994; Makogon, 2010). The challenges of natural gas hydrate for commercial deployment is the slow formation rate, storage capacity and storage stability.

One possibility to enhance the natural gas formation rate, methane hydrate capacity, and stability of hydrate is adding a promoter (Ganji *et al.*, 2007; Partoon and Javanmardi, 2013; Sun *et al.*, 2003). Tetrahydrofuran or THF is one effective promoter for methane hydrate formation due to it can alter the phase equilibrium of hydrate formation to a higher temperature and lower pressure (Florusse *et al.*, 2004; Kang and Lee, 2000). It has been reported that THF can form hydrates with water by itself without a gas molecule in the large cage of sII (Gough and Davidson, 1971). Seo *et al.* (2001) studied the mixed–CH_4 hydrate phase equilibrium in the presence of promoters including acetone, THF, 1,4-dioxane and propylene oxide. The result showed that the equilibrium temperature of the methane and THF mixed hydrated appeared to be the highest among the tested promoters, and THF was proven to be the strongest to stabilizing methane hydrates. Recently, Kumar *et al.* (2016) reported that mixed THF–CH_4 hydrates are more stable than pure THF hydrates based on calorimetric measurements. Veluswamy *et al.* (2016b) used THF as a hydrate promoter and reported rapid methane hydrate formation at 283.2 K and 7 MPa thus concluding that THF acts as both thermodynamic and kinetic promoter. The result showed that the methane uptake enhancement was about 11.6 times higher with the presence of THF as a promoter. Recently, the study by Veluswamy *et al.* (2016a) presented the mixed THF–CH_4 hydrate at three different temperatures – 283.2 K, 288.2 K and 293.2 K and

at experimental pressures of 7.2 MPa, which all conditions are in the sII region only. The final gas uptake was similar at all these temperatures although the kinetics of hydrate formation was impacted significantly. Moreover, Lin *et al.* (2018) investigated the effect of THF concentration at 283.2 K and 5 MPa. They reported the higher methane uptake and faster rate of hydrate formation in the presence of the stoichiometric concentration of THF. Therefore, this research aims to study the effects of temperature on the methane hydrate formation in the mixed THF–CH_4 hydrates with the presence of the stoichiometric of 5.56 mol% THF. The temperature in this work was chosen covering both sI and sII region. Moreover, this work study the effect of pressure in the presence of stoichiometric of 5.56 mol% THF on the methane hydrate formation at higher temperatures. In addition, this work evaluates the effect of methyl ester sulfonate (MES), a biodegradable anionic surfactant, on the kinetic promotion of mixed THF–CH_4 hydrates with the presence of the stoichiometric of 5.56 mol% THF.

5.3 Experimental Procedure

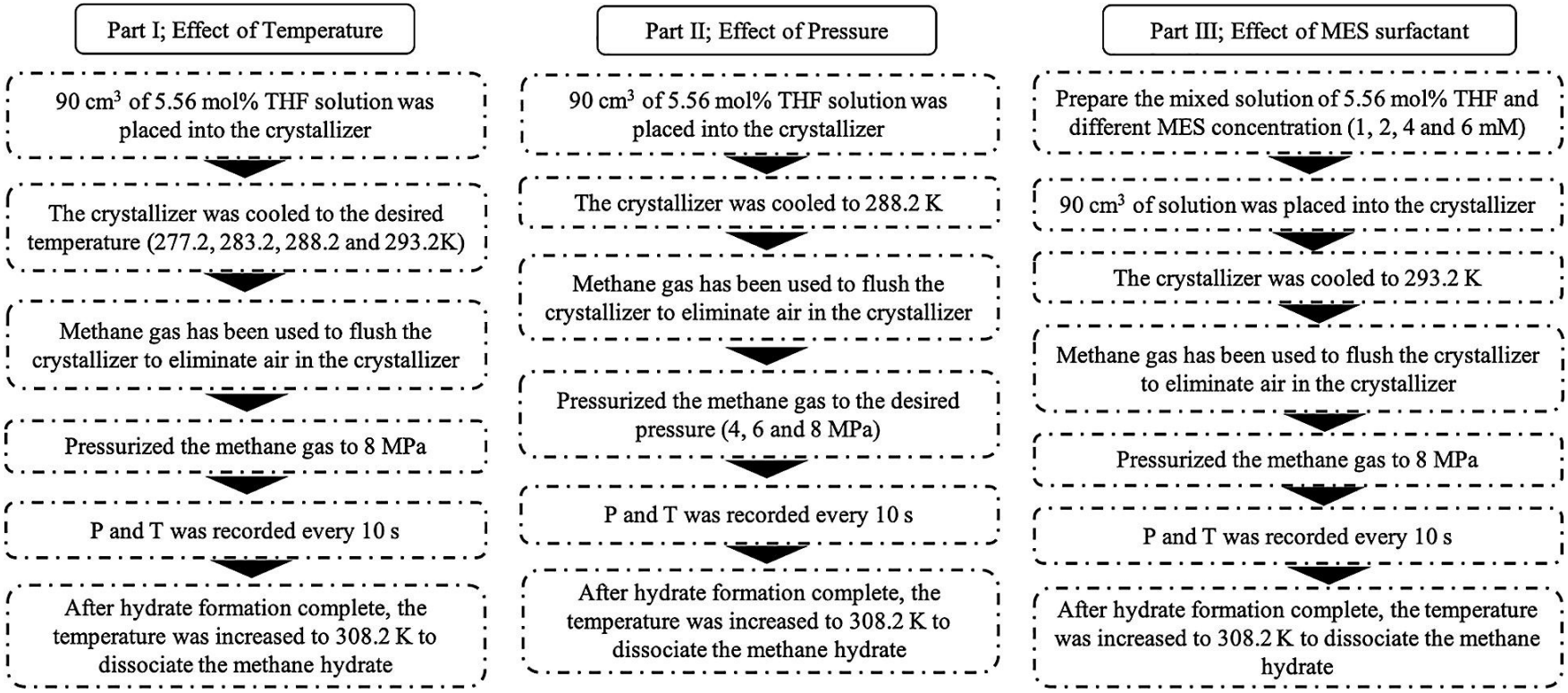

Figure 5.1 the procedure of the experiment.

5.2.1 Materials and Apparatus

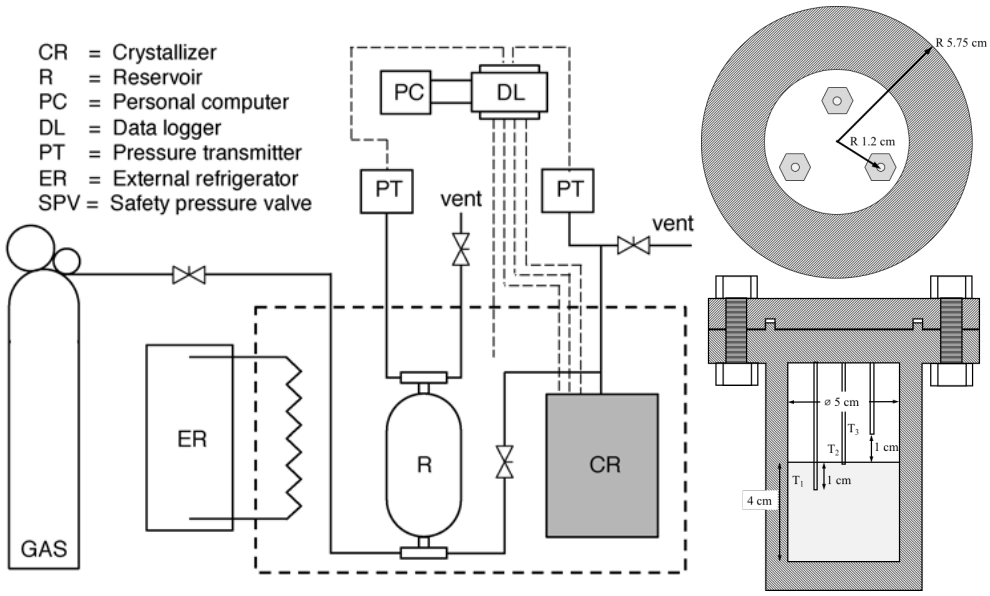

Figure 5.2 Schematic of experimental apparatus (left side) and cross-section of a crystallizer (right side). Modified from Siangsai *et al.* (2015).

Tetrahydrofuran (THF, AR grade 99.99 %) was obtained from Lab-Scan, Thailand. Methane (99.99 % purity) purchased from Linde Public Company, Thailand. Deionized water was used for the methane hydrate formation. The solution (5.56 mol% THF or the mix of 5.56 mol% THF and MES) was prepared in a volumetric flask. The methane hydrate formation and dissociation apparatus is in Figure 6.2a. The apparatus consists of 180 cm^3 high-pressure stainless steel crystallizer (CR) and 100 cm^3 supply vessel (R) immersed in a cooling bath. The external refrigerator (Model RC-20, Daeyang, Korea) circulated the mixed glycol and water to controlled temperature in a cooling bath. The pressure transmitter (PT) (Cole-Pamer®, Singapore) with a range of 0 - 21 Mpa and 0.13 % global error are used to measure the pressure in the system. Three K-type thermocouples with ±1.0 K accuracy were located at the gas phases, the interface between two phases, and in the solution represented by T1, T2, and T3 respectively as showed in Figure 6.2b. A data logger (AI210, Wisco

Industrial Instruments, Thailand) was connected to a computer to record the data during the experiment. All experiments were carried out in the quiescent condition with a fixed amount gas and solution in the closed system.

5.3.2 Hydrate Formation Experiment

90 $cm^3$of solution (5.56 mol% THF or the mix of 5.56 mol% THF and MES) was placed into the crystallizer. In order to eliminate the air in the system, the crystallizer was pressurized to 0.5 MPa by methane gas and depressurized to atmospheric pressure twice. The experimental temperatures were set at the desired temperature. Methane gas was introduced into the crystallizer at the desired pressure. The data was recorded every 10 s by the data logger after methane gas was introduced into the crystallizer. During the hydrate formation, the pressure in the crystallizer dropped due to the hydrate formation. The experiment continued until there was no further pressure drop at least 1 h. The pressure and temperature data were used to calculate the moles of methane consumed by equation (5.1);

$$\Delta n_{H,\downarrow} = n_{H,0} - n_{H,t} = \left(\frac{PV}{zRT}\right)_{\mathrm{G,0}} - \left(\frac{PV}{zRT}\right)_{\mathrm{G,t}} \tag{5.1}$$

where $\Delta n_{H,\downarrow}$ is the moles of gas consumed for the hydrate formation at the end of experiment. $n_{H,0}$ is the moles of methane at the start of experiment. $n_{H,t}$ is the moles of the methane at time t. Subscripts $G,0$ and G,t represent the gas phase at the start of the experiment and time t, respectively. P and T are the pressure and temperature in the system. V is the volume of gas phase in the crystallizer, R is the universal gas constant, and z is the compressibility factor calculated by Pitzer's correlation (Smith *et al.*, 2005).

5.3.3 Hydrate Dissociation Experiment

The hydrates were dissociated by increasing the temperature from the formation temperature at the same heating rate for all experiments to 308.2 K. The hydrate dissociates when the temperature in the crystallizer crosses the equilibrium

phase boundary. The moles of methane released from the hydrate at any time during the hydrate dissociation can be calculated by

$$\Delta n_{H,\uparrow} = n_{H,t} - n_{H,0} = \left(\frac{PV}{zRT}\right)_{G,t} - \left(\frac{PV}{zRT}\right)_{G,0} \quad (5.2)$$

when $\Delta n_{H,\uparrow}$ represents the moles of gas released from the hydrates. The methane recovery is calculated by equation (5.3) as a function of time for any dissociation experiment (Haligva *et al.*, 2010; Linga *et al.*, 2009).

$$\%\text{methane recovery} = \frac{(\Delta n_{H,\uparrow})}{(\Delta n_{H,\downarrow})} \times 100 \quad (5.3)$$

where $\Delta n_{H,\downarrow}$ is the moles of gas consumed for the hydrate formation at the end of experiment.

5.4 Result and Discussion

5.4.1 Effects of Temperature on the Methane Hydrate Formation

Results from the effect of temperature and pressure on the methane hydrate formation with the presence of stoichiometric 5.56 mole% THF are divided into three parts. The methane hydrate formation at 8 MPa and 277.2, 283.2, 288.2, and 293.2 K is discussed first. The temperature was chosen to study the effect of different starting points on the hydrate formation in the THF-methane phase diagram. The experiments conducted at 277.2 K and 283.2 K for 8.0 MPa are in the sI & sII region of the pure methane phase equilibrium diagram, while, the starting point of the experiments conducted at 288.2 and 293.2 K are only in the sII region of the mixed methane-THF hydrate phase equilibrium, which can be observed in Figure 5.3. Then, the methane hydrate formation at 288.2 K with different pressures from 8 to 4 MPa is reported. Later that, the hydrate formation at 293.2 K and 8 MPa in presence of different concentration of anionic surfactant is reported. Note that each experiment was repeated at least three times to ensure its reproducibility. In Figure 5.3, the

experimental pressure and temperature chosen for this work is mapped in the P-T phase equilibrium data for both CH_4–water and CH_4–THF-water system.

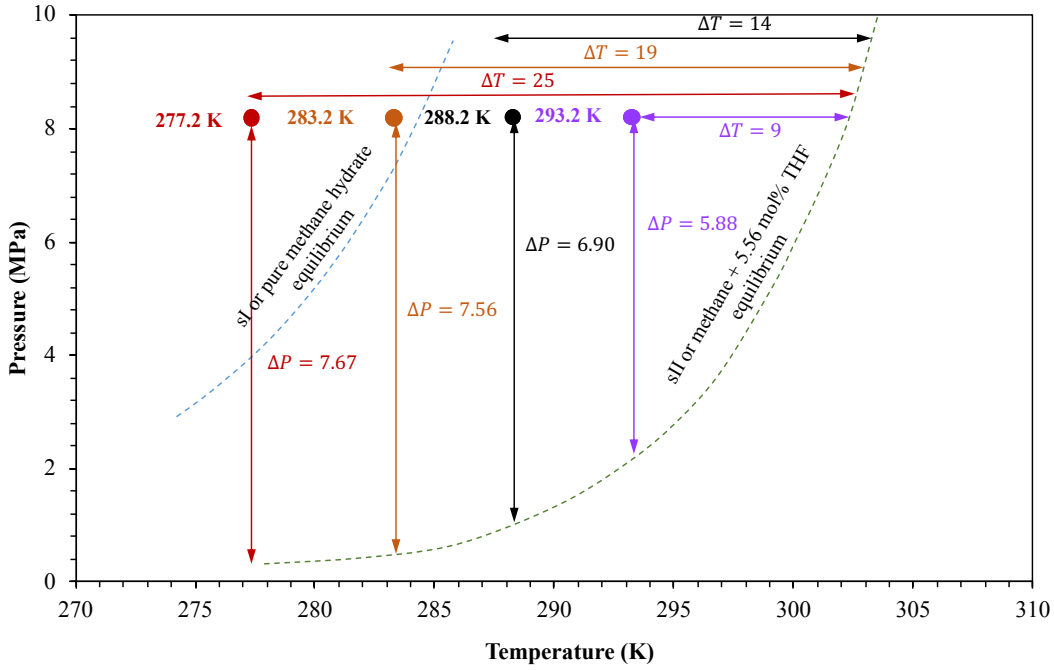

Figure 5.3 Temperature and pressure driving forces of the experiments at 277.2, 283.2, 288.2 and 293.2 K and 8 MPa, respectively. sI and sII equilibrium data were obtained from Nakamura *et al.* (2003) and Lee *et al.* (2012), respectively.

To further elucidate the effects of temperature on the hydrate formation kinetics, Figure 5.4 shows methane uptake profiles for the methane hydrate formation with the presence of 5.56 mol% THF at 8 MPa and different temperatures. The profiles start from the first hydrate nucleation and stop at 540 min. The standard deviation during the hydrate formation is included with the shaded region. From Figure 5.4, the fastest methane uptake is from the experiment conducted at 277.2 K, while the experiment conduct at 293.2 K is slowest methane uptake. It can see from the Figure 5.4 that the hydrate formation completed about 40, 100, 160 and 500 min after the nucleation for 277.2, 283.2,288.2 and 293.2 K, respectively. The methane hydrate formation kinetics can also be represented by t_{90}, which is the time to achieve 90% of final methane uptake and shown in Figure 5.5. Both the rate of methane hydrate formation observed from the slopes of methane uptake profile and t_{90} at 277.2 K are

significantly faster than that at the higher temperatures. This can be attributed to the higher driving force of hydrate formation at 277.2 K than the formation conducted at the other temperatures. The initial pressure and temperature driving forces for these four experiments are calculated from the equilibrium curve in Figure 5.3. From the figure, increasing the temperature from 277.2 K to 293.2 K, the initial pressure and temperature driving forces decrease from 7.67 to 5.88 MPa and 25 to 9 K resulting in the slow methane hydrate formation kinetics. In addition, the t_{90} increases up to 12.1 times higher from the increased temperature.

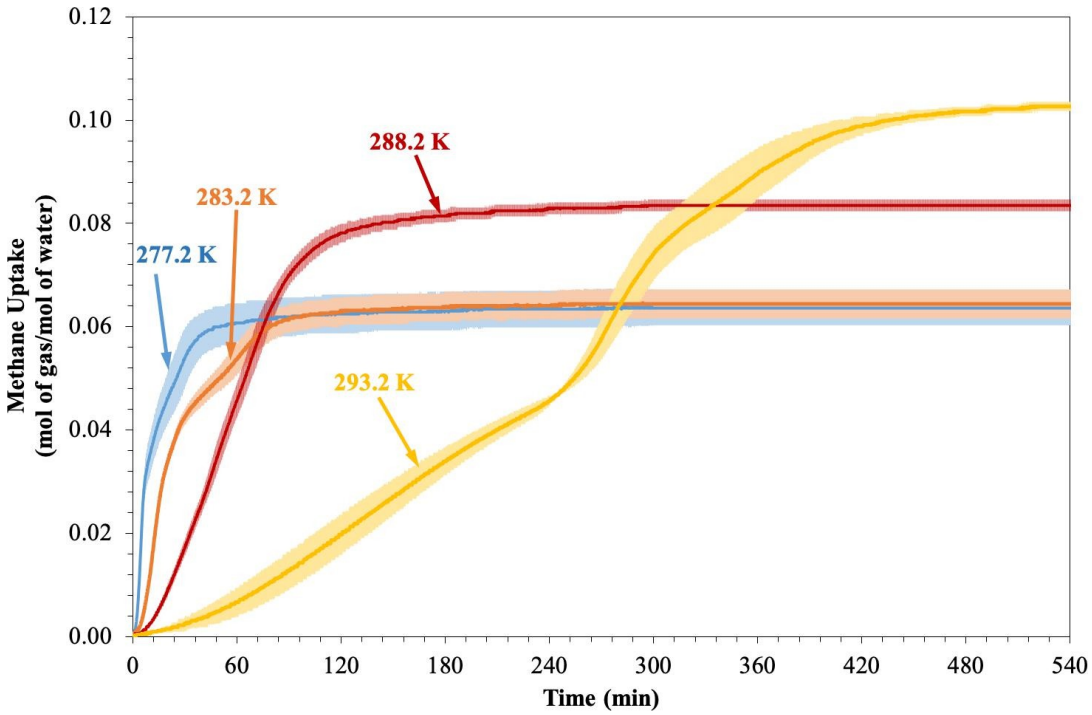

Figure 5.4 Methane uptake profiles for methane hydrate formation with the presence of 5.56 mol% THF at 277.2, 283.2, 288.2 and 293.2 K after nucleation.

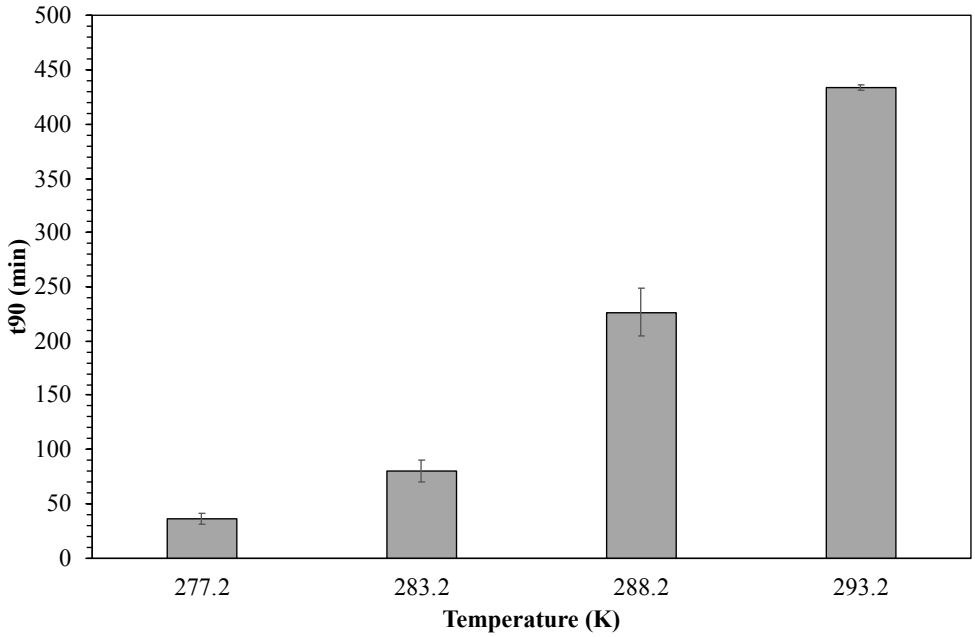

Figure 5.5 t_{90} of the methane hydrate formation with the presence of 5.56 mol% THF at 8 MPa and 277.2, 283.2, 288.2 and 293.2 K.

It is interesting to observe in Figure 5.4 that there was a distinctive slope change in the methane uptake profile about 255 min for the experiments conducted at 293.2 K. In order to further explain the two stages behavior of hydrate growth for methane hydrate formation experiments conducted at 293.2 K, the temperature profiles during the hydrate formation experiment till 500 min after starting experiment of all experimental temperature were shown in Figure 5.6. Figure 5.6 shows the temperature profiles at the gas and liquid interface, T2, conducted at 277.2, 283.2, 288.2, and 293.2 K and 8MPa from the start of the experiment to 500 min. As seen in the Figure 5.6, the experiments conducted at 277.2 K and 283.2 K show only one board peak of heat release, while those at 288.2K and 293.2 K show multiple temperature peaks including board peak and sharp peak. The multiple temperature peaks are resulted from the multiple hydrate nucleation as reported by Veluswamy *et al.* (2016a). The broaden peaks imply longer methane hydrate formation time. Kumar *et al.* (2019) reported mixed methane hydrate formation mechanism in the presence of THF as a promoter. They used *in-situ* Raman spectroscopy in order to analyze the molecular level during the real time mixed methane–THF formation. They found that on the real time methane

occupancy in the small cages and THF in the large cages of sII hydrates during the hydrate formation. Therefore, the presence of 5.56 mol% THF and the experimental conditions employed it is plausible that the hydrates formed is only sII structure.

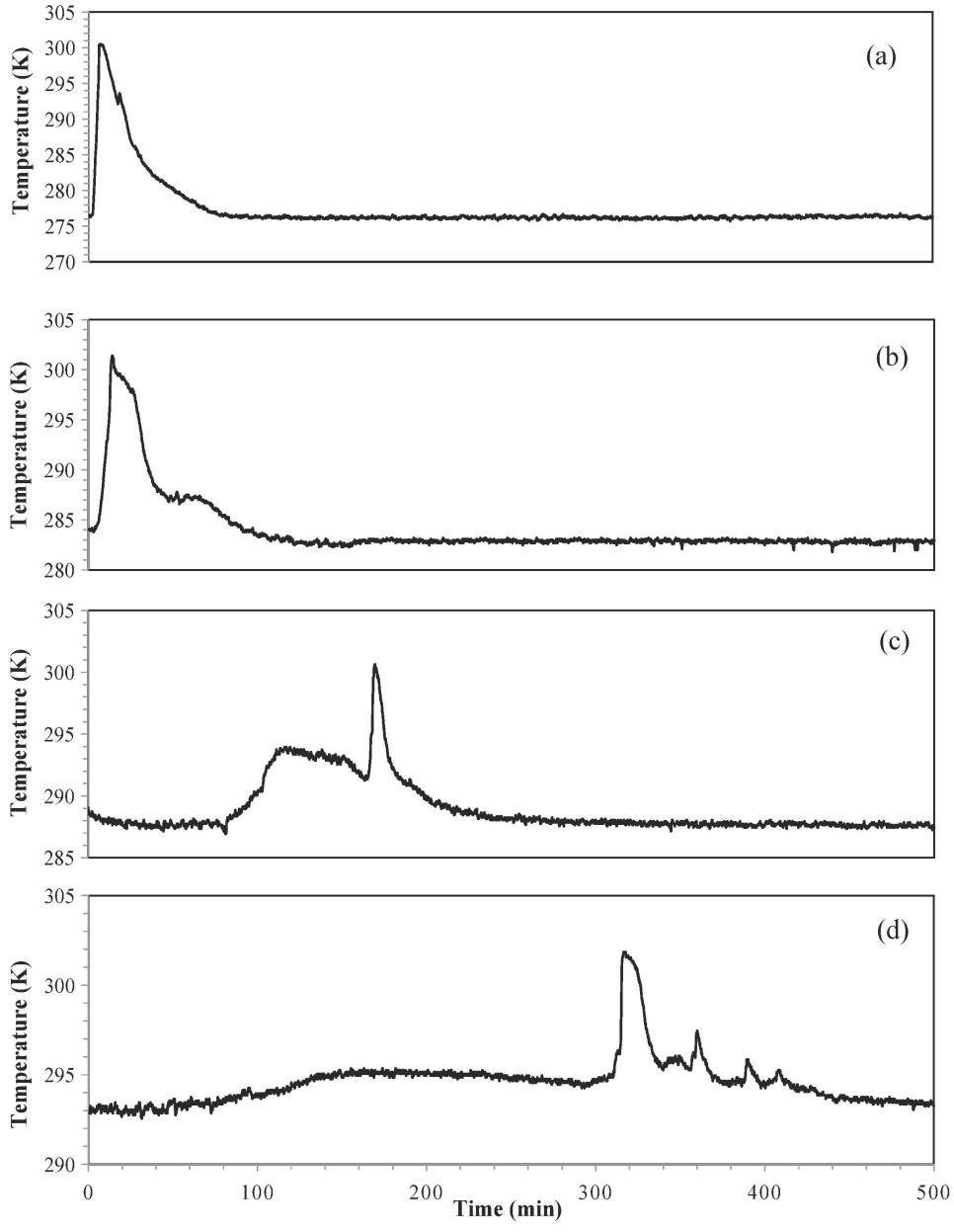

Figure 5.6 Temperature profiles at the gas and liquid interphase during the methane hydrate formation with the presence of 5.56 mol% THF at (a) 277.2 (Exp. No. A1, Table 6.1), (b) 283.2 (Epx. No. B2, Table 6.1), (c) 288.2 (Exp. No. C1, Table 6.1) and (d) 293.2 K (Exp. No. D3, Table 6.1) and 8 MPa.

Table 5.1 Hydrate formation at different temperatures and 8 MPa

Exp. No.	Experimental Temperature (K)	Induction Time (min)	t_{90} (min)	Methane Uptake (mole gas/mole of water)
A1		0.5	32.83	0.0700
A2	277.2	0.5	32.83	0.0629
A3		0.33	42.67	0.0624
B1		1.5	71.17	0.0701
B2	283.2	2.67	74.33	0.0655
B3		8.17	94.33	0.0644
C1		82.17	252.17	0.0940
C3	288.2	89.67	197.83	0.0884
C3		94.5	229.5	0.0884
D1		94.17	436.67	0.1041
D2	293.2	92.5	433.5	0.1067
D3		103.17	430.89	0.1064

Table 5.1 summarizes the THF-methane hydrate formation at 8 MPa and different experimental temperatures. The induction time, when the first nucleation is observed, of the hydrate formation with the presence of 5.56 mol% THF at 8 MPa is shown in Figure 5.7. As seen in the Figure 5.7, the hydrate nucleation starts within 5 min for the experiments at 277.2 and 283.2 K, while it takes longer than one hour for those at 288.3 and 293.2 K. It clearly shows that the induction time from the formation starting in the sI region is significantly faster than in the sII region. This could be attributed to the solubility of methane, which plays a critical role on the hydrate nucleation. The methane solubility dramatically decreases when the temperature increases (Lekvam and Bishnoi, 1997) It is the solubility that governs how much methane dissolves into the solution until reaching the supersaturation condition and methane nucleation afterwards. That is why increasing the temperature results in the long induction time.

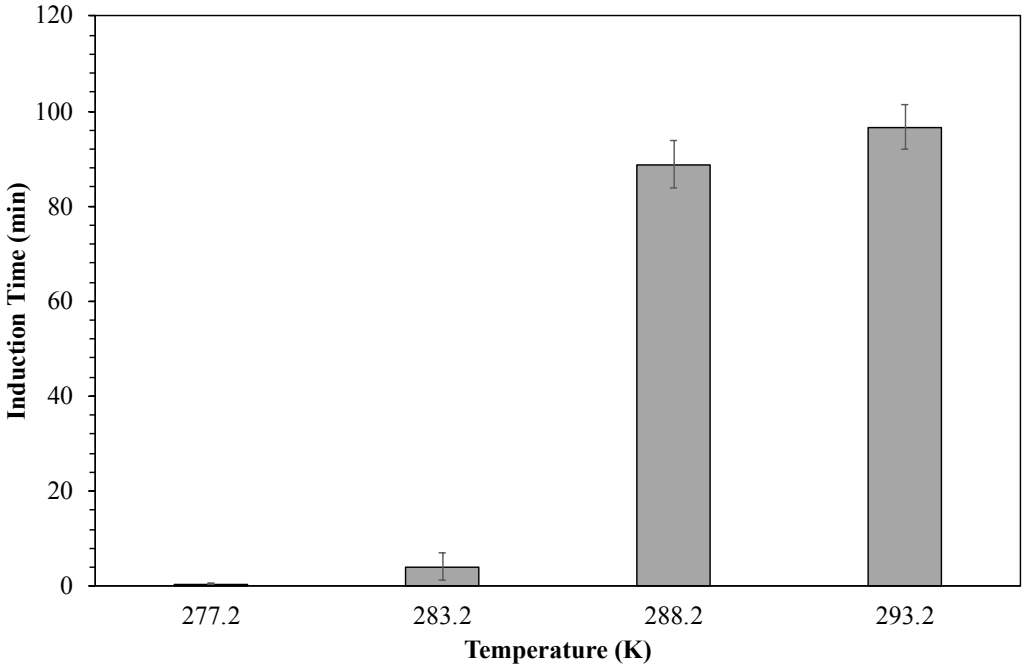

Figure 5.7 Induction time of the methane hydrate formation with the presence of 5.56 mol% THF at 8 MPa and 277.2, 283.2, 288.2 and 293.2 K.

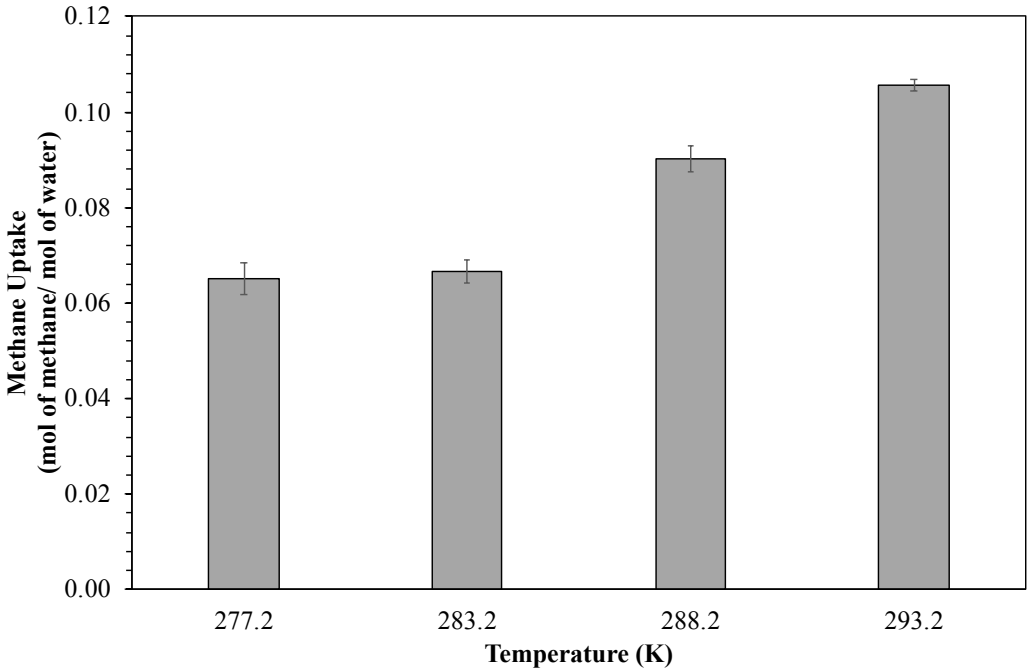

Figure 5.8 Methane uptake at the end of hydrate formation (ca. 660 min after the induction time) with the presence of 5.56 mol% THF at 8 MPa.

The methane uptake at the end of the methane hydrate formation with the presence of 5.56 mole% THF (ca. 660 min after the start of the experiment) conducted at 8 MPa and different temperatures is shown in Figure 5.8. As seen in the Figure 5.8, the methane uptake increases with the increase in the experimental temperature. The experiment conducted at 293.2 K has the highest methane uptake of 0.1057 ± 0.0012 mole gas/mole water, albeit slowest hydrate formation kinetics. Although the methane hydrate formation conducted at 277.2 K has higher hydrate growth kinetics than at 283.2K, the methane uptakes capacity is about the same. This could be attributed to the thermodynamics of the hydrate formation. The heat generated during the hydrate formation can hinder the hydrate growth. At 277.2 and 283.2 K, the heat released from the hydrate formation, observed from the temperature profile in Figures 5.6a and 5.6b, is distributed less effectively to the surrounding, resulting in the disruption of the hydrate growth. On the contrary, at 288.2 and 293.2 K, the first peak of the temperature profiles, Figures 5.6c and 5.6d, gradually increase meaning that the heat generated during the hydrate formation can be dissipated effectively as the methane uptake gradually increases. Additionally, the experiments conducted at 288.2 and 293.2 K show the sharp peak implying that methane is converted to gas hydrates immediately resulting in the higher methane uptake than that from the experiments at 277.2 and 283.2 K. Moreover, the broad peak of the experiment conducted at 293.2 K is broader than that at 288.2 K implying that the heat is distributed to the surrounding more effectively than at 288.2 K. Furthermore, the experiment conducted at 293.2 K shows multiple small peaks after the second peak, hence, the increased methane uptake, and it is at this condition that has the highest methane uptake. Another reason that the methane hydrates form faster in the experiments conducted at 277.2 and 283.2 K could be the dense and stiff hydrates at the interface blocking the gas to further form the hydrate crystals (Tanaka *et al.*, 2009). As the experiment conducted at 293.2 K has the slowest methane hydrate formation rate, there is a lower extent of hydrate layer blockage resulting in the highest methane to hydrate conversion.

The higher methane uptake from the experiment at 293.2 K may be best described by the corresponding theoretical predictions by de Deugd *et al.* (2001) and

Yoon (2012). de Deugd *et al.* (2001) proposed a model to calculate the fractional occupancy of methane and THF in the small cavity and large cavity by Langmuir adsorption model. The results indicated that, when the temperature was increased, the fractional occupancy of methane in both small cavity and large cavity increased, while the fractional occupancy of THF in the large cage of sII structure decreased with the increase in the temperature. Yoon (2012) reported that the methane gas occupied in the small 5^{12} cages of sII gradually increased with the increase in the temperature based on theoretical predictions of the occupancy behavior applying Soave-Redlich-Kwong (PSRK) method. The result indicated that. The theoretical calculation clearly substantiates why the methane uptake at 293.2 K is the highest.

5.4.2 Effects of Pressure on the Methane Hydrate Formation at High Temperatures

Results from the effect of temperature clearly indicate that the higher methane uptake can be achieved at a high temperature being in sII region with the presence of 5.56 mol % THF. Also, Kumar *et al.* (2019) reported that the mixed methane–THF hydrate at the lower pressure being in sII region showed extremely stable of mixed hydrate pellet for a period of two months. So that, to investigate the holistic effects of temperature, the pressure is decreased from 8 MPa to 4 and 6 MPa. Note that, for 6 MPa and 4 MPa, the methane hydrate formation experiment was conducted only at 288.2 K and they are in the sII region.

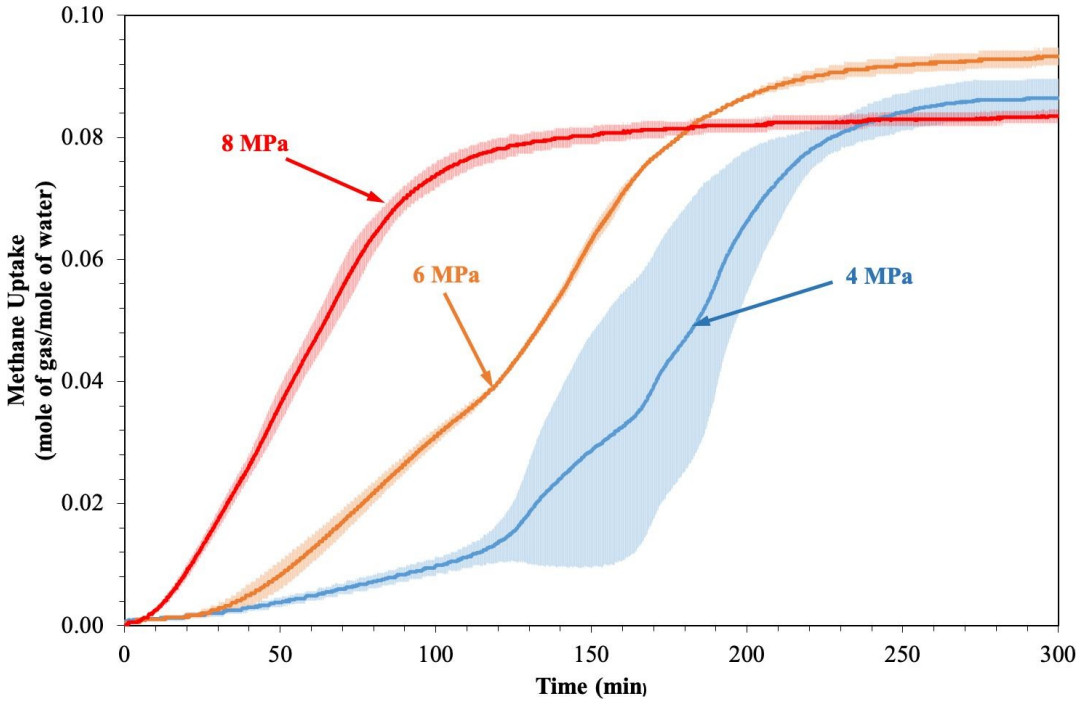

Figure 5.9 Methane uptake profiles for experiments conducted at 4, 6 and 8 MPa and 288.2 K after nucleation. The solid lines are the average data and shaded region represent the standard deviation.

Figure 5.9 shows the hydrate growth profiles during the hydrate formation observed at different starting pressures at 288.2 after 300 min from nucleation. As seen in the Figure 5.9, the hydrate formation at 8, 6, and 4 MPa completes within 160, 250, and 280 min, respectively. Moreover, the hydrate formation rate decreases with decreasing experimental pressure, which corresponds with t_{90} in Figure 5.10. It can be clearly seen that both the hydrate formation rate and t_{90} decrease with the lowered experimental pressures from 8 MPa to 4 MPa as the result of the decrease in the initial pressure driving force from 6.90 to 2.70 MPa.

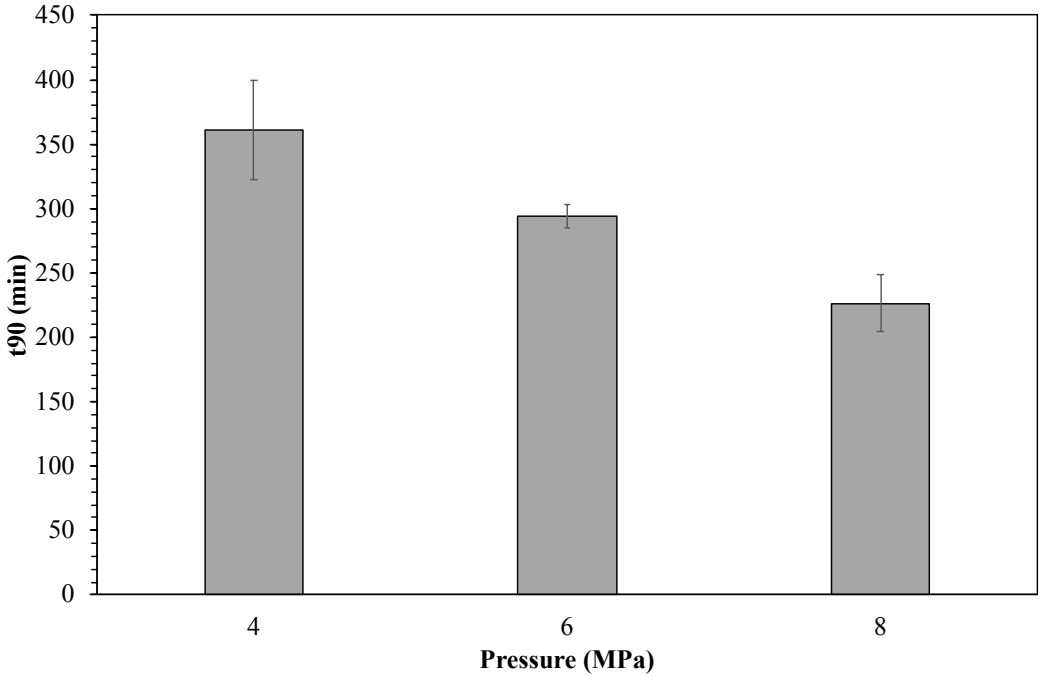

Figure 5.10 t_{90} of the methane hydrate formation with the presence of 5.56 mol% THF at 288.2 K and 4, 6 and 8 MPa.

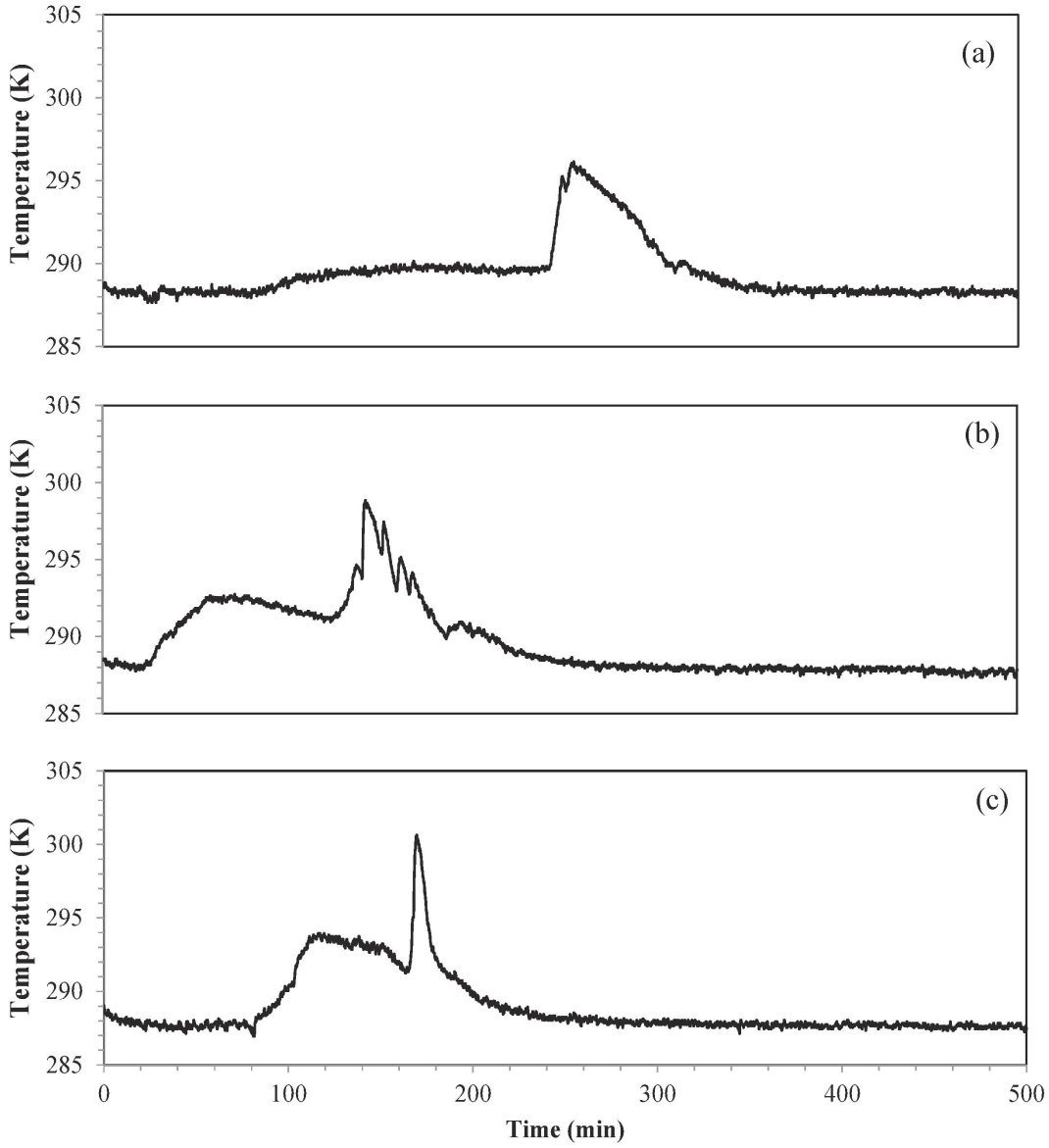

Figure 5.11 Temperature profiles at the gas and liquid interphase during the methane hydrate formation with the presence of 5.56 mol% THF at (a) 4 (Exp. No. E2, Table 2), (b) 6 (Exp. No. F3, Table 2), and (c) 8 MPa (Exp. No. C2, Table 2) and 288.2 K.

It can be observed in Figure 5.8 that there was a distinctive slope change in the methane uptake profile about 120 and 130 min for the experiments conducted at 6 and 4 MPa, respectively, so that the temperature profiles during the hydrate formation experiment was used in order to explain this phenomenon. Figure 5.11 presents the temperature profiles during the hydrate formation conducted at 4, 6, and

8 MPa and 288.2 K with the presence of 5.56 mole%. The temperature profiles consist of two main peaks resulted from the multiple nucleation during the formation, the behavior of which was also reported by Veluswamy *et al.* (2016a). It should be noted that there are two board temperature peaks for the formation at 4 and 6 MPa, while with 8 MPa, there are board and sharp peaks for the first and second peak, respectively. In general, the first peak is due to first nucleation, while the second peak means the secondary nucleation.

Table 5.2 Hydrate formation experimental conditions at difference pressure conducted at 288.2 K

Exp. No.	Experimental Pressure (MPa)	Induction Time (min)	t_{90} (min)	Methane Uptake (mole gas/mole of water)
E1		80.33	375.83	0.0855
E2	4	99.17	399.67	0.0876
E3		84.83	307.83	0.0895
F1		29.67	293.5	0.0970
F2	6	12.83	305.33	0.0980
F3		28.33	283.17	0.0945
C1		82.17	252.17	0.0940
C2	8	89.67	197.83	0.0884
C3		94.5	229.50	0.0884

The THF–CH_4 hydrate formation at 288.2 K and different experimental pressures is summered in Table 5.2. As seen in the Figure 5.12, the induction time of the experiments conducted at 4, 6, and 8 MPa are random confirming that the formation is stochastic in nature (Sloan and Koh, 2008; Veluswamy *et al.*, 2016a).

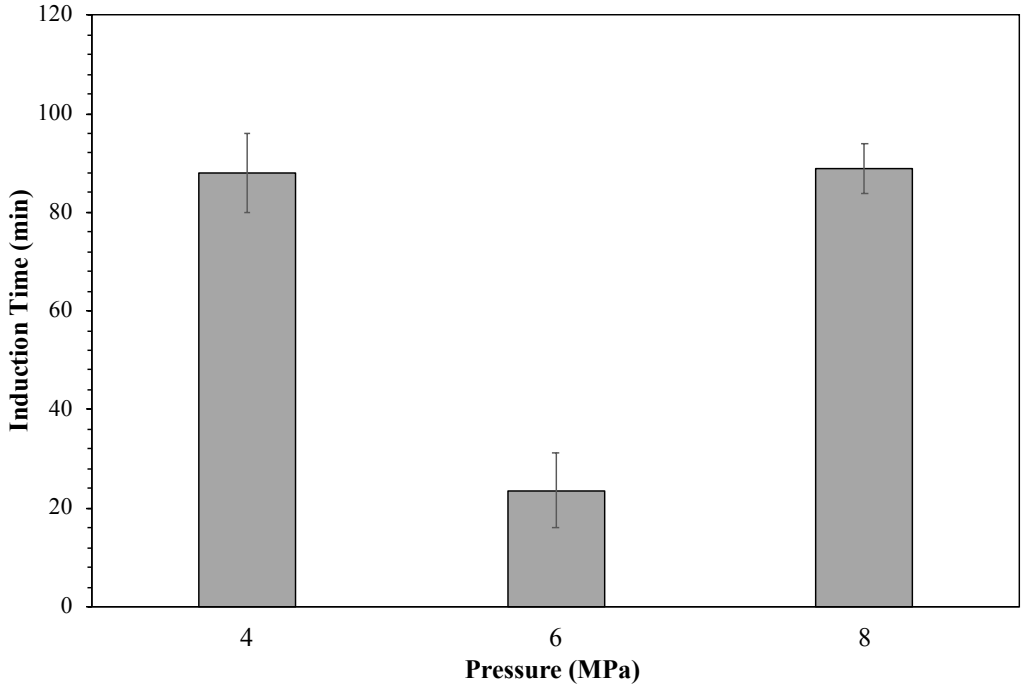

Figure 5.12 Induction time of the methane hydrate formation with the presence of 5.56 mol% THF at 288.2 K and 4, 6 and 8 MP.

Figure 5.13 shows the methane uptake at the end of hydrate formation (ca. 660 min after the start of the experiment) with the presence of 5.56 mol% THF at 288.2 K and different pressures. As seen in the Figure 5.13, the methane uptakes at the end of hydrate formation of all experiments are about the same in spite of the decrease in the pressure driving force. This could be attributed to the fact that, at the lower pressure, the low formation rate facilitates effective heat distribution to the surrounding and prevents the accumulated heat to hinder further hydrate formation.

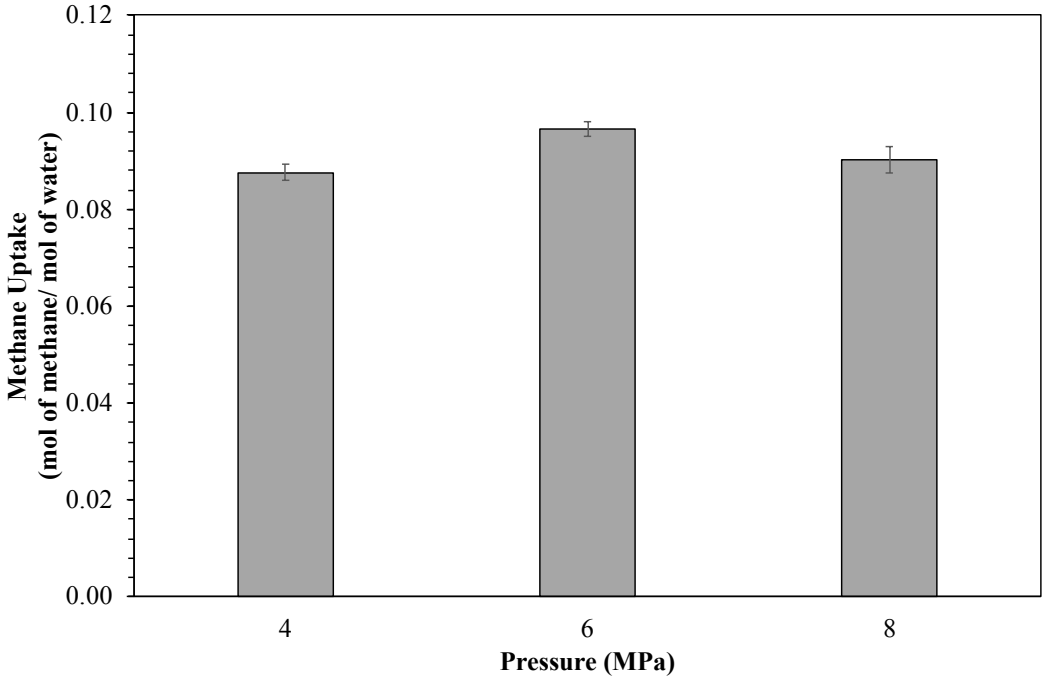

Figure 5.13 Methane uptake at the end of hydrate formation (ca. 600 min after the induction time) with the presence of 5.56 mol% THF at 288.2 K.

Figure 5.14 presents the P-T profiles observed during the hydrate formation with different pressures of 4, 6, and 8 MPa and 288.2 K. All experimental pressures start in the sII region. It can be observed that, while the temperature increases from the starting temperature, the pressure decreases due to the methane gas in the crystallizer is converted to methane hydrates. Moreover, the P-T profiles can be divided into three steps. From point A to point B, the temperature in the system slightly increases and, at the same time, the pressure in the system slightly decreases as the small amount of methane gas is converted to hydrates corresponding with the gradual increase of the first peak in the temperature profile, shown in Figure 5.11. After that, the temperature from point B rises immediately to point C on the equilibrium curve for all experiments conducted at 283.2 K showing that the temperature driving force is reduced due to the exothermic heat released during the hydrate formation, which corresponds with the second peak of the temperature profiles, Figure 5.11. From point C to point D, the temperatures decrease on the boundary of the equilibrium curve. After that, the temperatures steeply decrease back to the starting experimental temperature. It is interesting to note that, during this step, the pressure dramatically

decreases due to a lot of methane gas is converted to methane hydrates. The steep decrease in the pressure further implies that there is lower driving force available during the course of hydrate formation. The P-T profiles play an important role to hydrate technology development for gas storage application. From the above observation, it may be suggested that the hydrate formation should be controlled in such a way that it is operated isobarically while the temperature is maintained on the sII equilibrium boundary.

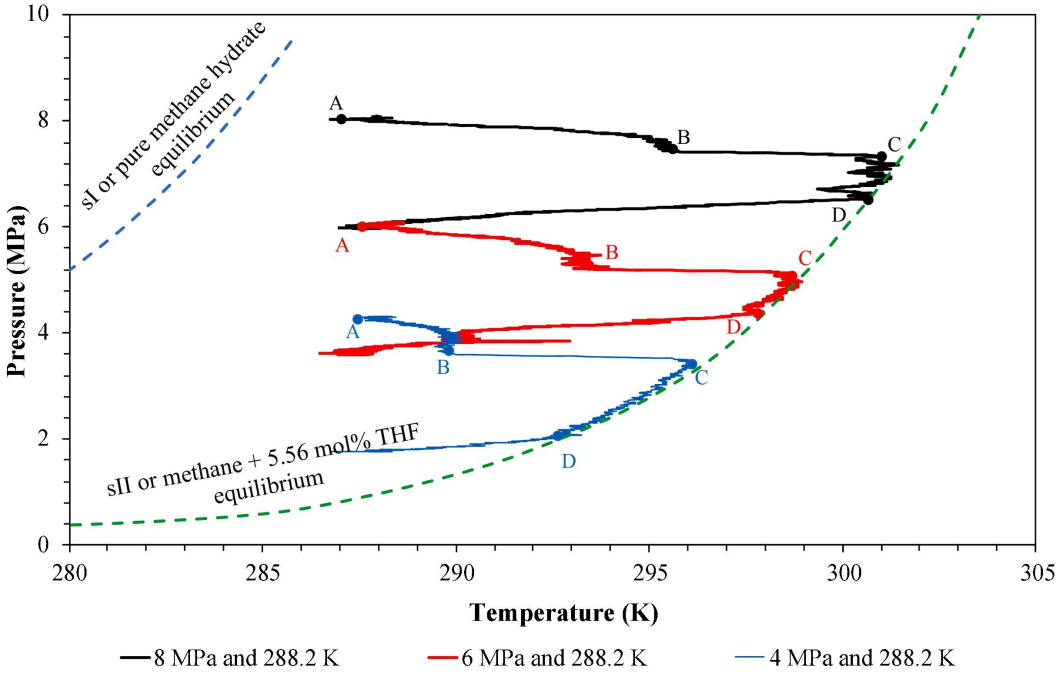

Figure 5.14. P–T profiles during hydrate formation for experiments at 288.2 K and different stating pressure of 8, 6, and 4 MPa,. sI and sII (mixed methane/5.56 mol% THF) equilibrium data were taken from Nakamura *et al.* (2003) and Lee *et al.* (2012), respectively.

Moreover, this work studies the methane hydrate dissociation after complete hydrate formation by using the thermal stimulation method to recover methane gas. The temperature in the system is increased to 308.2 K, which is outside the sII phase equilibrium. The final methane recovery of both temperature and pressure effects is in the range of 89.05 - 96.56 %. The result indicates both pressure and temperature did not affect the final methane recovery. The details about the percentage

of methnae recovery is given in Figure S5.1 in Supporting Information. As seen in the Figure S1, the final methane recovery is in the range of 89.05 - 96.56 %, 96.25 - 97.12%, and 95.32-96.00% for the experiments conducted at 8, 6, and 4 MPa, respectively. The result indicates both pressure and temperature did not affect on the final methane recovery.

5.4.3 Effect of MES Surfactant on the Methane Hydrate Formation

The result from the effect of temperature on the methane hydrate formation show that the methane uptake is at the highest with the presence of THF at 293.2 K and 8 MPa. However, the hydrate formation is slow and takes more than 400 min to reach the 90% of final methane uptake. In order to improve of the methane hydrate formation kinetics at 293.2 K and 8 MPa, the presence of anionic surfactant, methyl ester sulfonate (MES), is used as a co-promoter with THF. MES was chosen in this work because it is inexpensive and biodegradable. The concentration of MES was varied from 1 to 6 mM, which covers the value above and below the critical micelle concentration (CMC), 4 mM.

Figure 5.15 shows the effects of MES concentration. It can be clearly seen from the Figure 5.15 (top plot) that the presence of MES both lower and higher CMC improves the methane formation kinetics significantly with the completion of methane hydrate formation about 60 min after hydrate nucleation compared to more 500 min for the case without MES. Moreover, it can be observed that the final methane uptake is about the same for both with and without MES. Figure 5.15 (bottom plot) shows the promotion effect of MES on the methane hydrate formation within 60 min from nucleation. As evidently presented in Figure 5.15 (bottom plot), the methane uptake was merely 0.006 mole gas/mole water when operating without MES surfactant. In the case of adding MES surfactant of all concentration, the methane uptake increased to 0.9 mole gas/mole water in the end of 60 min after hydrate nucleation.

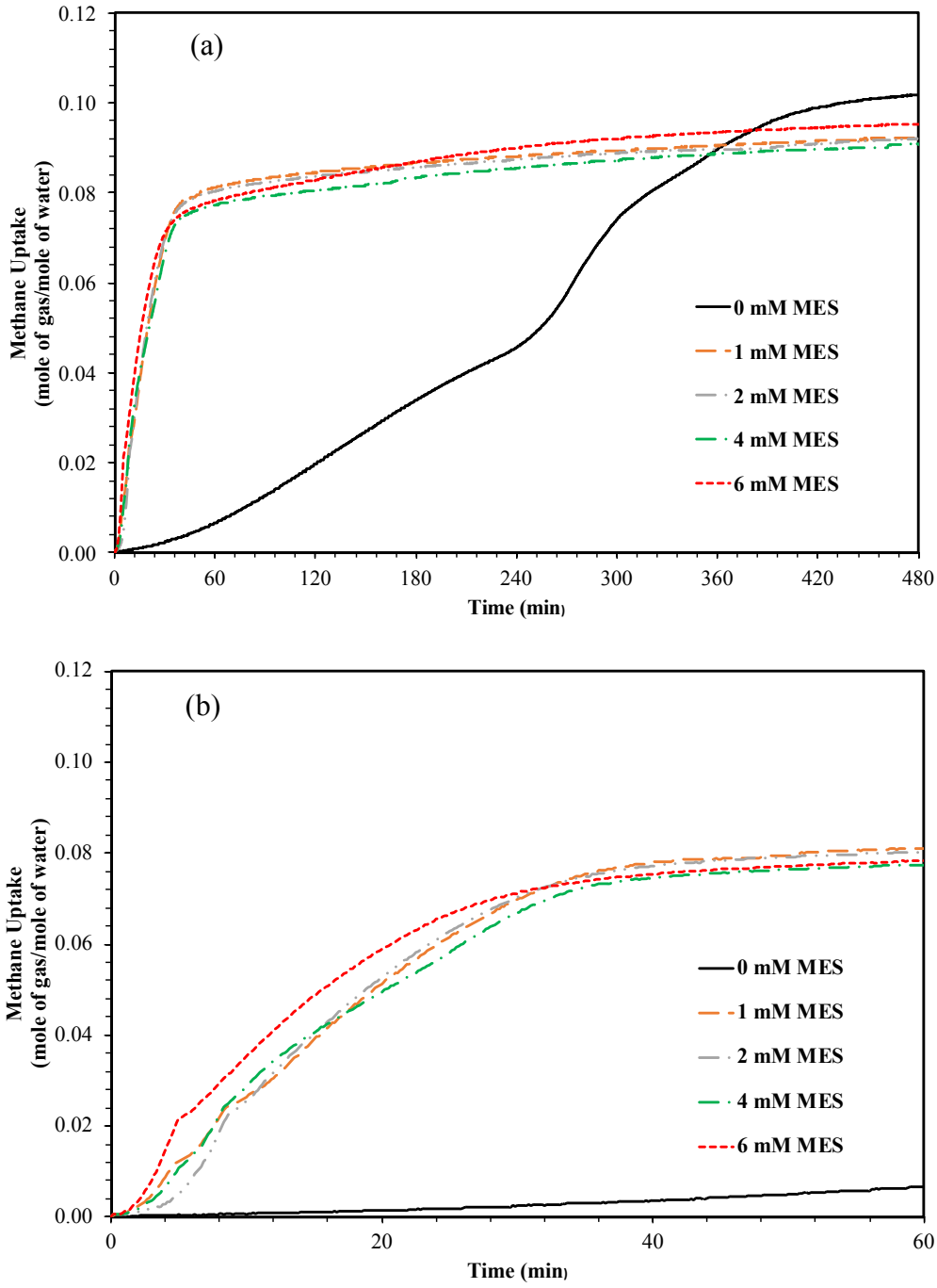

Figure 5.15 (a) Methane uptake profiles for experiments conducted at 8 MPa and 293.2 K after nucleation in the presence of mixed MES and 5.56 mol% THF (b) expanded to show the kinetic promotion over one hour of hydrate growth period.

Table 5.3 Hydrate formation at difference MES conducted at 293.2 K and 8 MPa

Exp. No.	MES Concentration (mM)	Induction Time (mim)	t_{90} (min)	Methane Uptake (mole gas/mole of water)
D1	0	94.17	436.67	0.1041
D2		92.5	433.5	0.1067
D3		103.17	430.89	0.1064
G1	1	70	351.63	0.0984
G2		73.2	338.67	0.0941
G3		71.1	346.76	0.0971
H1	2	32.1	303.3	0.0944
H2		31.33	292	0.0976
H3		36.66	306.5	0.0896
I1	4	17	298.87	0.0958
I2		16.66	292.33	0.0922
I3		20.2	260.33	0.0898
J1	6	15.58	261	0.0938
J1		18.67	267	0.0963
J3		16.67	284	0.0969

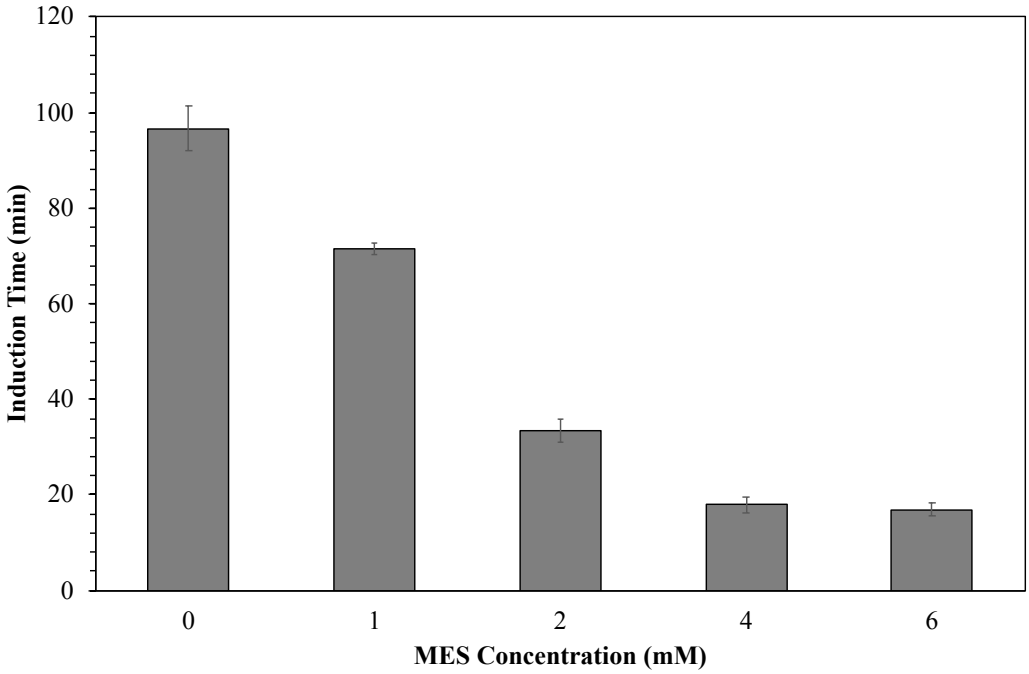

Figure 5.16 Induction time of methane hydrate formation at 8 MPa and 293.2 K with the presence of 5.56 mol% THF and different MES concentrations.

Table 5.3 summarized the methane hydrate formation in the presence of different MES concentration at 293.2 K and 8 MPa. Figure 5.16 presents the induction time observed for experiments with different surfactant concentrations. Results from the system with only 5.56 mol% THF have also been included for comparison. It can be seen from Figure 5.16 that the induction time decreases with increasing the concentration of MES. It could be attributed to the decrease in interfacial tension with the increase in the MES concentration. Zhang *et al.* (2007) reported that the surfactant concentration strongly affected the induction time. Moreover, it can be observed form the Figure 5.16 that the hydrate formation with presence of MES concentration above the CMC does not lead to further decrease in the induction time. This result is consistent to the study by Zhong and Rogers (2000). They reported that the increase in the surfactant concentration promoted the induction time on the hydrate formation. However, the concentration of surfactant exceeded the CMC would not lead to further decrease in the induction time.

5.5 Conclusions

The experiments were performed to study the effect of the stoichiometric THF (5.56 mol%) on methane hydrate formation in the quiescent reactor at different temperatures and pressures. The experiment was conducted at 8 MPa and four different temperatures, 277.2, 283.2, 288.2, and 293.2 K. The experimental temperature was divided into two regions corresponding to the sI (277.2 and 283.2 K) and sII (288.2 and 293.2 K) regions in the methane + 5.56 mol% THF hydrate formation phase diagram. The result showed that the formation starting with the temperature in the sI region had higher methane hydrate formation rate due to the higher temperature and pressure driving forces. On the contrary, starting with the temperature in the sII region, the formation had higher methane uptake due to two-stage hydrate growth and effective heat distribution to the surrounding. The formation was also conducted at 288.2 K with three different pressures, 4, 6, and 8 MPa, to study the effects of pressure. The result showed that, using the lower pressure, the formation rate deceased as the result of the decrease in the pressure driving force. The methane uptake was similar at the investigated pressures. Moreover, the methane hydrate/THF hydrate formation kinetics at 293.2 K and 8 MPa was enhanced by using MES surfactant. The presence of MES showed faster hydrate nucleation and shorter t_{90}. The increase in MES concentration decrease both induction time and t_{90}. The methane uptake in the presence of MES are about the same of all concentration. The methane recovery did not significant different with changing hydrate formation condition. Average gas recovery of 89.05 - 97.25%% was achieved on dissociating hydrates formed from the different starting pressure and temperature condition.

5.6 Acknowledgements

This work was supported by The Royal Golden Jubilee Ph.D. Program (2.P.CU/58/J.1), Thailand Research Fund; The Petroleum and Petrochemical College (PPC), Chulalongkorn University, Thailand; Center of Excellence on Petrochemical and Materials Technology (PETROMAT), Thailand; Grant for International Research Integration: Chula Research Scholar, Ratchadaphiseksomphot Endowment Fund,

Chulalongkorn University, Thailand; Thailand Energy Conservation Fund, Energy Policy and Planning Office Ministry of Energy; Department of Chemical and Biomolecular Engineering, Faculty of Engineering, National University of Singapore (NUS); UOP, A Honeywell Company, USA.

5.7 Supporting Information

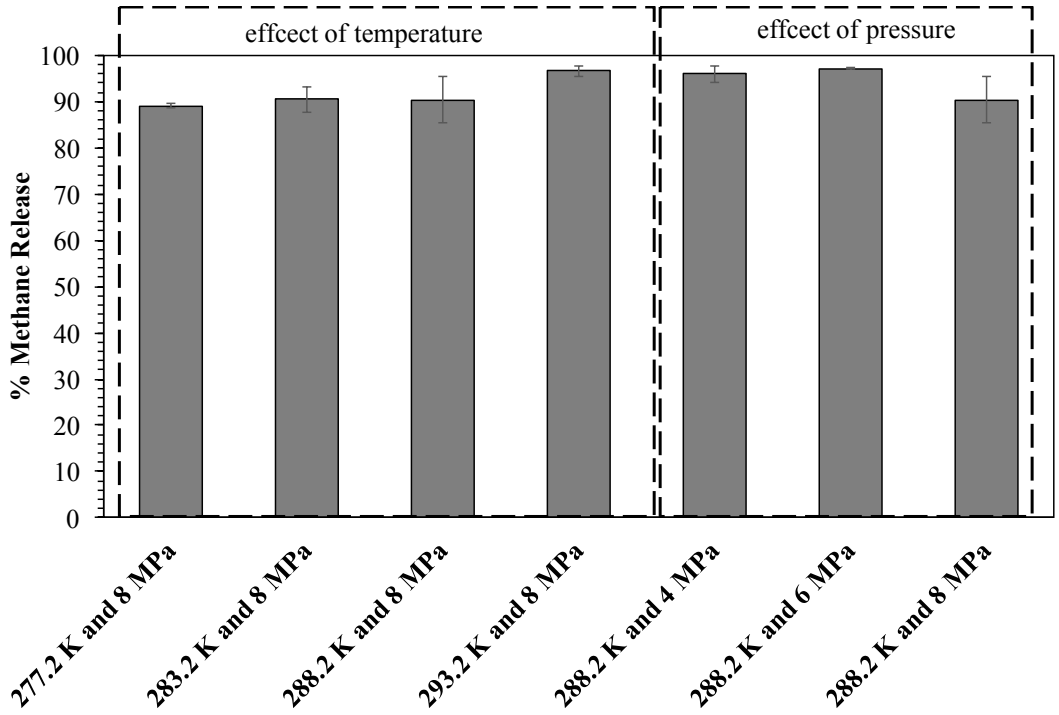

Figure S5.1 presents the methane release percentage for the different systems studied.

5.8 References

Babu, P., Kumar, R., and Linga, P. (2013). Medium pressure hydrate based gas separation (HBGS) process for pre-combustion capture of carbon dioxide employing a novel fixed bed reactor. International Journal of Greenhouse Gas Control, 17, 206-214.

Babu, P., Linga, P., Kumar, R., and Englezos, P. (2015). A review of the hydrate based gas separation (HBGS) process for carbon dioxide pre-combustion capture. Energy, 85, 261-279.

Babu, P., Nambiar, A., He, T., Karimi, I. A., Lee, J. D., Englezos, P., and Linga, P. (2018). A review of clathrate hydrate based desalination to strengthen energy–water nexus. ACS Sustainable Chemistry & Engineering, 6(7), 8093-8107.

de Deugd, R. M., Jager, M. D., and de Swaan Arons, J. (2001). Mixed hydrates of methane and water-soluble hydrocarbons modeling of empirical results. AIChE Journal, 47(3), 693-704.

Demirbas, A. (2010a). Methane hydrates as potential energy resource: Part 1 – Importance, resource and recovery facilities. Energy Conversion and Management, 51(7), 1547-1561.

Demirbas, A. (2010b). Natural Gas. In A. Demirbas (Ed.), *Mathane Hydrate* (pp. 57-76). London, England: Springer-Verlag London.

Englezos, P. (1993). Clathrate hydrates. Industrial & Engineering Chemistry Research, 32(7), 1251-1274.

Florusse, L. J., Peters, C. J., Schoonman, J., Hester, K. C., Koh, C. A., Dec, S. F., Marsh, K. N., and Sloan, E. D. (2004). Stable low-pressure hydrogen clusters stored in a binary clathrate hydrate. Science 306(5695), 469-471.

Ganji, H., Manteghian, M., Sadaghiani zadeh, K., Omidkhah, M. R., and Rahimi Mofrad, H. (2007). Effect of different surfactants on methane hydrate formation rate, stability and storage capacity. Fuel, 86(3), 434-441.

Gough, S. R., and Davidson, D. W. (1971). Composition of tetrahydrofuran hydrate and the effect of pressure on the decomposition. Canadian Journal of Chemistry, 49(16), 2691-2699.

Gudmundsson, J. S., Parlaktuna, M., and Khokhar, A. A. (1994). Storage of natural gas as frozen hydrate. SPE Production & Facilities, 9(01), 69-73.

Haligva, C., Linga, P., Ripmeester, J. A., and Englezos, P. (2010). Recovery of methane from a variable-volume bed of silica sand/hydrate by depressurization. Energy & Fuels, 24(5), 2947-2955.

Han, S., Rhee, Y.-W., and Kang, S.-P. (2017). Investigation of salt removal using cyclopentane hydrate formation and washing treatment for seawater desalination. Desalination, 404, 132-137.

IGU. (2018). Global gas report 2018. In (pp. 60).

Kang, K. C., Linga, P., Park, K.-n., Choi, S.-J., and Lee, J. D. (2014). Seawater desalination by gas hydrate process and removal characteristics of dissolved ions (Na+, K+, Mg2+, Ca2+, B3+, Cl−, SO42−). Desalination, 353, 84-90.

Kang, S.-P., and Lee, H. (2000). Recovery of CO2 from Flue Gas Using Gas Hydrate: Thermodynamic Verification through Phase Equilibrium Measurements. Environmental Science & Technology, 34(20), 4397-4400.

Kumar, A., Daraboina, N., Kumar, R., and Linga, P. (2016). Experimental investigation to elucidate why tetrahydrofuran rapidly promotes methane hydrate formation kinetics: Applicable to energy storage. The Journal of Physical Chemistry C, 120(51), 29062-29068.

Kumar, A., Veluswamy, H. P., Linga, P., and Kumar, R. (2019). Molecular level investigations and stability analysis of mixed methane-tetrahydrofuran hydrates: Implications to energy storage. Fuel, 236, 1505-1511.

Lee, Y.-J., Kawamura, T., Yamamoto, Y., and Yoon, J.-H. (2012). Phase equilibrium studies of tetrahydrofuran (THF) + CH4, THF + CO2, CH4 + CO2, and THF + CO2 + CH4 hydrates. Journal of Chemical & Engineering Data, 57(12), 3543-3548.

Lekvam, K., and Bishnoi, P. R. (1997). Dissolution of methane in water at low temperatures and intermediate pressures. Fluid Phase Equilibria, 131(1), 297-309.

Lin, Y., Veluswamy, H. P., and Linga, P. (2018). Effect of Eco-Friendly Cyclodextrin on the Kinetics of Mixed Methane–Tetrahydrofuran Hydrate Formation. Industrial & Engineering Chemistry Research, 57(17), 5944-5950.

Linga, P., Haligva, C., Nam, S. C., Ripmeester, J. A., and Englezos, P. (2009). Recovery of methane from hydrate formed in a variable volume bed of silica sand particles. Energy & Fuels, 23(11), 5508-5516.

Linga, P., Kumar, R., and Englezos, P. (2007). The clathrate hydrate process for post and pre-combustion capture of carbon dioxide. J Hazard Mater, 149(3), 625-629.

Lozano-Castelló, D., Alcañiz-Monge, J., de la Casa-Lillo, M. A., Cazorla-Amorós, D., and Linares-Solano, A. (2002). Advances in the study of methane storage in porous carbonaceous materials. Fuel, 81(14), 1777-1803.

Makogon, Y. F. (2010). Natural gas hydrates – A promising source of energy. Journal of Natural Gas Science and Engineering, 2(1), 49-59.

Nakamura, T., Makino, T., Sugahara, T., and Ohgaki, K. (2003). Stability boundaries of gas hydrates helped by methane—structure-H hydrates of methylcyclohexane and cis-1,2-dimethylcyclohexane. Chemical Engineering Science, 58(2), 269-273.

Partoon, B., and Javanmardi, J. (2013). Effect of mixed thermodynamic and kinetic hydrate promoters on methane hydrate phase boundary and formation kinetics. Journal of Chemical & Engineering Data, 58(3), 501-509.

Ricaurte, M., Dicharry, C., Renaud, X., and Torré, J.-P. (2014). Combination of surfactants and organic compounds for boosting CO2 separation from natural gas by clathrate hydrate formation. Fuel, 122, 206-217.

Rios, R. B., Stragliotto, F. M., Peixoto, H. R., Torres, A. E. B., Bastos-Neto, M., Azevedo, D. C. S., and Cavalcante Jr, C. L. (2013). Studies on the adsorption behavior of CO2-CH4 mixtures using activated carbon. Brazilian Journal of Chemical Engineering, 30, 939-951.

Sapag, K., Vallone, A., Blanco, A. G., and Solar, C. (2010). Adsorption of Methane in Porous Materials as the Basis for the Storage of Natural Gas. In P. Potocnik (Ed.), *Natural Gas* (pp. 205-244). New York: IntechOpen.

Seo, Y. T., Kang, S. P., and Lee, H. (2001). Experimental determination and thermodynamic modeling of methane and nitrogen hydrates in the presence of THF, propylene oxide, 1,4-dioxane and acetone. Fluid Phase Equilibria, 189(1), 99-110.

Siangsai, A., Rangsunvigit, P., Kitiyanan, B., Kulprathipanja, S., and Linga, P. (2015). Investigation on the roles of activated carbon particle sizes on methane hydrate formation and dissociation. Chemical Engineering Science, 126, 383-389.

Sloan, E. D., and Koh, C. A. (2008). *Clathrate Hydrates of Natural Gases*. New York: CRC Press.

Smith, J. M., Van Ness, H. C., and Abbott, M. M. (2005). *Introduction to Chemical Engineering Thermodynamics*. Singapore: McGraw-Hill.

Sun, Q., Chen, G., Guo, X., and Liu, A. (2014). Experiments on the continuous separation of gas mixtures via dissolution and hydrate formation in the presence of THF. Fluid Phase Equilibria, 361, 250-256.

Sun, Z., Wang, R., Ma, R., Guo, K., and Fan, S. (2003). Natural gas storage in hydrates with the presence of promoters. Energy Conversion and Management, 44(17), 2733-2742.

Tanaka, R., Sakemoto, R., and Ohmura, R. (2009). Crystal growth of clathrate hydrates formed at the interface of liquid water and gaseous methane, ethane, or propane: Variations in crystal morphology. Crystal Growth & Design, 9(5), 2529-2536.

Tang, J., Zeng, D., Wang, C., Chen, Y., He, L., and Cai, N. (2013). Study on the influence of SDS and THF on hydrate-based gas separation performance. Chemical Engineering Research and Design, 91(9), 1777-1782.

Veluswamy, H. P., Kumar, A., Seo, Y., Lee, J. D., and Linga, P. (2018). A review of solidified natural gas (SNG) technology for gas storage via clathrate hydrates. Applied Energy, 216, 262-285.

Veluswamy, H. P., Kumar, S., Kumar, R., Rangsunvigit, P., and Linga, P. (2016a). Enhanced clathrate hydrate formation kinetics at near ambient temperatures and moderate pressures: Application to natural gas storage. Fuel, 182, 907-919.

Veluswamy, H. P., Wong, A. J. H., Babu, P., Kumar, R., Kulprathipanja, S., Rangsunvigit, P., and Linga, P. (2016b). Rapid methane hydrate formation to develop a cost effective large scale energy storage system. Chemical Engineering Journal, 290, 161-173.

Wang, X., French, J., Kandadai, S., and Chua, H. T. (2010). Adsorption measurements of methane on activated carbon in the temperature range (281 to 343) K and pressures to 1.2 MPa. Journal of Chemical & Engineering Data, 55(8), 2700-2706.

Yang, M., Song, Y., Jiang, L., Liu, W., Dou, B., and Jing, W. (2014). Effects of operating mode and pressure on hydrate-based desalination and CO2 capture in porous media. Applied Energy, 135, 504-511.

Yoon, J.-H. (2012). A theoretical prediction of cage occupancy and heat of dissociation of THF-CH4 hydrate. Korean Journal of Chemical Engineering, 29(12), 1670-1673.

Zakaria, Z., and George, T. (2011). The performance of commercial activated carbon absorbent for adsorbed natural gas storage. International Journal of Recent Research and Applied Studies, 9(2), 6.

Zhang, J. S., Lee, S., and Lee, J. W. (2007). Does SDS micellize under methane hydrate-forming conditions below the normal Krafft point? Journal of Colloid and Interface Science, 315(1), 313-318.

Zhang, T., Walawender, W. P., and Fan, L. T. (2010). Grain-based activated carbons for natural gas storage. Bioresource Technology, 101(6), 1983-1991.

Zhong, Y., and Rogers, R. E. (2000). Surfactant effects on gas hydrate formation. Chemical Engineering Science, 55(19), 4175-4187.

CHAPTER VI
INNOVATIVE APPROACH TO ENHANCE THE METHANE HYDRATE FORMATION AT NEAR AMBIENT TEMPERATURE AND MODERATE PRESSURE FOR GAS STORAGE APPLICATIONS

6.1 Abstract

Solidified natural gas (SNG) technology via hydrates is a promising and potential method for storing natural gas. It offers a compact mode of natural gas storage with high degree of safety. In this work, we present the synergistic effects of tetrahydrofuran (THF), hollow silica (HS) and sodium dodecyl sulfate (SDS) in enhancing the kinetics of mixed methane-THF hydrate formation at 6 MPa and 293.2 K in an unstirred reactor configuration. HS at the low loading of 0.5 %w HS/v in 5.56 mol% THF solution used in the current study is an innovative approach to improve the surface contact area resulting in kinetic enhancement at moderate conditions (low driving force). However, the mixture of 0.5 %w HS/v in 5.56 mol% THF solution resulted in a long induction time (about 400 min) which is not favorable for the SNG technology. Addition of SDS decreased the induction time and increased the hydrate formation rate under similar experimental conditions. The induction time significantly decreased with the increase in the SDS concentration. Additionally, the presence of SDS played a key role in influencing the temperature profile and the hydrate morphology during mixed hydrate formation. The methane gas uptake was 0.0591 (±0.0007) and 0.0615 (±0.0023) mol of methane/mol of water without and with SDS respectively. Thermal stimulation with ΔT = 15 Kwas employed to recover methane from hydrates. The results showed that up to 95 % of methane gas can be recovered from the hydrates formed with and without SDS. Interestingly, the presence of HS was effective in preventing the foam generation during hydrate dissociation in the presence of SDS.

Keywords: Methane, Hydrate, Hollow silica, Tetrahydrofuran, Sodium dodecyl sulfate, Morphology

6.2 Introduction

Natural gas is recognized as the clean fossil fuel that is characterized by soot-free combustion as well as the reduction of carbon dioxide emissions. The demand of natural gas is projected to grow at about the same rapid rate (nearly 4% annual average) as it has since 2005, the highest for any fossil fuel, and will be continuously increasing up to 2040 based on the forecast by International Energy Agency (IEA) (EIA, 2017). Veluswamy *et al.* (2018) provided a comparison between conventional technologies, including liquefied natural gas (LNG), compressed natural gas (CNC) and absorbed natural gas (ANG) along with solidified natural (SNG) in their review article. SNG has been highligted as a promising option due to several advantages. SNG technology caters to storing and transporting natural gas in the form of clathrate hydrates. The natural gas hydrates or clathrate hydrates are non-stoichiometric crystalline compounds similar to ice. They are formed by the physical bonding between the water molecules and the light hydrocarbon molecules (small gas molecule), such as methane, ethane, propane etc., in which the light hydrocarbons are encapsulated in the water framework at specific pressure and temperature (Sloan and Koh, 2008). These conditions and size of guest gas molecule control the hydrate structure. Three hydrate structures - structure I (sI), structure II (sII) and structure H (sH) have been reported to exist (Englezos and Lee, 2005; Jager *et al.*, 1999; Khokhar *et al.*, 1998; Sloan and Koh, 2008).

Methane is the main component in natural gas hydrates. About 10 quadrillion cubic meters of gas is estimated to be stored in the hydrate reservoirs, distributed in the sediment under deep-sea and permafrost regions around the world (Boswell and Collett, 2011; Demirbas, 2010; Englezos and Lee, 2005; Makogon, 2010). At standard temperature and pressure, the pure methane hydrates of 1 cubic meter can encage methane gas of about 150 to 180 cubic meters (Koh *et al.*, 2011; Linga *et al.*, 2007; Sloan and Koh, 2008) .This characteristic of the natural gas hydrates is the key factor for enabling the SNG technology for natural gas storage. Other key advantages of SNG technology include being a compact mode of storage with high energy volumetric storage capacity, the safest option of natural gas storage due to its non-explosive nature, environmentally benign due to the use of only water and natural gas with the

operation at moderate temperature and pressure conditions (Veluswamy *et al.*, 2018). Despite these several advantages of SNG technology, challenges that hinder the SNG deployment on the commercial scale include slow kinetics of hydrate formation and cost of refrigeration cost during the storage of SNG at 248 K along with the stability of hydrate at storage conditions.

To overcome the slow hydrate formation kinetics, an increase in the contact area between gas and water during the hydrate formation process has been considered. New reactor design such as the stirred reactor (Mech *et al.*, 2016; Verrett *et al.*, 2012; Zhong *et al.*, 2015), spray reactor (Englezos and Lee, 2005; Tang *et al.*, 2006), or gas bubble reactor (Luo *et al.*, 2007; Vysniauskas and Bishnoi, 1983) were employed to improve the gas/liquid contact and to minimize the negative effect of the thin hydrate film covering between gas and liquid phase. However, these choices are not cost-effective and impractical on the industrial scale. Other possible methods for improving the methane hydrate formation kinetics include the employment of porous media and using kinetic promoter during the hydrate formation. The presence of porous media in the hydrate system acts as the third surface. It improves the gas-water contact area aiding the gas molecule to dissolve easily into the liquid phase resulting in the improvement of hydrate formation rate and gas storage capacity at mild conditions (Cha *et al.*, 1988; Siangsai *et al.*, 2015; Zhong *et al.*, 2013). However, the porous media, such as activated carbon or silica sand, added to the system will increase the weight of the reactor. It is the drawback for choosing some porous media for enhancing the hydrate formation kinetics. Among porous media used for methane hydrate formation, hollow silica (HS) is attractive because of its unique properties such as low density, high pore volume, high porosity, high specific area and good thermal insulation (Chen *et al.*, 2013). Prasad *et al.* (2014) reported the methane hydrate formation in HS matrix at moderate pressure. This condition is significantly lower than pure water system at the same hydrate yield showed that the methane uptake and hydrate yield in the HS were higher than silica sand and pure water Chari *et al.* (2015). Additionally, they found that the stirring did not influence on the methane hydrate formation kinetics and yield in the HS system. Veluswamy *et al.* (2016c) reported that using HS to water ratio beyond 1:6 enhanced the formation kinetics of methane hydrate and methane uptake. Surfactant has a strong influence on the kinetics of hydrate

formation and storage capacity because it can reduce the interfacial surface tension and increase the gas solubility(Bolden *et al.*, 1983; Kalogerakis *et al.*, 1993; Roy *et al.*, 1997). Ganji *et al.* (2007) studied the effects of different types of surfactant on the methane hydrate formation and found that the anionic surfactant especially SDS was the best one for utilizing methane hydrates for storage and transportation. Lin *et al.* (2004) studied the effects of SDS on the kinetics of methane hydrates and found that the presence of SDS enhanced the hydrate formation rate and observed the maximum storage capacity of 170 v/v. Moraveji *et al.* (2017) studied the effects of three types of surfactants on methane hydrate formation rate and induction time. They found that the hydrate formation rate and the induction time were significantly affected by the anionic surfactant (SDS) compared to other surfactants. However, with the use of porous material or surfactant, the methane hydrate formed sI structure that results in the limitation of hydrate stability. Generally, sI structure or pure methane hydrate forms at low temperature (sub cooling) and high pressure, with high energy requirement for hydrate formation and storage.

To operate at mild conditions (higher temperature and lower/moderate pressure), the thermodynamic promoter was chosen for the hydrate formation process. Tetrahydrofuran (THF) was reported as an effective thermodynamic promoter to stabilize the hydrate by shifting phase equilibrium to higher temperature and lower pressures (Florusse *et al.*, 2004; Mohammadi and Richon, 2009; Seo *et al.*, 2001).THF forms sII hydrates by itself without the aid of guest gas molecule. Large cages of sII structure are preferably occupied by THF, while smaller cages are empty(Kumar *et al.*, 2016; Sloan and Koh, 2008). Prasad *et al.* (2009) used micro-Raman for investigation of mixed methane-THF hydrate and indicated THF molecules occupied the large cages of sII while the small cages of sII structure were occupied by the methane gas. Further, Kumar *et al.* (2019) characterized the mixed hydrates of methane-THF at the molecular level using *in-situ* Raman spectroscopy. They documented the real-time cage occupancy wherein the small cages were occupied by methane and large cages by THF during the mixed hydrate formation. Moreover, the mixed methane-THF hydrate pellet showcased extreme stability for two months at 1.5 atm and 271.5 K. High-pressure differential scanning calorimetry analysis revealed that the stability of mixed methane-THF hydrates is higher than that of pure THF

hydrates. Veluswamy *et al.* (2016d) reported that the presence of 5.6 mol% THF at 7 MPa and 283.2 K predominantly increased the kinetics of methane hydrate formation and enhanced methane uptake about 11.6 times when compared with the pure methane at 9.5 MPa and 272.2 K. Veluswamy *et al.* (2016b) also investigated the mixed methane-THF at the experimental pressure of 7.2 MPa and different temperatures, 283.2, 288.2 and 293.2 K. They found that the final gas uptake was similar at all temperatures. Moreover, they used SDS as a co-promoter to enhance the methane hydrate formation kinetics at the higher temperature of 293.2 K. Although the mixed methane-THF hydrates were formed in sII region, they used higher pressure of 7.2 MPa.

Thus, the aim of this work was to enhance the mixed methane-THF hydrate formation at lower pressure and higher temperature of 6 MPa and 293.3 K, respectively. This work used a small amount of HS, 0.5 %w/v, to improve the surface contact area and studied the effects of HS on the mixed hydrate formation. In addition, this work also examined the effects of SDS on the kinetic promotion of mixed methane-THF hydrates with the presence of mixed 0.5 %w/v HS and the stoichiometric concentration of 5.56 mol% THF. In addition, morphology during the hydrate formation and dissociation was investigated to understand how the promoters enhanced the formation and contributed to the dissociation.

6.3 Experimental Section

6.3.1 Materials

The P-type of hollow silica powder (HS) (CAS No. 7631-86-9) of 99% purity, having a mean diameter of 30-70 μm and bulk density of < 0.1 g/cm^3, was purchased from Nanoshel, India. HS was the same material in earlier studies of Chari *et al.* (2013b), Veluswamy *et al.* (2016c) and Prasad *et al.* (2014). Analytical reagent grade tetrahydrofuran (THF) (CAS No. 109-99-9) of 99.99 % purity was purchased from Lab-Scan, Thailand. Sodium dodecyl sulfate (SDS) (CAS No. 151-21-3) of 99.9 % in the power form was purchased from Aldrich, Germany. Methane gas (CAS No. 74-82-8) of 99.99% purity was purched from Linde Public Company, Thailand. All experiment in this work used deionized water.

6.3.2 Experimental Apparatus for the Hydrate Formation Kinetic Experiment

The experimental setup for the gas hydrate formation and dissociation is schematicaly shown in Figure 6.1 (left side). Details of the set up are provided in previous studies (Inkong *et al.*, 2019a; Inkong *et al.*, 2019b). In brief, the stainless streel crystallizer (CR) designed for the the maximun working pressure of 20 MPa with 180 cm^3 volume was connected with a 100 cm^3 reservoir (R). The temperatures of crystallizer and gas reservoir were maintained with a cooling bath with an external refrigerator (ER) (Model RC-20, Daeyang, Korea) using a 4:1 ratio of water to glycol. The pressure in the system was measured by a pressure transmitter (Cole-Pamer®, Singapore) with 0.13 % accuracy within the range of 0-21 MPa. Three K-type thermocouples with ±1.0 K accuracy was strategically placed in different locations inside the crystallizer, Figure 6.1(right side), to measure the temperature at each location. The thermocouples T1, T2 and T3 were placed in the solution, at the interface and in the gas phase, respectively. The pressure and temperature during the experiment were tracked by a data logger (AI210, Wisco Industrial Instruments, Thailand), which was connected to a personal computer.

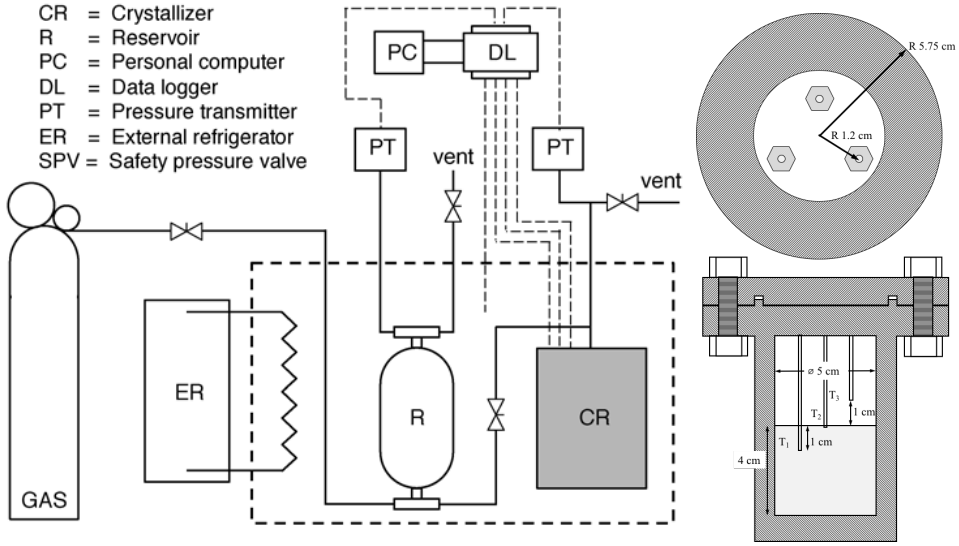

Figure 6.1 Detailed schematic of experimental setup (left side) and schematic of a crystallizer (right side). Modified from Siangsai *et al.* (2015)

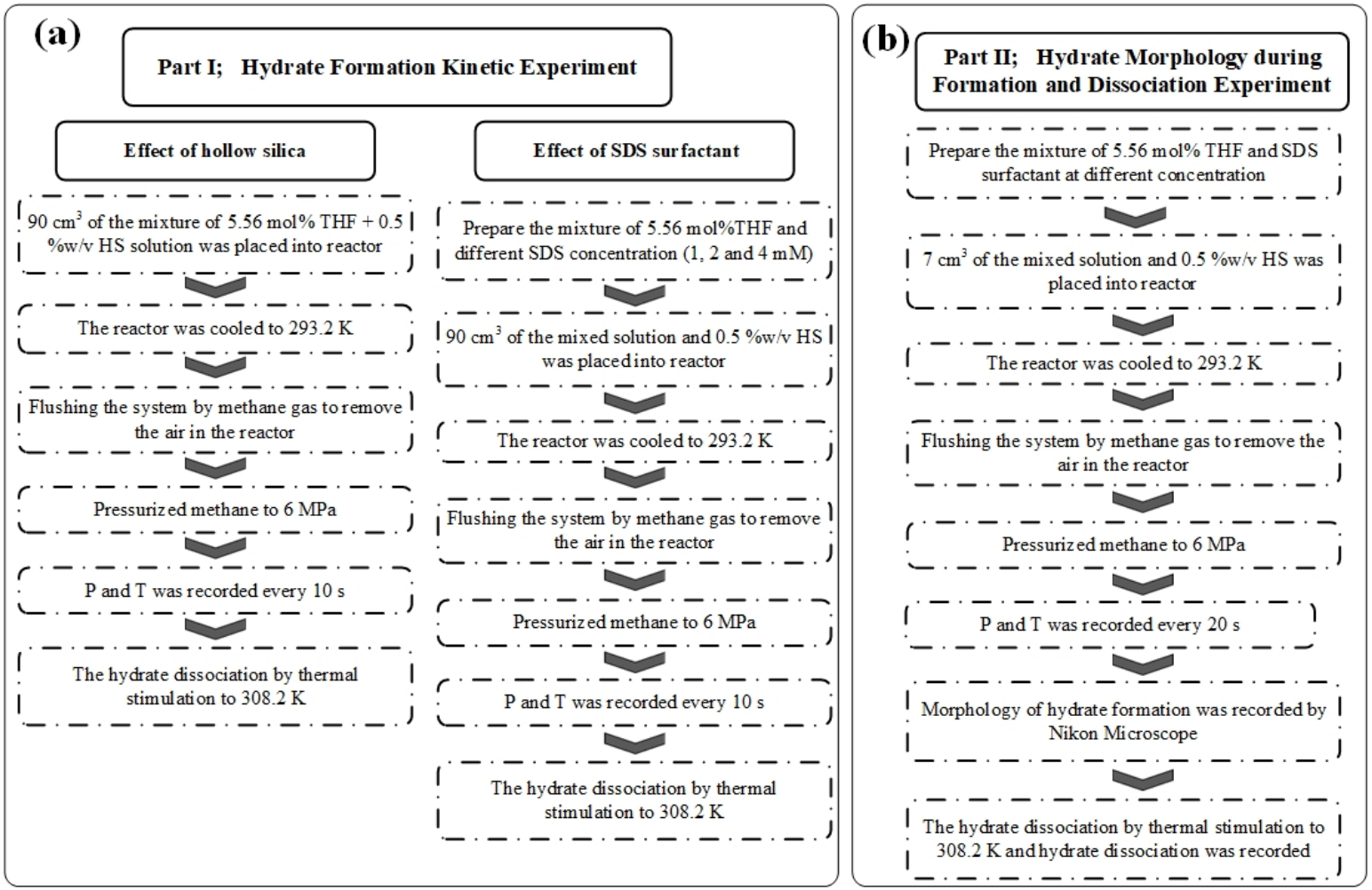

Figure 6.2 Details of experimental procedures.

6.3.3 Experimental Apparatus for the Morphology of Hydrate Formation and Dissociation

A detailed description and schematic of the experimental aparatus in the morphology experiments are in line with those from (Veluswamy *et al.*, 2016a); Veluswamy *et al.* (2016c). In summary, the transparent sapphire was used to fabricate the reactor column to withstand up to 10 MPa with 30 mm inner diameter and 80 mm height. The transparent reactor column was supported by two stainless steel lids. During the experiments, the temperature was measured by a T type Omega constantan thermocouple with 0.1 K error and pressure was measured by a Rosemount pressure transmitter with 0.1% error in the range of 0-20 MPa. The Polyscience SD15R external refrigerator was used to circuate the coolant fuild to control the temperature in the water bath. Data acquisition system supplied by National Instruments recorded the temperature and pressure in the reactor during the experiments every 20 s. The hydrate morphology during formation and dissociation was captured every 20 s by Stereoscopic zoom microscope SMZ1000 from Nikon coupled with Nikon Digital Sight (DS-Fi1) camera and Optika Pro HDMI camera.

6.3.4 Hydrate Formation Experiment

Figure 6.2 presents the experimental procedures for kinetic and morphology studies. 0.5 %w HS/v was calculated based on the volume of mixture of stochiometric concentration of THF (5.56 mol% THF) and SDS concentrations. SDS concentration employed in current study was varied from 0 to 4 mM (0 to 1152 ppm). As seen from Figure 6.2, both kinetic and morphology studies have about the same procedure except for the sample volume. For the kinetic study, each experiment used 90 cm^3 of the solution whereas the morphological experiments used only 7 cm^3 of the solution. The solution was transferred to crystallizer and then connected to the set up. To remove any air in the system, methane gas was pressurized to 0.5 MPa and depressurized to atmospheric twice. After the temperature inside the crystallizer reached the desired temperature (293.2 K), methane gas was introduced into the crystallizer to the pressure of 6 MPa. Every 10 s for the kinetic experiments and 20 s for the morphology experiments, pressure and temperature data was recorded. The hydrate formation completed when the pressure inside the crystallizer was constant for

at least 1 h. The moles of methane gas involved in the formation and the methane gas uptake at given any time (t) was calculated by equations (6.1) and (2)

$$\text{Mole of gas consumed} = \left(\frac{PV}{zRT}\right)_{t=0} - \left(\frac{PV}{zRT}\right)_{t} \quad \text{(mol of methane)} \tag{6.1}$$

$$\text{Methane gas uptake} = \frac{\left(\Delta n_{H,\downarrow}\right)_t}{n_{H_2O}} \quad \text{(mol of methane /mole of water)} \tag{6.2}$$

where $\Delta n_{H,\downarrow}$ is the number of moles of gas consumed at the end of experiment. P and T represent the pressure and temperature recored in the crystallizer. V is the volume of gas phase in the crystallizer, R is the universal gas constant (82.06 cm^3atm /mol.K), and z is the compressibility factor calculated by Pitzer's correlation.(Smith *et al.*, 2005)

The hydrate formation rate was presented in the terms of the normalized initial hydrate formation rate (NR_{30}) for the first 30 min after hydrate nucleation. NR_{30} was calculated by equation (6.3) (Veluswamy *et al.*, 2015);

$$NR_{30} = \frac{R_{30}}{V_{water}} \quad \text{(mol of methane/min/m}^3\text{ of water)} \tag{6.3}$$

where V_{water} is the amount of water (m^3) taken in the crystallizer, and R_{30} is the hydrate growth rate (mol of methane/min) for the 30 min after hydrate nucleaiton was calculated by using the least squares method. The methane hydrate growth was plotted versus time and then used this method to find the for the best fit of the rate of hydrate growth in the first 30 min after hydrate nucleation.

6.3.5 Hydrate Dissociation Experiment

To recover methane from the methane hydrates, the crytallizer temperature was increased to 308.2 K. The equilibrium temperature of the mixed THF-methane hydrate at 6 MPa K was 300.1 K (Lee *et al.*, 2012), thereby using 308.2 K ensured complete hydrate dissociation. During hydrate dissociation, the pressure in the crystallizer increased due to the gas released from dissociating hydrates. The pressure

and temperature during the dissocation of hydrates were mesured by the pressure transducer and recorded by data logger. The hydrate dissociation experiment completed when the pressure in the crystallizer was constant at experimental temperature (308.2 K). The moles of methane gas released from the hydrates during the dissociation at given any time (*t*) was calculated by equation (6.4).

$$\Delta n_{H,\uparrow} = n_{H,t}\text{-}n_{H,0}=\left(\frac{PV}{zRT}\right)_{G,t} - \left(\frac{PV}{zRT}\right)_{G,0} \tag{6.4}$$

Methane recovery was calculated by equation (6.5) (Babu *et al.*, 2013; Linga *et al.*, 2009).

$$\%\text{methane recovery} = \frac{(\Delta n_{H,\uparrow})}{(\Delta n_{H,\downarrow})_{End}} \times 100 \tag{6.5}$$

where $\Delta n_{H,\uparrow}$ is moles of released gas from hydrate during the hydrate dissociation at any given time.

$(\Delta n_{H,\downarrow})_{End}$ is moles of gas consumption for hydrate formation at the end of experiments.

6.4 Results and Discussion

This work investigated the mixed methane-THF hydrate formation at a higher temperature and lower pressure (6 MPa and 293.2 K and) to examine the possibility of reducing the cooling energy/compression cost required for hydrate formation. This experimental condition was chosen because this condition ensures the hydrate formation in the sII region only (Lee *et al.*, 2012). This work also investigated the effects of low loading HS on the mixed methane-THF hydrate formation. The stoichiometric concentration of THF (5.56 mole% THF) was used in all experiments. Kinetics of mixed hydrate formation in the presence of low loading HS and the effect of the presence of anionic surfactant, SDS, at the low loading of HS during at 6 MPa and 293.2 K were examined. To complement the kinetic study, the morphology of the mixed methane-THF hydrate in the presence of low loading of HS in 5.56 mol% THF with and without SDS during the hydrate formation at 6 MPa and 293.2 K was also

presented and discussed alongside. Note that each experiment in the kinetic study was repeated at least three times and two times for the morphology study to ensure its reproducibility.

6.4.1 Effects of Hollow Silica (HS) on the Mixed Methane-THF Hydrate Formation

Table 6.1 Three separate methane hydrate formation experiments with HS at 6 MPa and 293.2 K

No. Exp.	Induction Time* (min)	t_{90} (min)**	Methane Capacity (mol of methane /mol water)	***NR_{30} (mol of methane /min/m^3 of water)	%Recovery
0.5 %w/v HS + 5.56 mol % THF +CH_4					
B1	432.83	666.13	0.0596	12.65 (R^2 = 0.953)	97.01
B2	495.30	748.97	0.0581	18.49 (R^2 = 0.981)	97.59
B3	516.50	736.67	0.0597	14.06 (R^2 = 0.955)	97.41

* Induction time is the time taken for first hydrate nucleation from the start of experiment

** Time required to reach 90% of the final methane uptake calculated form the start of experiment

*** Rate of hydrate formation calculated for 30 min from the induction time

It should be noted that there is no mixed methane-THF hydrate formation at 6 MPa and 293.2 K without HS observed during 48 h.This can be attributed to the low driving force (both pressure and temperature driving force) available at this experimental condition. The temperature and pressure diving forces used in this work are 3.88 MPa and 7 K, respectively. There were calculated from the difference of the experimental condition and the equilibrium diagram of sII (Lee *et al.*, 2012). Additionally, the reactor type employed in this work is an unstirred reactor, which only has a fixed gas/liquid contact area (at the interface). Furthermore, the reactor could

increase the mass transfer resistance for the gas diffusion into the liquid phase to form mixed methane-THF hydrate.(Makino *et al.*, 2005; Sugahara *et al.*, 2009)

To form mixed methane-THF hydrates at 6 MPa and 298.2 K, HS was used to increase the surface contact area between gas and liquid phase. HS acts like a third surface and facilitates the gas diffusion into the liquid phase. HS was reported to act as a kinetic promoter for methane hydrate formation(Chari *et al.*, 2015). However, many reports proposed that HS can enhance the methane hydrate formation at lower temperatures in the range of 273 - 275 K (Chari *et al.*, 2015; Chari *et al.*, 2013a; Chari *et al.*, 2013b; Prasad *et al.*, 2014; Veluswamy *et al.*, 2016c). There have never been reports on using HS for the same purpose at the high temperature. Nevertheless, many reports proposed that the pure methane hydrate formation by using HS result in high methane uptake at high concentrations of HS in water solution (Chari *et al.*, 2015; Veluswamy *et al.*, 2016c). But, in this work, a low loading of HS, 0.5 %w HS/v, is used to promote the mixed methane-THF hydrate at the low driving force (pressure and temperature). The results of the mixed methane-THF hydrate kinetics and the final methane uptake in the presence of 0.5 %w HS/v in 5.56 mol% THF solution are presented in Table 6.1.

HS was added in concentration akin to a kinetic promoter (0.5 %w/v) to promote the hydratate formation and not like a fixed bed support (studied involving higher concentrations in the literature). From our preliminary experiments, improved kinetics was not evident at lower concentrations of HS (< 0.5 %w/v). Hence, 0.5 %w/v HS was considered as optimal and used for the evaluation of formation kinetics. From Table 6.1. it can be clearly seen that the addition of this concentration of HS increase the hydrate formation compared to no hydrate formation when there is no HS.

The methane gas uptake profiles from experiments conducted with 0.5 %w HS/v in 5.56 mol% THF solution are provided in Figure 6.3. The time in the figure starts from zero, which corresponds to the time for the first hydrate crystal formation observed from the first temperature spike during the hydrate formation. The spike of the temperature was due to the exothermic nature of the hydrate formation process. It can be seen from the figure that all three experiments show comparable methane growth uptake profiles with only small deviation indicating the consistency of hydrate formation and growth. In addition, the methane uptakes leveloff at about 160 mins

after nucleation. However, all experiments were carried out for longer than 360 min after nucleation to ensure the complete hydrate formation.

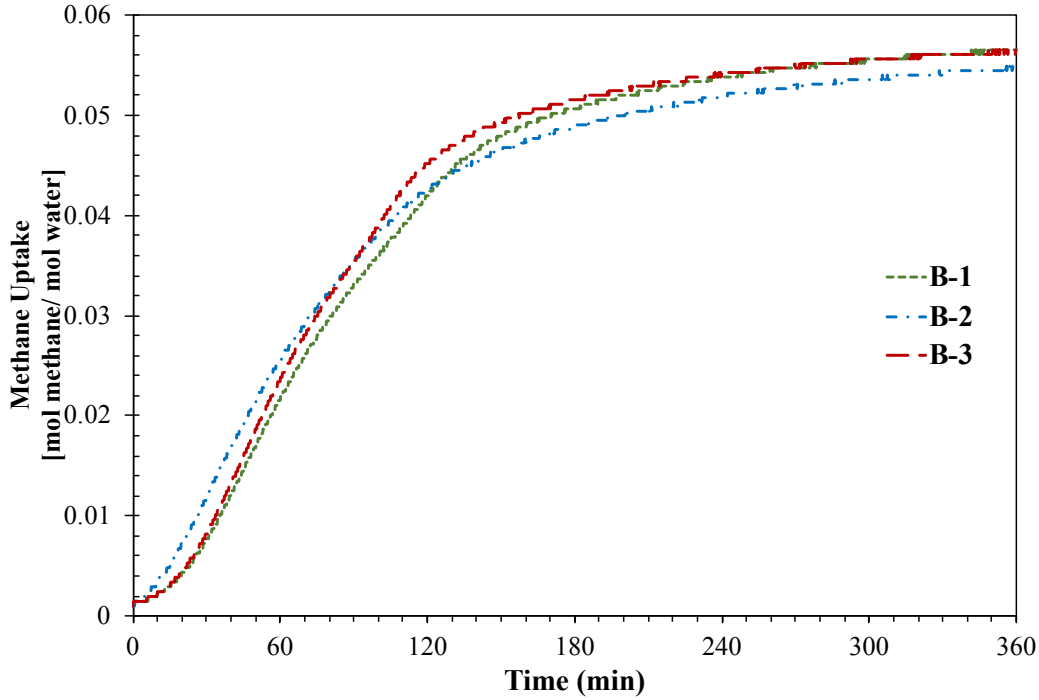

Figure 6.3 Methane uptake profiles during the hydrate formation after hydrate nucleation at 6 MPa and 293.2 K in the presence of 0.5 %w HS/v in 5.56 mol% THF.

The presence of the lower amount HS in the 5.56 mol% THF solution can promote the mixed methane-THF hydrate formation at 6 MPa and 293.2 K due to the characteristic property of HS. Figure S6.1 (Supporting Information) presents the SEMs of the morphology of HS. It can be seen from the figure that HS has a smooth surface, and there is a cavity inside the HS. The cavity of HS is also confirmed by the TEM image shown in Figure S6.2. The cavity inside the HS (brighter area) is covered with a thin wall (darker area) with uniform thickness. Both SEMs and TEMs confirm that the HS is a porous media that possesses high porosity and high specific surface area. Moreover, the important property of HS is its low density, which results in HS floating at the interface of gas and liquid solution phases, improving/providing the third additional surface. It is believed that the presence of HS at the interface between gas and the solution phase increases the movement of THF solution to the gas phase

through the network of capillary channels during the hydrate formation (Veluswamy *et al.*, 2016c).

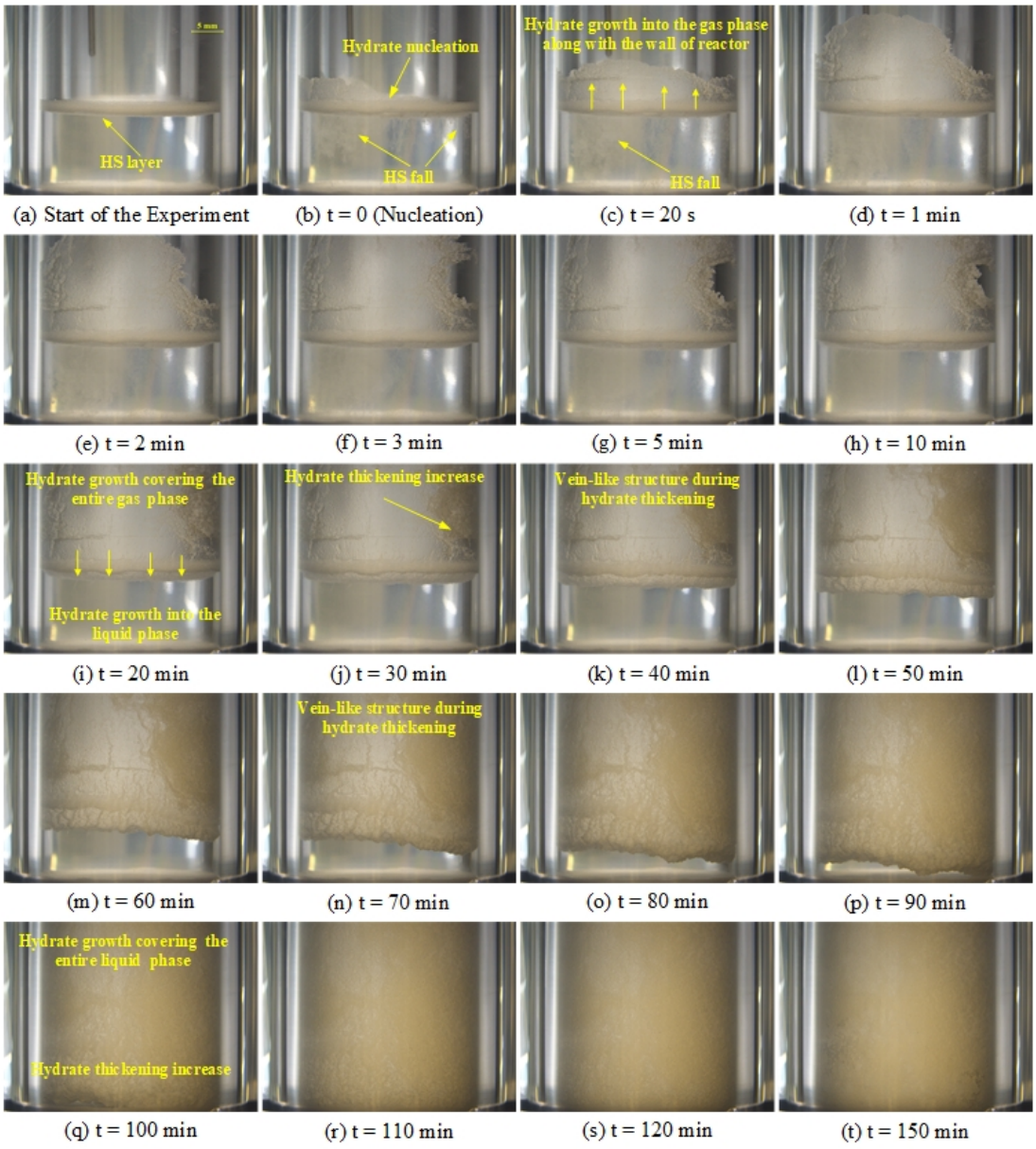

Figure 6.4 (a−t) Morphology of methane hydrate formation using 7 mL of the mixture of 0.5 %w HS /v in 5.56 mol% THF solution at 6 MPa and 293.2 K.

To understand the mixed methane-THF hydrate formation mechanism in the presence of HS, a series of observations during the nucleation and hydrate growth for the experiment conducted with 0.5 %w HS/v in 5.56 mol% THF solution at 6 MPa

and 293.2 K is presented in Figure 6.4. Figure 6.4a shows the start of the experiment with the gas phase and thermocouple. It can be clearly observed from Figure 6.4a that the uniform layer of HS floats along the gas/liquid interface. Figure 6.4b shows the hydrate nucleation along the gas/liquid interface, which is consistently observed in the quiescent systems as it offers the higher surface area for gas and liquid phase interaction. Moreover, it can be clearly observed from Figure 6.4b that some HS particles at the interface fall down during the hydrate formation. This could be attributed to the mixed methane-THF hydrates form inside the cavity of HS (Chari *et al.*, 2015; Chari *et al.*, 2013a; Prasad *et al.*, 2014). The overall density of the mixed methane-THF hydrates and HS particle is higher than water as resulting in the hydrate particles falling down from the interface. Figure 6.4c (20 s after the hydrate nucleation) shows hydrate growth in the upward direction. It is postulated that the presence of HS at the interface of gas and the THF solution increases the movement of THF solution to the interface through the network of the capillary channels generated by the property of HS. These channels exist in the HS particles due to their highly interconnected micropores. The migration of THF solution via the capillary force of HS to gas phase favors the hydrate formation upward towards the gas phase Veluswamy *et al.* (2016c). reported the presence of HS improved the movement of water to the gas-hydrate interface through capillary channels during the methane hydrate formation. Figures 6.4d-6.4h (40 s - 10 min after the hydrate nucleation) show that the mixed methane-THF hydrates progressively grow along the wall into the upward direction until the reactor column in the gas phase is covered by the gas hydrates. After the mixed methane-THF hydrates covers the reactor column in the gas phase direction, the hydrates grow slowly in the downward directions as shown in Figures 6.4i-6.4q (20 min - 90 min after hydrate nucleation). As an evidence for the mixed methane-THF hydrates growing along the wall of the reactor before growing in the downward direction, a video covering the entire reactor column during the hydrate formation is provided in the Supporting Information (Video SV6.1). Moreover, it can be observed from Figures 6.4i-6.4p that during the mixed methane-THF hydrate growth in the downward direction, vein-like formations can be observed, indicating the thickening or hardening of hydrates. After 100 min from nucleation (Figure 6.4q), hydrates cover the entire bulk solution and the thickening of hydrates at the bottom part of the reactor

column can be clearly seen (Figure 6.4r). Afterwards, there is no further significant morphology observations, Figures 6.4r-6.4t.

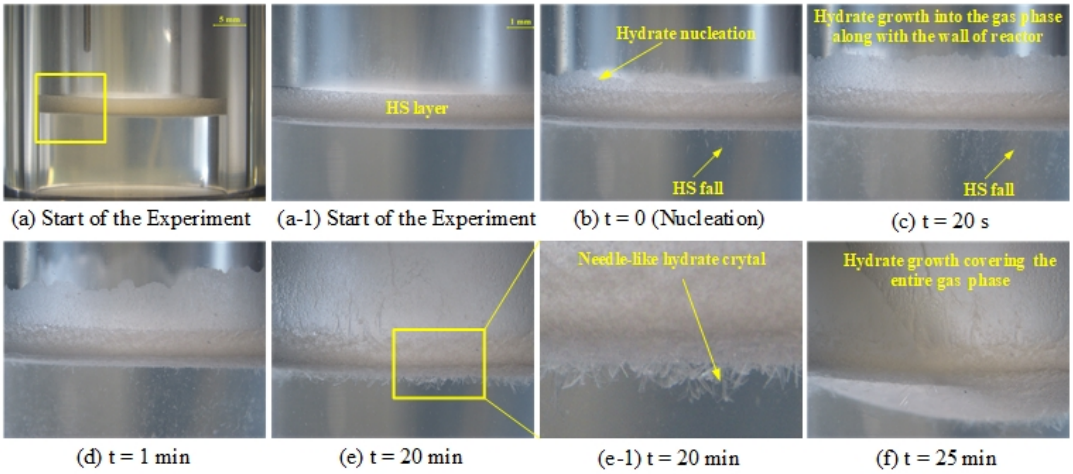

Figure 6.5 (a−f) Morphology of methane hydrate formation at the interface of the mixture of 0.5 %w HS/v in 5.56 mol% THF solution at 6 MPa and 293.2 K.

Figure 6.5 presents the recorded observations with the details of the mixed methane-THF hydrates growth at the selected time intervals along with the zoomed interface. Figure 6.5(a-1), the zoomed picture from Figure 6.5a, shows the uniform layer of HS particle floats at the gas/liquid interface. Figures 6.5b-6.5c show the mixed methane-THF hydrate nucleation and mixed methane-THF hydrate growth along with the wall of the reactor column in the upward direction. As the mixed methane-THF hydrates grow in the upward direction, it can be observed that some HS particles moved down in the THF solution because of the difference in density of HS and the mixed methane-THF hydrates in the HS as discussed earlier. From this figure, it is clear that the mixed methane-THF hydratse first grow on the top of the HS layer. Then, the growth takes place along the wall of the reactor column. The hydrates grow progressively in the upward direction as seen in Figures 6.5c-6.5d. The hydrate growth in the upward direction is owing to the combination of the capillary effect of HS and hydrate particles. Veluswamy *et al.* (2016d) observed the morphology of mixed methane-THF hydrate in the glass vial 1.5 cm^3. They found that the hydrate channels were formed during the growth of mixed hydrates and reported that these channels facilitated the migration of solution from the bulk liquid in the upward direction by the

capillary action. Figure 6.5e (20 min after hydrate nucleation) shows the mixed methane-THF hydrate growth in the downward direction. Interestingly, the needle-shaped crystals grow into the bulk solution from the lower liquid/hydrate interface. For better clarity, the bottom part of the hydrates are zoomed and presented in the Figures 6.5e-6.5l. The behavior can be explained by dendritic crystals, which grow into the solution, that drive the hydrate expansion into the bulk solution.(Veluswamy *et al.*, 2016d)

As shown in Table 6.1, the methane uptake after complete hydrate formation is 0.0596 ± 0.0050 mol of methane/mol of water. In order to compare and analyze the methane uptake for the mixed low loading HS in 5.56 mol% THF solution with only HS or only THF, the gas uptake for these experiments is presented in Figure 6.6 along with that reported in literatures. Chari *et al.* (2013a) and Chari *et al.* (2015) reported the methane uptake at 0.0671 ± 0.0034 and 0.0700 ± 0.0041 mol of methane gas/mol of water from the formation with HS at 8 and 274.15 K; and at 8.85 MPa and 275 K, respectively. Veluswamy *et al.* (2016b) showed about the same methane uptake, ca. 0.07 mol of methane gas/mol of water, from the hydrate formation with THF at 7.2 MPa and 283.2, 288.2 and 293.2 K. However, these studies were performed at very low temperature and high pressure to achieve the high methane uptake. The methane uptake in this work is not significantly different from those in literature despite of the lower pressure (6 MPa) and higher temperature (293.2 K). This demonstrates that the presence of the low loading HS in 5.56 mol% THF solution can favorably promote mixed methane-THF hydrate formation even at 6 MPa and 293.2 K without significant change in the methane uptake.

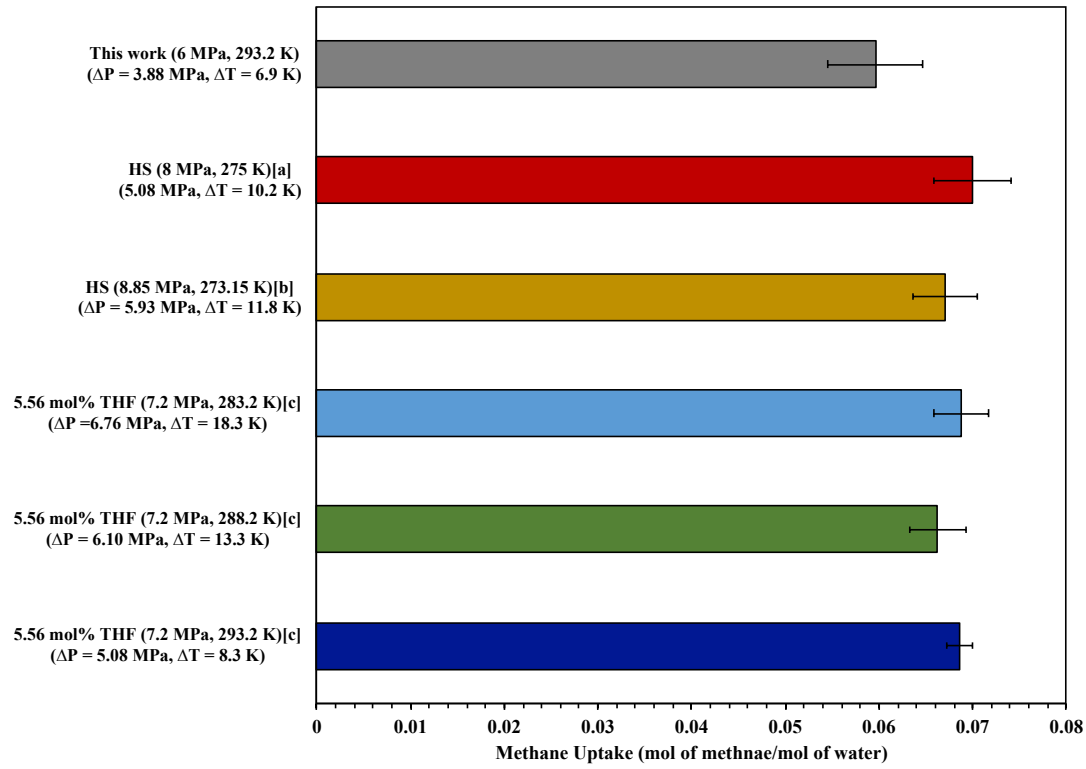

Figure 6.6 Comparison of the methane uptakes in this work with literature ([a] Chari *et al.* (2015), [b] Chari *et al.* (2013b) and [c] Veluswamy *et al.* (2016b)).

6.4.2 Effects of Sodium Dodecyl Sulfate (SDS) and the Hollow Silica (HS) on Mixed Methane-THF Hydrate Formation

The result from the previous section summarized in Table 6.1 shows that the first hydrate nucleation takes longer than 400 min to form from the start of the experiment accompanied with the slow rate of hydrate formation (requiring at least 4 hrs for completion of hydrate formation). This is a drawback for using the hydrate technology for commercial storage and transportation applications. In order to decrease the induction time and increase the rate of mixed methane-THF hydrate formation at 6 MPa and 293.2 K, an anionic surfactant was added to improve the kinetics of hydrate formation. Many publications reported that the anionic surfactant promoted the methane hydrate formation kinetic especially SDS (Ganji *et al.*, 2007; Lin *et al.*, 2004; Sun *et al.*, 2004). SDS is a well-known kinetic promoter for methane hydrate formation in an unstirred tank reactor even though with very low concentrations (Kumar *et al.*, 2015; Okutani *et al.*, 2008; Veluswamy *et al.*, 2016b;

Zhong and Rogers, 2000).

In order to improve induction time and the rate of hydrate formation of the mixed methane-THF hydrates in the presence of the mixture 0.5 %w/v HS in 5.56 mol% THF at 6 MPa and 293.2 K, SDS concentration was varied between 1 to 4 mM (228 to 1152 ppm). Figure 6.7 presents the effects of SDS concentration on the induction time and NR_{30}. It can be seen that the induction time dramatically decreased whereas NR_{30} significantly increased in the presence of SDS. The presence of SDS decreases the surface tension resulting in the ease of methane gas to diffuse into the liquid phase, hence, promoting the hydrate growth rate. Evidently, the presence of both HS and SDS result in the synergistic effects for the hydrate nucleation and the rate of hydrate formation. Moreover, it can be seen from Figure 6.7 that the induction time decrease with the increase in SDS concentration. This could be attributed to the decreased interfacial tension between gas and liquid phase with the increase in SDS concentration and consequently the rapid gas hydrate nucleation (Kashchiev and Firoozabadi, 2002; Wang *et al.*, 2015). The results are also consistent with the report by Zhong and Rogers (2000), who proposed that the induction time strongly depended on the SDS concentration and increased proportionally to its concentration.

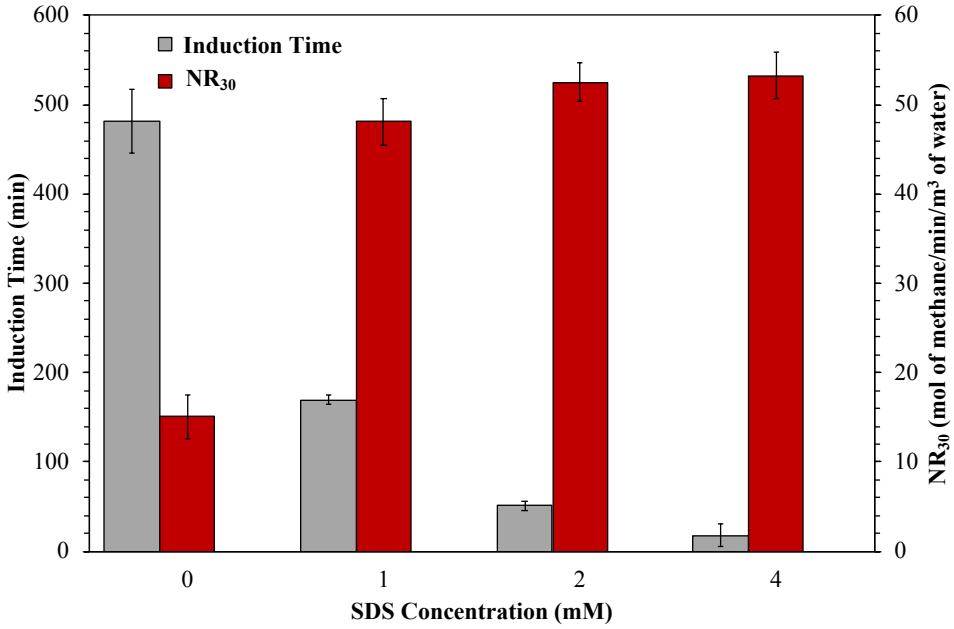

Figure 6.7 Induction time and NR_{30} along with error bars at different SDS concentration in 0.05 % w HS/v in 5.56 mol% THF at 6 MPa and 293.2 K.

Figure 6.8 shows methane uptake starting from nucleation for methane formation experiments conducted with different SDS concentrations in 0.5 %w HS/v and 5.56 mol% THF solution at 293.2 K and 6 MPa. Figure 6.8a shows that, with 1 mM SDS, the methane uptake continuously increases and reaches a plateau approximately 100 min after hydrate nucleation. When the SDS concentration is increased to 2 mM, as shown in Figure 6.8b, a deflection point about 60 min after hydrate nucleation, which indicates the increase in the hydrate formation rate(Veluswamy *et al.*, 2016b) can be observed. The delfection points can also be seen with 4 mM SDS. The expanded uptake profiles during 40 -160 min are provided in Figure 6.8d for better observation of deflection point. The mixed methane-THF hydrate formation in the presence of SDS completes in just 180 min after the hydrate nucleation for all experiments.

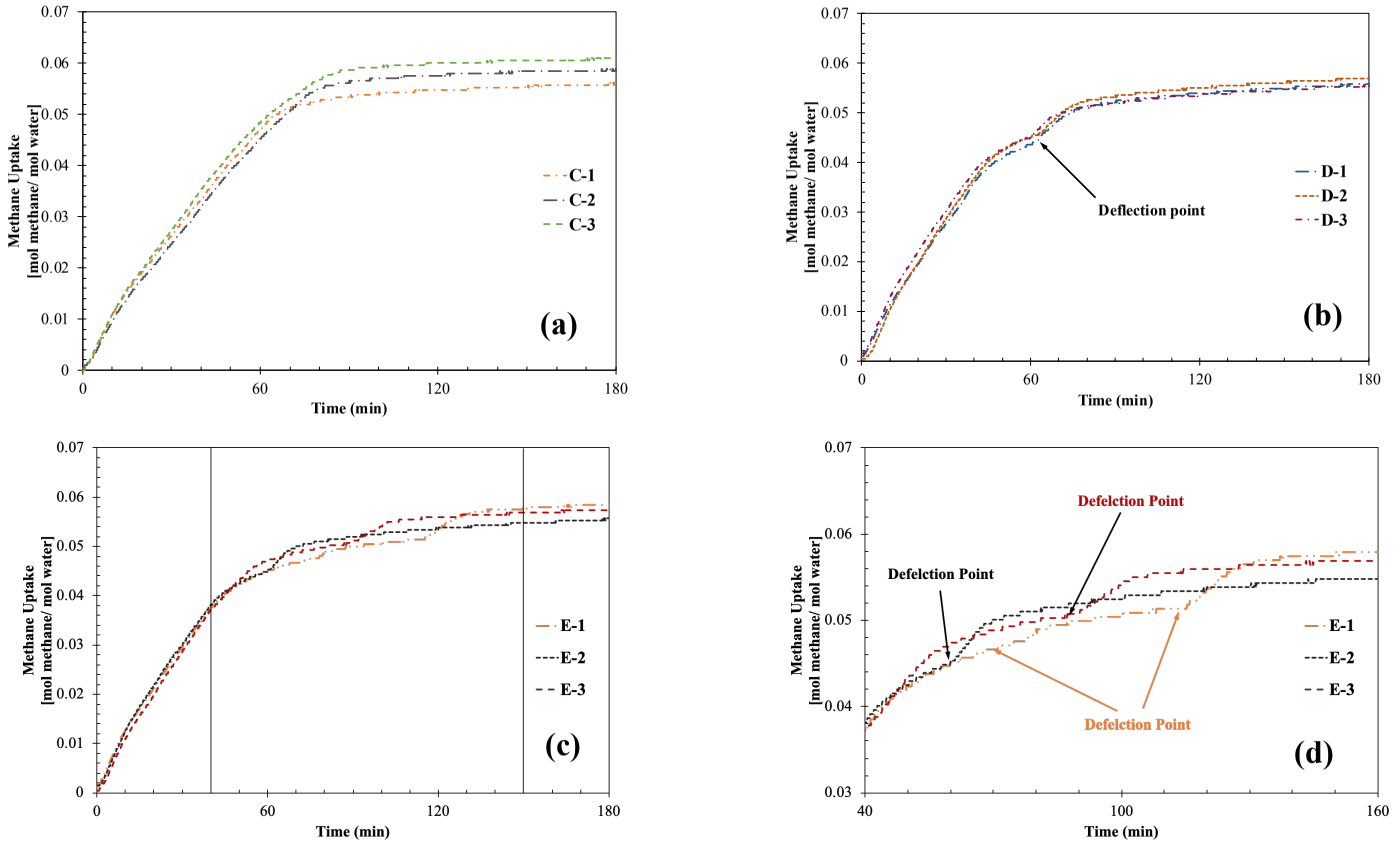

Figure 6.8 Methane uptake profiles during the hydrate formation after hydrate nucleation at 6 MPa and 293.2 K in the presence of 0.5 %w HS/v in 5.56 mol% THF and a) 1 mM SDS, b) 2 mM SDS, and c) 4 mM SDS d) expanded methane uptake profiles of 4 mM SDS during 40 - 160 min.

In order to further explain the deflection points during the hydrate growth with 2 and 4 mM SDS, the temperature profiles at interphase (T2) are presented in the Figure 6.9. Temperature profiles start from the first nucleation untill the completion for three separate experiments with 2 and 4 mM SDS. Figure 6.9a shows two distinct peaks for all experiments with 2mM SDS. The increase in the first broad peak is from the first nucleation followed by another temperature increase about 62 (±2) min from the first hydrate nucleation. The time of observation of the second peak corresponds to the deflection point in the methane uptake profiles. The increase in the gas uptake after the deflection point results in the secondary nucleation as evidenced from the temperature peak.(Veluswamy *et al.*, 2016b) It is interesting to note from Figure 6.9b that the experiments with 4mM SDS also show multiple peaks. The first temperature peaks are broader rising immediately due to the first nucleation followed by the second peak rises around 70 min and the temperature rises again around 115 min. The time, at which the second and third hydrate nucleation take place, is summarized in the Table 6.2. Moreover, it can be seen from Figure 6.9 that the first stage hydrate nucleation shows the broadest peak corresponding to the large amount of heat release during the hydrae formation, which, in turn, implies a large amount of the methane gas converted to hydrates. For the second or third stage hydrate nucleation, the extent of methane conversion is lower than the first nucleation as indicated by the slight increase in the temperature profile.

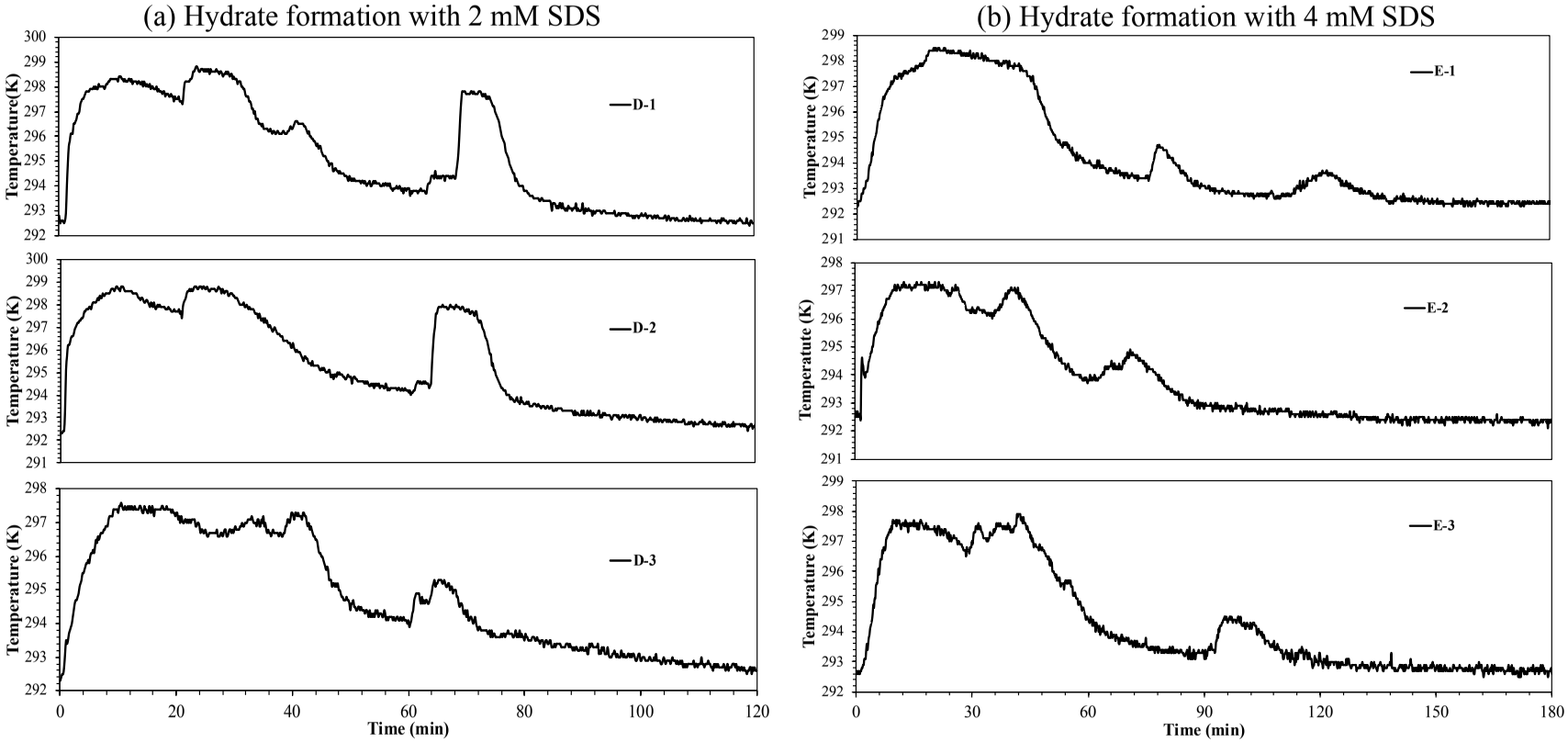

Figure 6.9 Temperature profiles in the reactor during hydrate formation at 6 MPa and293.2 K in the presence of 0.5 %w HS/v in 5.56 mol% THF and a) 2 mM SDS and b) 4 mM SDS.

Table 6.2 Methane hydrate formation with different concentrations of SDS in 0.5 %w HS/v and 5.56 mol% THF solution at 6 MPa and 293.2 K

No. Exp	*Induction Time (min)	**Second Nucleation (min)	**Third Nucleation (min)	***t_{90} (min)	Methane Capacity (mol of methaen /mol water)	****NR_{30} (mol of methane /min/m^3 of water)	%Recovery
1 mM SDS+ 0.5 %w/v HS +5.56 mol % THF +CH_4							
C1	168.50	-	-	228.67	0.0573	50.00 (R^2= 0.988)	97.40
C2	176.83	-	-	267.13	0.0600	44.44 (R^2= 0.988)	96.10
C3	163.50	-	-	255.50	0.0614	49.88 (R^2= 0.991)	97.90
2 mM SDS+ 0.5 %w/v HS +5.56 mol % THF +CH_4							
D1	57.00	128.83	-	187.33	0.0612	50.50 (R^2= 0.995)	97.09
D2	52.17	123.17	-	188.17	0.0621	55.55 (R^2= 0.991)	96.34
D3	43.00	131.83	-	138.33	0.0616	51.55(R^2= 0.995)	96.41
4 mM SDS+ 0.5 %w/v HS +5.56 mol % THF +CH_4							
E1	32.83	69.00	114.82	183.67	0.0645	51.55 (R^2= 0.993)	96.79
E2	27.00	64.83	-	137.33	0.0600	56.55 (R^2= 0.995)	96.09
E3	3.00	88.83	-	108.33	0.0616	55.00 (R^2= 0.993)	96.41

* Induction time is taken for first hydrate nucleation

** The time of second and third nucleation reported from the first hydrate nucleation

*** Time required to for 90% of the final methane uptake calculated from the start of experiment

**** Rate of hydrate formation calculated for 30 min from induction time

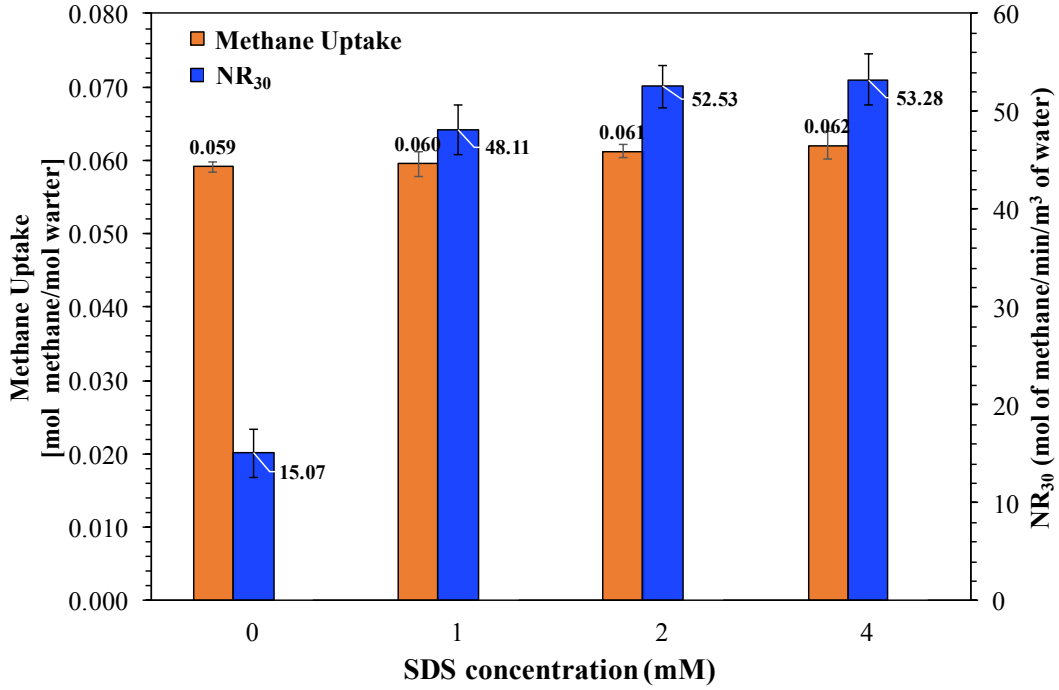

Figure 6.10 Methane uptakes at the end of hydrate formation (ca. 600 min after hydrate nucleation) and NR_{30} with the presence of 0.5 % HS w/v in 5.56 mol% THF solution and different concentrations of SDS at 6 MPa and 293.2 K.

The final methane uptakes after hydrate formation complete (ca. 600 min after the start of the experiment) of the mixed methane-THF hydrate formation with and without SDS are presented in Figure 6.10. The final methane uptakes from the formation with and without SDS are similar. However, NR_{30} significantly increases with the presence of SDS. The results are consistent with the literatures, which reported that surfactants served only as a kinetic promoter for hydrate formation.(Kalogerakis *et al.*, 1993; Veluswamy *et al.*, 2015; Verrett *et al.*, 2012; Watanabe *et al.*, 2005; Zhong and Rogers, 2000)

Figure 6.11 presents a series of morphology observations during the

hydrae formation with 4 mM SDS in 0.5 %w HS/v and 5.56 mol% THF solution at 6 MPa and 293.2 K. It is very interesting that, with SDS, the morphology during the hydrate formation is different from the the system without SDS (Figure 6.5). The rapid formation of mixed methane-THF hydrates in the presence of SDS can be clearly observed. Figure 6.11a shows the start of the experiment with uniform layer of HS particles along the gas/liquid interface. Figure 6.11b shows the hydrate nucleation along the interface with some HS particles falling down to the bottom of the reactor. It is similar to the phenomenon observed from the system without SDS (Figures 6.4b and 6.11b). At about 20 s after the nucleation, the mixed methane-THF hydrates form along the walls of the reactor column both upwardly and downwardly, as seen from Figure6.11c. The rapid mixed methane-THF hydrate growth in both directions is owing to the synergistic effects of HS and SDS by providing the third surface to increase the contact area between the gas and liquid and also the lower interfacial tension to increase the gas dissolution into the liquid phase. The mixed methane-THF hydrate continues to grow in both directions of the reactor column, as seen from Figures 6.11d-6.11e. Two min after the start of hydrate nucleation, the mixed methane-THF hydrates completely envelop the reactor walls in both directions. After the hydrates form throughout the bulk solution, there is no significant change in the morphology, Figures 6.11f-6.11l. The video during the hydrate formation with 4 mM SDS in 0.5 %w HS/v and 5.56 mol% THF solution conducted at 6 MPa and 293.2 K is provided in the Supporting Information, VS6.2. Comparison between Figures 6.4 and 6.11 clearly demonstrates the presence of SDS in the mixture of 0.5 %w/v and 5.56 mol% THF solution results in the hydrate growth in both upward and downward directions at a much faster pace. The morphology during the formation with 1 and 2 mM SDS is about the same to that with 4 mM, and details are provided in Supporting Information (Figures S6.3-S6.4). However, slightly faster hydrate formation can be observed with 4 mM SDS than the other two SDS concentrations.

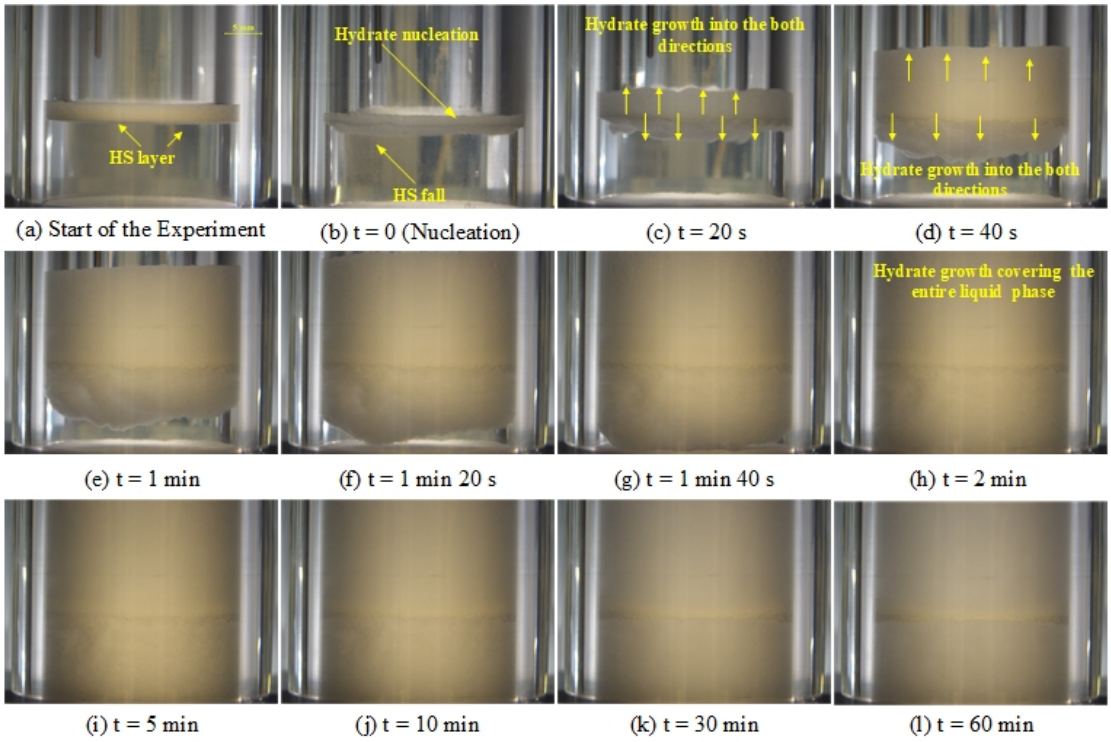

Figure 6.11 (a–l) Morphology of methane hydrate formation using 7 mL of the mixture of 0.5 %w HS/v in 5.56 mol% THF and 4 mM SDS solution at 6 MPa and 293.2 K.

6.4.3 Hydrate Dissociation

As shown above, the mixed methane-THF hydrate formation can be promoted and enhanced at the high temperature and low pressure with HS. In order to utilize the gas hydrate technology in the storage and transportation application, methane recovery from the hydrates also play a critical role. After the completion of the methane hydrate formation, the hydrates were dissociated by the thermal stimulation method. The temperature was increased from 293.2 K to 308.2 K (15 K temperature driving force). Figure 6.12 presents the P–T profiles during the dissociation from hydrates formed without SDS, experiment B-1, and with 4 mM SDS, experiment E-2. Note that the pressure in the figure starts from zero, which is from the subtraction of the starting pressure before dissociation to each pressure during the dissociation. From P-T profiles in the Figures 6.12(a) and 6.12(c), it can be seen that during the first 30 min of hydrate dissociation, the temperature is below the equilibrium temperature of 5.56 mol% THF-methane hydrate of 298.2 K (Lee *et al.*,

2012). Thus, the slight increase in pressure during this period is a result of the thermal expansion of gas that remains in the reactor and reservoir. After 30 min, the temperature gradually increases and crosses the equilibrium temperature with hydrates starting to dissociate. Therefore, the hydrate stable zone is the range of temperature from the experimental temperature to the dissociation temperature. Furthermore, Figure 6.12(a) shows a sharp increase in pressure, which is resulted from the methane gas released from the cage of hydrates. Moreover, at 50 min, the temperature of the liquid phase in the reactor (T1) deviates from the temperature of the interface (T2) and gas phase (T3) to reach to the temperature of the water. 65 min and 74 min from the start of the dissociation, T2 and T3 suddenly increase and gradually increased to reach the water temperature. From the temperature profiles, it is clear that the hydrate dissociation takes place from the bottom to the top of the reactor. Figures 6.12a and 6.12c indicate that the pressure and temperature in the reactor are stable about 110 min after the start of the experiment indicating the completion of gas hydrate dissociation. In addition, both pressure and the temperature profiles from the dissociation are similar regardless of the presence of SDS during the formation. However, the pressure and temperature in the reactor from the dissociation of hydrate formed with SDS are stable around 90 min after the start of the experiment indicating faster completion of gas hydrate dissociation than the system without SDS.

In order to observe the effects of SDS concentration on the dissociation kinetics, the average normalized gas recovery from hydrates formed at each SDS concentration is presented in Figure 6.13. Normalized gas recovery is defined as the difference between the amounts of gas formed in the hydrates and the amount of gas recovered from the hydrates, which is then divided by the amount of gas recovered. The figure shows that the hydrate dissociation slightly increases with the increasing in the SDS concentration. The results are consistent with the literature, which reported that the hydrate dissociation rates increases with increasing the surfactants concentration.(Ganji *et al.*, 2007; Lin *et al.*, 2004) The final methane recovery from the hydrates formed with and without SDS is in the range of 96 - 98% , Figure S6.5 in Supporting Information.

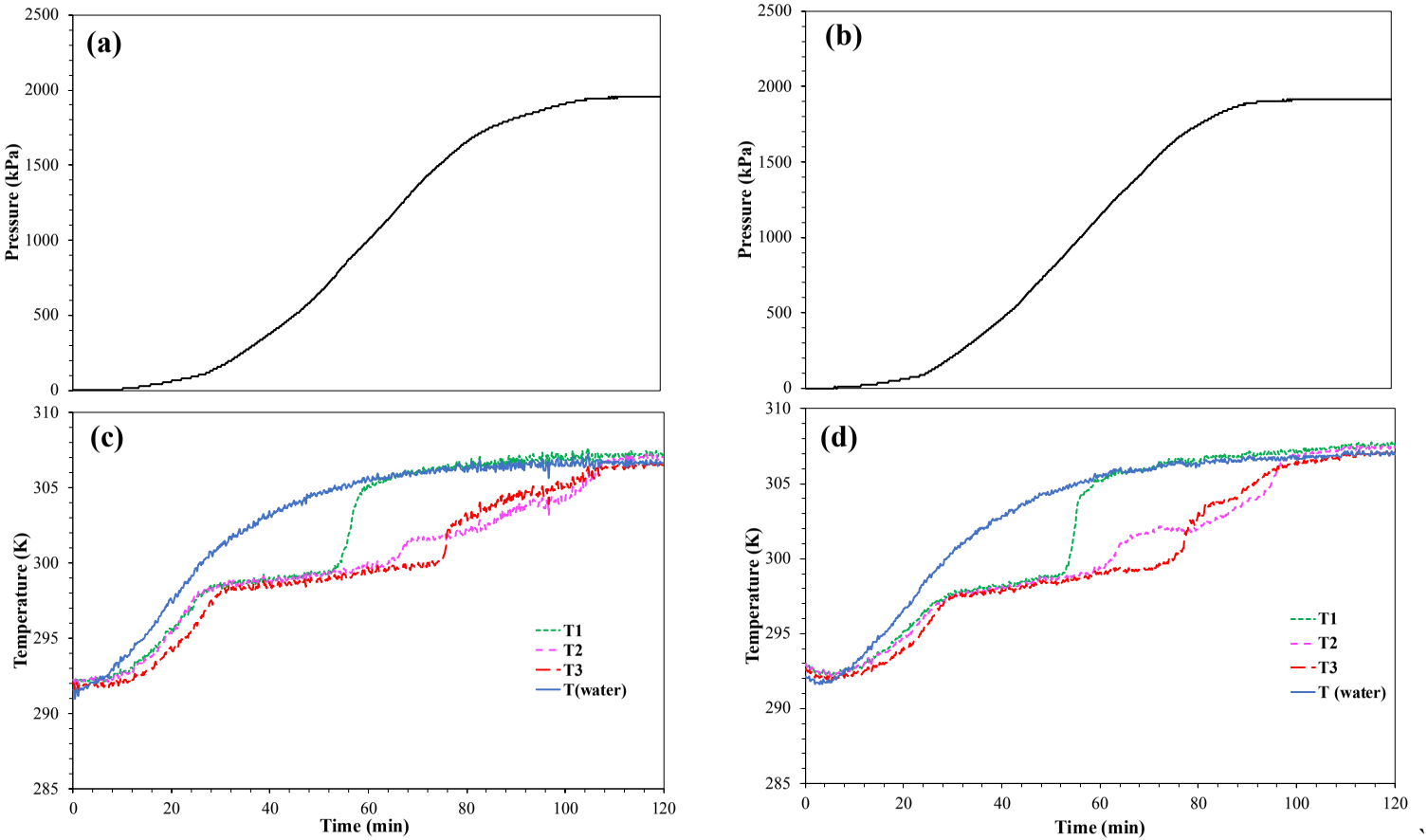

Figure 6.12 Pressure profiles during hydrate dissociation for (a) B-1 and (b) E-1; temperature profiles of the reactor and water during hydrate dissociation for (c) B-1 and (d) E-1.

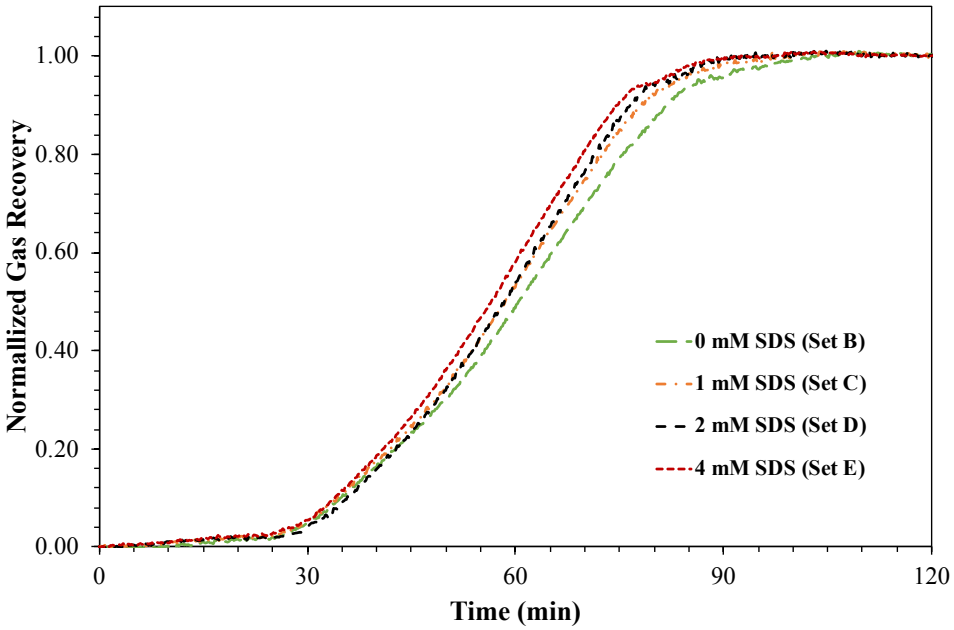

Figure 6.13 Average normalized recovery curves for the hydrate formation at 293.2 K and 6 MPa in the presence of 0.05 %w HS/v in 5.56 mol%THF and different SDS concentrations.

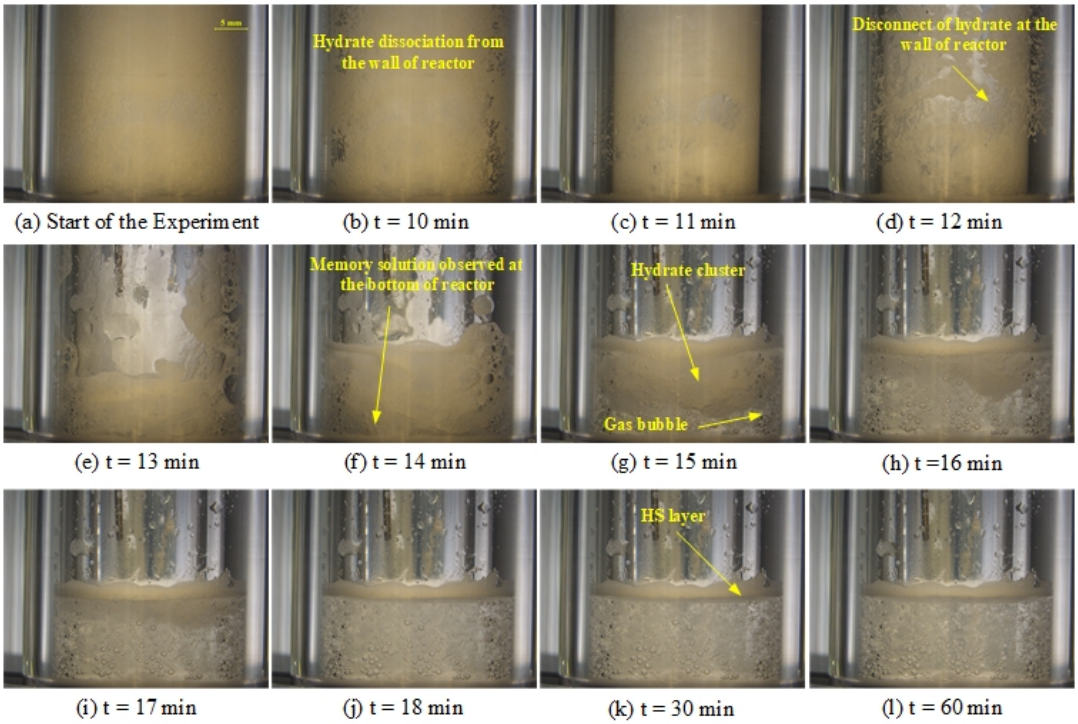

Figure 6.14 (a−l) Morphology during dissociation of hydrates formed with 0.5 %w HS/v in 5.56 mol% THF solution.

As described in the experimental procedure, the hydrate morphology during the decomposition experiments by thermal stimulation increasing temperature from 293.2 to 308.2 K was performed. Figure 6.14a presents the morphology of hydrates formed from 0.5 %w/v HS and THF solution at the start of hydrate dissociation (as observed at the end of formation experiment). After 10 min from the start of decomposition as in Figure 6.14b, traces of decomposing hydrates are observed along the walls of the reactor column. This is because as the reactor is immersed in the water bath, the wall of the reactor column gets heated first by the conduction heat transfer. Following this, the hydrate layer on the wall of the reactor gradually dissociates, as observed in Figures 6.14c-6.14e. Solution clearly becomes visible at the bottom and the wall of the reactor after 14 min (Figure 6.14f). At 15 min after hydrate formation (Figure 6.14g), gas bubbles appear in the solution during the hydrate decomposition due to the impending pressure in the system (bubbles held from going to the gas phase). With further progress in time, the hydrate cluster continuously decomposes, and the solution gets regenerated (Figures 6.14h-6.14i) with increased gas bubbles. At 18 min after hydrate formation (Figure 6.14j), the hydrate cluster completely decomposes and gas bubbles remain in the solution. These bubbles disappear when the gas is vented to the atmosphere. One interesting observation after of hydrate dissociation in the presence of 0.5 %w/v HS in THF solution is that the HS particles still float at the interface between gas and solution phase. Thus it is plausible to get the repeatable performance of kinetics of hydrate formation. Afterwards, no significant morphology change can be observed, Figures 6.14k-6.14l. Supporting Video SV6.3 shows the dissociation of methane hydrates formed from 0.5 %w/v HS and THF solution.

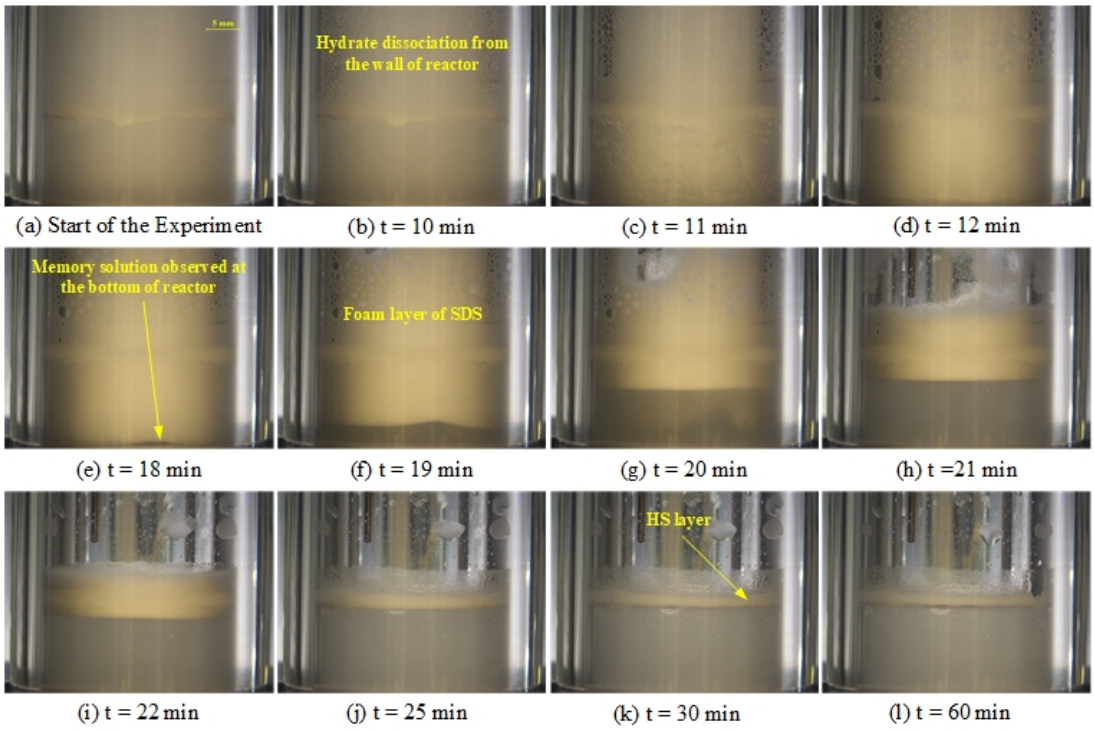

Figure 6.15 (a−l) Morphology during dissociation of hydrates formed with 0.5 % HS w/v in 5.56 mol% THF and 4 mM SDS solution.

Figure 6.15 represents a series of morphology observations made during the dissociation of hydraes formed with 4 mM SDS in 0.5 %w/v HS and 5.56 mol% THF. Hydrate morphology at the start of the hydrate dissociation process is shown in Figure 1 5 a. 10 min after the start of hydrate dissociation experiment (Figure 6.15b), hydrate dissociation starts to take place along the walls. Later on, the bubble foam can be observed due to the presence of the surfactant in the hydrates, as shown in Figures 6.15c-6.15d. At about 18 min, Figure 6.15e, the memory solution finally appears at the bottom of the reactor, indicating substantial hydrate dissociation. It should be noted that at this point, most memory solution is covered with the bubble foam. One minute further at 19 min, Figure 6.15f, the memory solution at the bottom of the reactor that is visible with a foam layer on top. Figures 6.15g-6.15j show that the memory solution at the bottom of the reactor increases with the decrease in the foam layer on the top. It should also be noted that bubbles in the solution appear during the hydrate decomposition. This trend continues until 30 min after the start of hydrate dissociation (Figure 6.15k) when all the memory solution is clearly visible, and most of the

generated foam disappears. Moreover, at this point, the layer of HS floats on the interface of gas/THF solution and some particles are attached to the wall of the reactor column wetted with THF solution. Finally, there is no further changes in the reactor column, Figure 6.15l. The video SV6.4 in Supporting Information presents the morphology during the dissociation.

The morphology observed during the dissociation clearly shows that the presence of HS in the formation is effectively reduce the foam generated by SDS making the system much easier and more efficient to handle. To highlight the action of HS in the foam reduction during the hydrate dissociation, Figure S6.4 in the Supporting Information is presented. This shows the series of hydrate dissociation pattern from the hydrates formed with the mixture of 4 mM SDS and 5.56 mol% THF (without HS). It further substantiates that the presence of HS reduces the foam formation during the dissociation. Note that, with only 4 mM SDS and 5.56 mol% THF, methane hydrates cannot form. To form the hydrates at this particular condition, a special procedure was employed. That included immediately reducing the methane pressure to 3 MPa and compressing the pressure back to 6 MPa in 10 s.

6.5 Conclusions

Experiments were performed to enhance the methane hydrate formation at lower driving force both temperature and pressure in the quiescent reactor (the pressure and temperature driving force about 3.88 MPa and 7 K, respectively). Firstly, the experiments were performed in the presence of only the stoichiometric 5.56 mole% THF at starting experimental of 6 MPa and 293.2 K. However, the presence of only of 5.56 mole% THF cannot form (nucleate) methane hydrates at this condition. The addition of 0.5 %w HS/v promoted the hydrate formation but it took longer than 400 min with slow rate of hydrate formation. To decrease the induction time to form the mixed methane-THF hydrates, SDS was used. The presence of SDS decreased the induction time to lower than 200 min with faster rate of hydrate formation. Furthermore, the induction time decreased with the increase in the SDS concentration. The presence of SDS in the mixture of 0.5 %w HS/v and 5.56 mol% THF significantly improved the hydrate formation rate, methane uptake and the rate of hydrate

dissociation. Morphology during the hydrate formation clearly showed the effects of SDS. Without SDS, the hydrate formation started from the interface between gas and liquid phase predominatly in the upward direction due to the capillary force of HS particles before growing in the downward direction. On the other hand, with SDS, the formation took place both upwardly and downwardly simultaneously. Methane recovery in the range of 95 - 97 % was achieved from the gas hydrates with and without SDS. A HS layer was observed at the interface after the completion of hydrate dissociation showcasing the plausibility of repeated kinetic performance and regenerability of the solution. From the hydrate dissociation morphology, the presence of HS along with SDS is effective in reducing or preventing the foam generation during the hydrate dissociation.

6.6 Acknowledgements

This work was supported by The Royal Golden Jubilee Ph.D. Program (2.P.CU/58/J.1), Thailand Research Fund; The Petroleum and Petrochemical College (PPC), Chulalongkorn University, Thailand; Center of Excellence on Petrochemical and Materials Technology (PETROMAT), Thailand; Grant for International Research Integration: Chula Research Scholar, Ratchadaphiseksomphot Endowment Fund, Chulalongkorn University, Thailand; Thailand Energy Conservation Fund, Energy Policy and Planning Office Ministry of Energy; Department of Chemical and Biomolecular Engineering, Faculty of Engineering, National University of Singapore (NUS), UOP, A Honeywell Company, USA.

6.7 Supporting Information

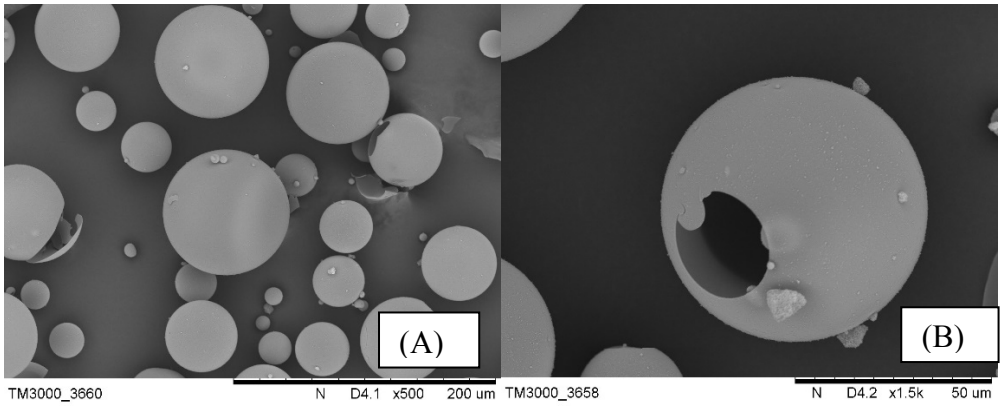

Figure S6.1 Morphology of hollow silica by scanning electron microscope (SEM) (a) Particle of hollow silica in different sizes, (b) Breakage hollow silica.

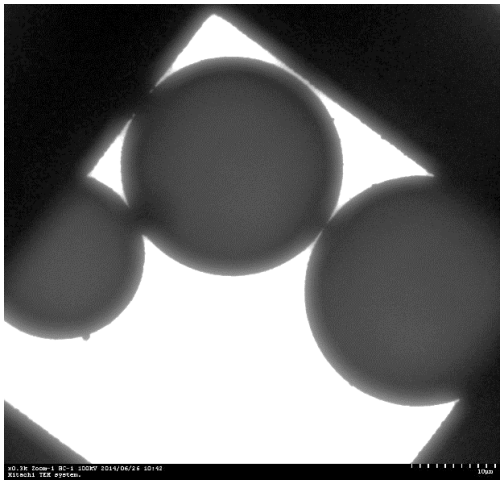

Figure S6.2 Particles of hollow silica by transmission electron microscope (TEM).

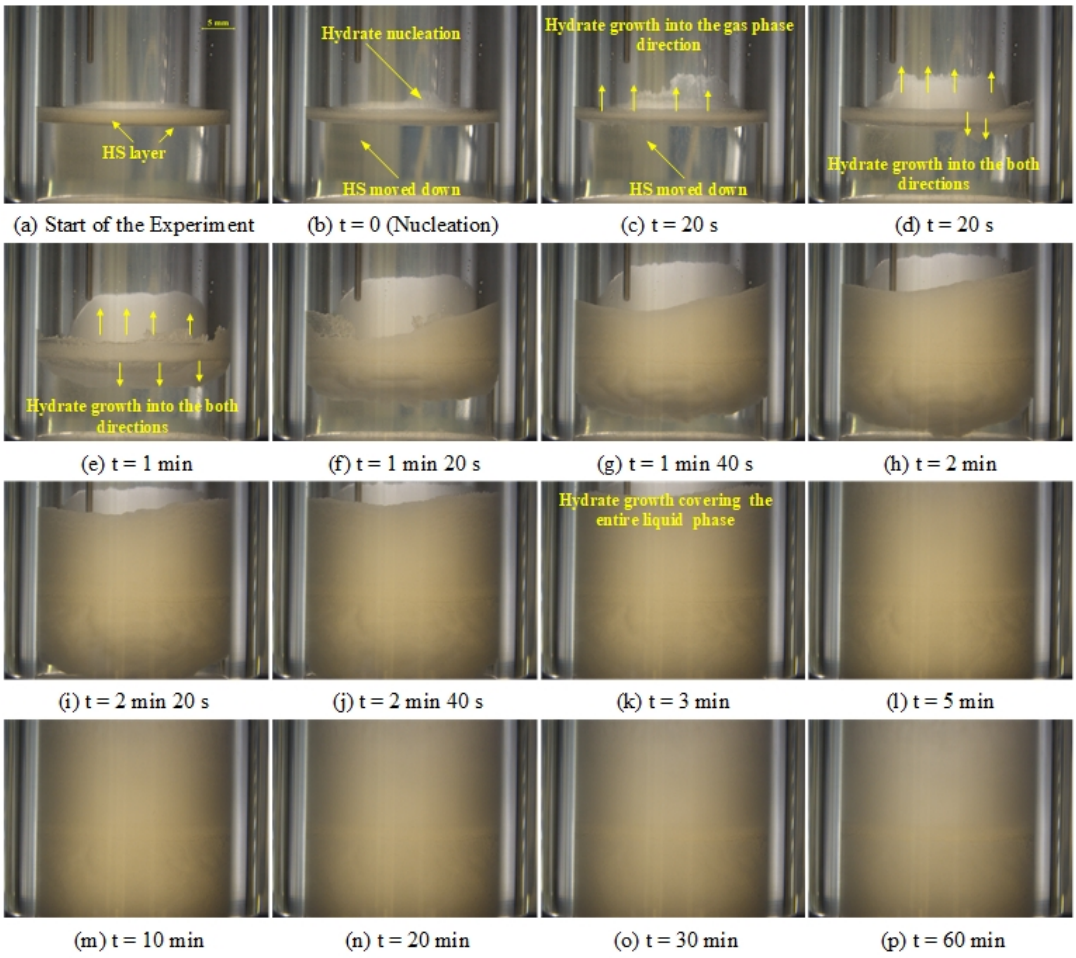

Figure S6.3 (a-p) The morphology of methane hydrate formation of the mixture of 0.5 w/v % HS in 5.56 mol% THF solution and 1 mM SDS solution.

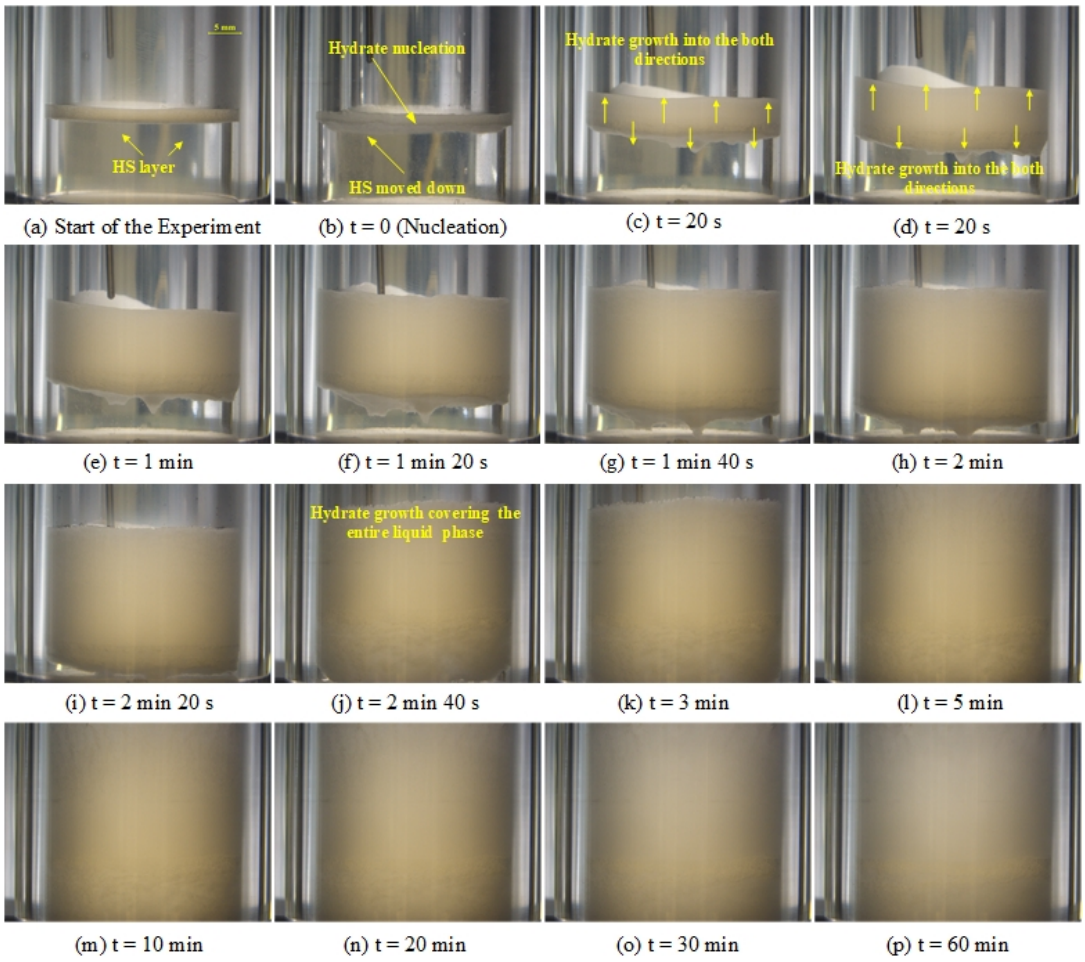

Figure S6.4 (a-p) The morphology of methane hydrate formation of the mixture of 0.5 w/v % HS in 5.56 mol% THF solution and 2 mM SDS solution.

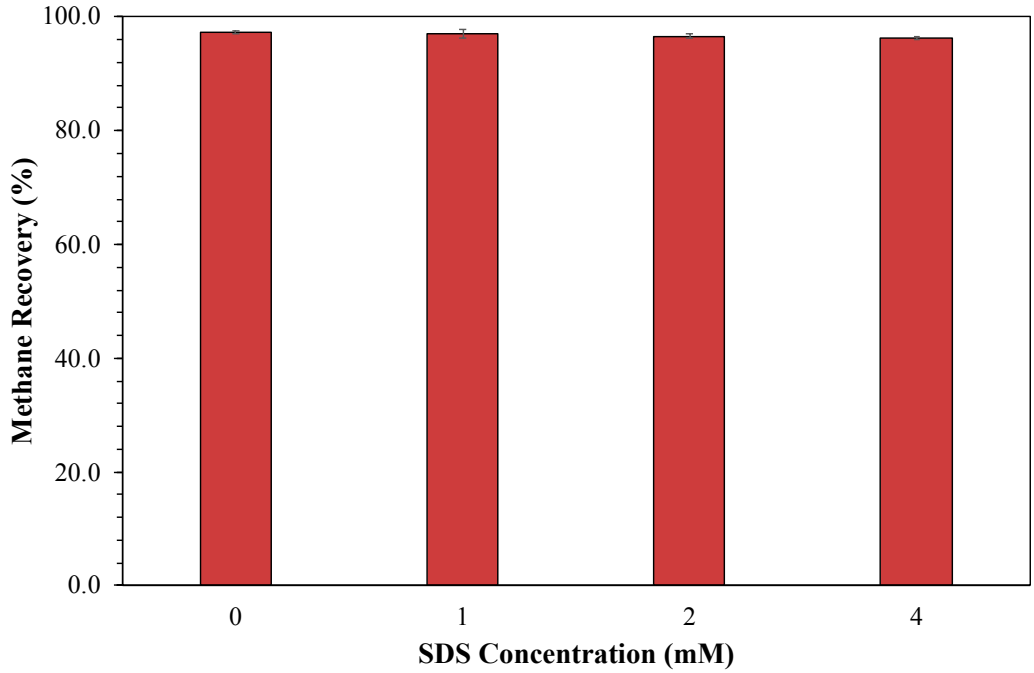

Figure S6.5 Methane recovery at different SDS concentrations.

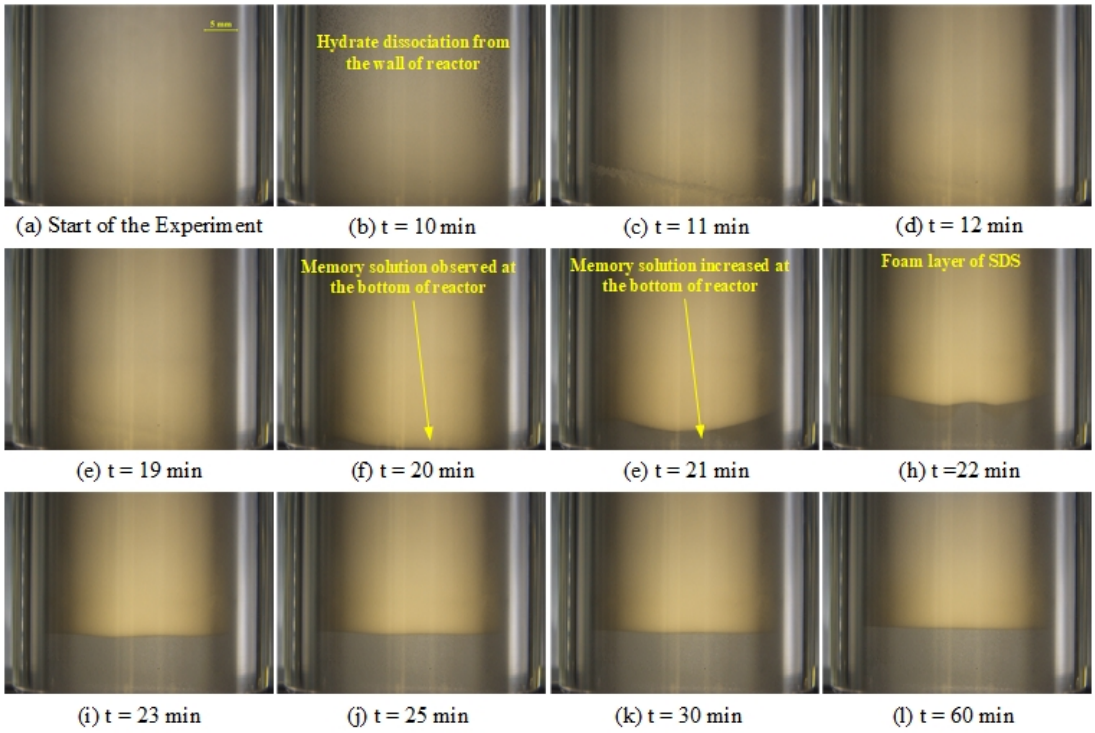

Figure S6.6 (a−l) Morphology of methane hydrate dissociation of the mixture of 5.56 mol% THF and 4 mM SDS solution.

6.8 References

Babu, P., Kumar, R., and Linga, P. (2013). Pre-combustion capture of carbon dioxide in a fixed bed reactor using the clathrate hydrate process. Energy, 50, 364-373.

Bolden, P. L., Hoskins, J. C., and King, A. D. (1983). The solubility of gases in solutions containing sodium alkylsulfates of various chain lengths. Journal of Colloid and Interface Science, 91(2), 454-463.

Boswell, R., and Collett, T. S. (2011). Current perspectives on gas hydrate resources. Energy & Environmental Science, 4(4), 1206-1215.

Cha, S. B., Ouar, H., Wildeman, T. R., and Sloan, E. D. (1988). A third-surface effect on hydrate formation. The Journal of Physical Chemistry, 92(23), 6492-6494.

Chari, V. D., Prasad, P. S. R., and Murthy, S. R. (2015). Hollow silica: A novel material for methane storage. Oil & Gas Science and Technology, 70(6), 1125-1132.

Chari, V. D., Raju, B., Prasad, P. S. R., and Rao, D. N. (2013a). Methane hydrates in spherical silica matrix: optimization of capillary water. Energy & Fuels, 27(7), 3679-3684.

Chari, V. D., Sharma, D. V. S. G. K., Prasad, P. S. R., and Murthy, S. R. (2013b). Methane hydrates formation and dissociation in nano silica suspension. Journal of Natural Gas Science and Engineering, 11, 7-11.

Chen, H., Yan, Z., Li, B., Li, Y., and Wu, Q.-H. (2013). Manipulation of mesoporous silica hollow spheres by control of silica precursors. Materials Letters, 112, 78-80.

Demirbas, A. (2010). Methane hydrates as potential energy resource: Part 1 – Importance, resource and recovery facilities. Energy Conversion and Management, 51(7), 1547-1561.

EIA. (2017). Annual Energy Outlook 2017 with projections to 2050. 126.

Englezos, P., and Lee, J. D. (2005). Gas hydrates: A cleaner source of energy and opportunity for innovative technologies. Korean Journal of Chemical Engineering, 22(5), 671-681.

Florusse, L. J., Peters, C. J., Schoonman, J., Hester, K. C., Koh, C. A., Dec, S. F., Marsh, K. N., and Sloan, E. D. (2004). Stable low-pressure hydrogen clusters stored in a binary clathrate hydrate. Science 306(5695), 469-471.

Ganji, H., Manteghian, M., Sadaghiani zadeh, K., Omidkhah, M. R., and Rahimi Mofrad, H. (2007). Effect of different surfactants on methane hydrate formation rate, stability and storage capacity. Fuel, 86(3), 434-441.

Inkong, K., Rangsunvigit, P., Kulprathipanja, S., and Linga, P. (2019a). Effects of temperature and pressure on the methane hydrate formation with the presence of tetrahydrofuran (THF) as a promoter in an unstirred tank reactor. Fuel, 255, 115705.

Inkong, K., Veluswamy, H. P., Rangsunvigit, P., Kulprathipanja, S., and Linga, P. (2019b). Investigation on the kinetics of methane hydrate formation in the presence of methyl ester sulfonate. Journal of Natural Gas Science and Engineering, 71, 102999.

Jager, M. D., de Deugd, R. M., Peters, C. J., de Swaan Arons, J., and Sloan, E. D. (1999). Experimental determination and modeling of structure II hydrates in mixtures of methane+water+1,4-dioxane. Fluid Phase Equilibria, 165(2), 209-223.

Kalogerakis, N., Jamaluddin, A. K. M., Dholabhai, P. D., and Bishnoi, P. R. (1993). *Effect of surfactants on hydrate formation kinetics*. Paper presented at the SPE International Symposium on Oilfield Chemistry, New Orleans, Louisiana.

Kashchiev, D., and Firoozabadi, A. (2002). Driving force for crystallization of gas hydrates. Journal of Crystal Growth, 241(1), 220-230.

Khokhar, A. A., Gudmundsson, J. S., and Sloan, E. D. (1998). Gas storage in structure H hydrates. Fluid Phase Equilibria, 150-151, 383-392.

Koh, C. A., Sloan, E. D., Sum, A. K., and Wu, D. T. (2011). Fundamentals and applications of gas hydrates. Annu Rev Chem Biomol Eng, 2, 237-257.

Kumar, A., Daraboina, N., Kumar, R., and Linga, P. (2016). Experimental investigation to elucidate why tetrahydrofuran rapidly promotes methane hydrate formation kinetics: Applicable to energy storage. The Journal of Physical Chemistry C, 120(51), 29062-29068.

Kumar, A., Sakpal, T., Linga, P., and Kumar, R. (2015). Enhanced carbon dioxide hydrate formation kinetics in a fixed bed reactor filled with metallic packing. Chemical Engineering Science, 122, 78-85.

Kumar, A., Veluswamy, H. P., Linga, P., and Kumar, R. (2019). Molecular level investigations and stability analysis of mixed methane-tetrahydrofuran hydrates: Implications to energy storage. Fuel, 236, 1505-1511.

Lee, Y.-J., Kawamura, T., Yamamoto, Y., and Yoon, J.-H. (2012). Phase equilibrium studies of tetrahydrofuran (THF) + CH4, THF + CO2, CH4 + CO2, and THF + CO2 + CH4 hydrates. Journal of Chemical & Engineering Data, 57(12), 3543-3548.

Lin, W., Chen, G. J., Sun, C. Y., Guo, X. Q., Wu, Z. K., Liang, M. Y., Chen, L. T., and Yang, L. Y. (2004). Effect of surfactant on the formation and dissociation kinetic behavior of methane hydrate. Chemical Engineering Science, 59(21), 4449-4455.

Linga, P., Haligva, C., Nam, S. C., Ripmeester, J. A., and Englezos, P. (2009). Recovery of methane from hydrate formed in a variable volume bed of silica sand particles. Energy & Fuels, 23(11), 5508-5516.

Linga, P., Kumar, R., and Englezos, P. (2007). The clathrate hydrate process for post and pre-combustion capture of carbon dioxide. J Hazard Mater, 149(3), 625-629.

Luo, Y. T., Zhu, J. H., Fan, S. S., and Chen, G. J. (2007). Study on the kinetics of hydrate formation in a bubble column. Chemical Engineering Science, 62(4), 1000-1009.

Makino, T., Sugahara, T., and Ohgaki, K. (2005). Stability boundaries of tetrahydrofuran + water system. Journal of Chemical & Engineering Data, 50(6), 2058-2060.

Makogon, Y. F. (2010). Natural gas hydrates – A promising source of energy. Journal of Natural Gas Science and Engineering, 2(1), 49-59.

Mech, D., Gupta, P., and Sangwai, J. S. (2016). Kinetics of methane hydrate formation in an aqueous solution of thermodynamic promoters (THF and TBAB) with and without kinetic promoter (SDS). Journal of Natural Gas Science and Engineering, 35, 1519-1534.

Mohammadi, A. H., and Richon, D. (2009). Phase equilibria of clathrate hydrates of tetrahydrofuran + hydrogen sulfide and tetrahydrofuran + methane. Industrial & Engineering Chemistry Research, 48(16), 7838-7841.

Moraveji, M. k., Ghaffarkhah, A., and Sadeghi, A. (2017). Effect of three representative surfactants on methane hydrate formation rate and induction time. Egyptian Journal of Petroleum, 26(2), 331-339.

Okutani, K., Kuwabara, Y., and Mori, Y. H. (2008). Surfactant effects on hydrate formation in an unstirred gas/liquid system: An experimental study using methane and sodium alkyl sulfates. Chemical Engineering Science, 63(1), 183-194.

Prasad, P. S. R., Sowjanya, Y., and Dhanunjana Chari, V. (2014). Enhancement in methane storage capacity in gas hydrates formed in hollow silica. The Journal of Physical Chemistry C, 118(15), 7759-7764.

Prasad, P. S. R., Sowjanya, Y., and Shiva Prasad, K. (2009). Micro-Raman investigations of mixed gas hydrates. Vibrational Spectroscopy, 50(2), 319-323.

Roy, S., Mehra, A., and Bhowmick, D. (1997). Prediction of solubility of nonpolar gases in micellar solutions of ionic surfactants. J Colloid Interface Sci, 196(1), 53-61.

Seo, Y. T., Kang, S. P., and Lee, H. (2001). Experimental determination and thermodynamic modeling of methane and nitrogen hydrates in the presence of THF, propylene oxide, 1,4-dioxane and acetone. Fluid Phase Equilibria, 189(1), 99-110.

Siangsai, A., Rangsunvigit, P., Kitiyanan, B., Kulprathipanja, S., and Linga, P. (2015). Investigation on the roles of activated carbon particle sizes on methane hydrate formation and dissociation. Chemical Engineering Science, 126, 383-389.

Sloan, E. D., and Koh, C. A. (2008). *Clathrate Hydrates of Natural Gases*. New York: CRC Press.

Smith, J. M., Van Ness, H. C., and Abbott, M. M. (2005). *Introduction to Chemical Engineering Thermodynamics*. Singapore: McGraw-Hill.

Sugahara, T., Haag, J. C., Prasad, P. S. R., Warntjes, A. A., Sloan, E. D., Sum, A. K., and Koh, C. A. (2009). Increasing hydrogen storage capacity using

tetrahydrofuran. Journal of the American Chemical Society, 131(41), 14616-14617.

Sun, C.-Y., Chen, G.-J., and Yang, L.-Y. (2004). Interfacial tension of methane + water with surfactant near the hydrate formation conditions. Journal of Chemical & Engineering Data, 49(4), 1023-1025.

Tang, L.-G., Li, X.-S., Feng, Z.-P., Lin, Y.-L., and Fan, S.-S. (2006). Natural Gas Hydrate Formation in an Ejector Loop Reactor: Preliminary Study. Industrial & Engineering Chemistry Research, 45(23), 7934-7940.

Veluswamy, H. P., Ang, W. J., Zhao, D., and Linga, P. (2015). Influence of cationic and non-ionic surfactants on the kinetics of mixed hydrogen/tetrahydrofuran hydrates. Chemical Engineering Science, 132, 186-199.

Veluswamy, H. P., Hong, Q. W., and Linga, P. (2016a). Morphology study of methane hydrate formation and dissociation in the presence of amino acid. Crystal Growth & Design, 16(10), 5932-5945.

Veluswamy, H. P., Kumar, A., Seo, Y., Lee, J. D., and Linga, P. (2018). A review of solidified natural gas (SNG) technology for gas storage via clathrate hydrates. Applied Energy, 216, 262-285.

Veluswamy, H. P., Kumar, S., Kumar, R., Rangsunvigit, P., and Linga, P. (2016b). Enhanced clathrate hydrate formation kinetics at near ambient temperatures and moderate pressures: Application to natural gas storage. Fuel, 182, 907-919.

Veluswamy, H. P., Prasad, P. S. R., and Linga, P. (2016c). Mechanism of methane hydrate formation in the presence of hollow silica. Korean Journal of Chemical Engineering, 33(7), 2050-2062.

Veluswamy, H. P., Wong, A. J. H., Babu, P., Kumar, R., Kulprathipanja, S., Rangsunvigit, P., and Linga, P. (2016d). Rapid methane hydrate formation to develop a cost effective large scale energy storage system. Chemical Engineering Journal, 290, 161-173.

Verrett, J., Posteraro, D., and Servio, P. (2012). Surfactant effects on methane solubility and mole fraction during hydrate growth. Chemical Engineering Science, 84, 80-84.

Vysniauskas, A., and Bishnoi, P. R. (1983). A kinetic study of methane hydrate formation. Chemical Engineering Science, 38(7), 1061-1072.

Wang, F., Jia, Z.-Z., Luo, S.-J., Fu, S.-F., Wang, L., Shi, X.-S., Wang, C.-S., and Guo, R.-B. (2015). Effects of different anionic surfactants on methane hydrate formation. Chemical Engineering Science, 137, 896-903.

Watanabe, K., Imai, S., and Mori, Y. H. (2005). Surfactant effects on hydrate formation in an unstirred gas/liquid system: An experimental study using HFC-32 and sodium dodecyl sulfate. Chemical Engineering Science, 60(17), 4846-4857.

Zhong, D.-L., Daraboina, N., and Englezos, P. (2013). Coal mine methane gas recovery by hydrate formation in a fixed bed of silica sand particles. Energy & Fuels, 27(8), 4581-4588.

Zhong, D.-L., Lu, Y.-Y., Sun, D.-J., Zhao, W.-L., and Li, Z. (2015). Performance evaluation of methane separation from coal mine gas by gas hydrate formation in a stirred reactor and in a fixed bed of silica sand. Fuel, 143, 586-594.

Zhong, Y., and Rogers, R. E. (2000). Surfactant effects on gas hydrate formation. Chemical Engineering Science, 55(19), 4175-4187.

CHAPTER VII
CONCLUSIONS AND RECOMMENDATIONS

7.1 Conclusions

In order to improve the gas hydrate technology for natural gas storage and transportation, the hydrate formation and dissociation by using hydrate promoters were performed.

In Chapter IV, the effects of MES, bio-based and biodegradable anionic surfactant, on the methane hydrate formation at 277.2 K and 8 MPa was performed. The idea in this chapter to use bio-based materials as the hydrate promoter is to decrease the risk of the environment and humans impact by using the synthetic surfactant and to find a new hydrate promoter. The methane hydrate formation and dissociation experiments were carried out with 1-8 mM. The results indicated that all concentrations of MES significantly enhanced the methane hydrate formation rate and methane consumption compared with pure water (no methane hydrate formation for 48 h). The increase in the MES concentration decreased the induction time and increased the final methane uptake. The multiple hydrate nucleation was observed in all MES concentrations during the hydrate formation. The hydrate morphology during the hydrate formation of all MES concentrations showed similar hydrate growth pattern. The hydrate nucleation started at the interface of gas and liquid, followed by the hydrate growth in the upward direction and then downward direction. Hydrate dissociation was performed by thermal stimulation method by increasing the temperature to 298.2 K. Methane recovery was not significantly different with different MES concentrations, and the recovery was higher than 95%. During the dissociation, the hydrate dissociation started from the wall of the reactor column followed by the bulk hydrates inside the reactor.

However, in Chapter IV, the hydrate formation was performed at the low temperature and high pressure. This condition is unpractical in the industrial scale. So, in Chapter V, the hydrate formation was conducted by using THF which was thermodymanic promoter by changing the hydrate phase equilibrium to higher temperature and lower pressure. In Chapter V, the experiments were performed to

study the effects of temperature and pressure on methane hydrate formation by using THF concentration of 5.56 mol%. First, the effect temperature was conducted at 8 MPa and four different temperatures, 277.2, 283.2, 288.2, and 293.2 K. The experiment temperature was divided into two regions. 277.2 and 283.2 K are in the sI region of pure methane hydrate phase equilibrium, while at 288.2 and 293.2 K are in the sII region in the mixed methane+5.56 mol% THF hydrate phase equilibrium. The results showed that the formation starting in the sI region had higher mixed methane hydrate formation rate due to the higher temperature and pressure driving forces. The hydrate formation starting in the sII region had higher methane uptake because of two-stage hydrate growth during the hydrate formation and effective heat distribution to the surrounding. Later, the formation was also conducted at three different pressures, 4, 6, and 8 MPa, and at 288.2 K. The results showed that the formation rate decreased as the result from the decrease in the pressure driving force. However, the decrease in pressure did not change the final methane uptake. Moreover, kinetics of the mixed hydrate formation at 293.2 K and 8 MPa was enhanced by using MES. The presence a small amount of MES decreased the time for hydrate formation nucleation and increased rate of hydrate formation. The presence of MES did not affect the final methane uptake. The average gas recovery in the rage of 89.05-97.25% was achieved from the dissociating hydrates formed from the different starting pressure and temperature conditions.

In Chapter VI, the experiments were performed to enhance the methane hydrate formation at 6 MPa and 293.2 K. This condition is lower driving force both temperature and pressure by using three hydrate promoters including THF, HS, and SDS. The results indicated that there was no hydrate formation with only 5.56 mole% THF at 6 MPa and 293.2 K. However, the presence of 0.5 %w HS/v promoted the hydrate formation at this condition. Nevertheless, the induction time was longer than 400 min with slow hydrate formation rate. To improve the kinetics of the mixed methane hydrates at this condition, SDS was employed. SDS concentration was varied from 1 to 4 mM. The presence of SDS predominantly decreased the induction time and significantly increased the rate of hydrate formation. Furthermore, the increase in the SDS concentration decreased the time for hydrate nucleation. The methane uptakes with and without SDS were about the same for all SDS concentrations. Moreover, the

presence of SDS totally changed the morphology of the mixed hydrate formation. For the mixed hydrae formation without SDS, the nucleation of mixed hydrate started from the interface between gas and liquid phase and predominantly grew in the upward direction because of the capillary force between HS particles before growing into the downward direction. On the contrary, with the presence SDS, after the hydrate nucleation formed at the interphase, the mixed hydrates grew both upward and downwardly simultaneously. Methane recovery in the range of 95- 97 % was achieved from the mixed hydrates with and without SDS. From the hydrate dissociation morphology, after the completion of hydrate dissociation, the HS layer at the interface was observed showcasing the plausibility of repeated kinetic performance and regenerability of the solution. Furthermore, the presence of HS along with SDS was effective in reducing or preventing the foam generation during the hydrate dissociation.

7.2 Recommendations

The are several possible parameters to promote the hydrate formation and dissociation including the conditions of hydrate formation, promoter, and reactor design. To apply the gas hydrate technology to store and transport the natural gas on large scale, the hydrate formation condition should be operated at the moderate condition such as high temperature and low pressure condition. For the promoter, there are several promoters to enhance the hydrate formation such as activated carbon, silica sand, nano silica, and clay, or chemicals such as cyclopentane or acetone, ethylene glycol, etc. to promote the hydrate formation. However, choosing a hydrate promoter should take the impact on the environment and humans into consideration.

Moreover, the hydrate formation using a surfactant as the hydrate promoter inherited is the foam generation during the hydrate dissociation. To avoid foam problems generated during the hydrate dissociation, alternatives to decrease the foam generation such as using a new reactor design to remove foam during the hydrate dissociation or mixing with an antifoam like silicon surfactant or non-ionic surfactant.

For further investigation, another strategy to improve the hydrate formation at moderate condition is to vary HS concentration to find the optimum HS concentration for improving the rate of hydrate formation without adding the co-promoter. Moreover, using hybrid reactor is an alternative method to decrease the time to form the hydrate nucleation and the hydrate formation kinetics.

Apart from the hydrate formation condition and hydrate promoter, the continuous or semi-bath reactor should be applied instead of a bath reactor to determine the optimum condition for hydrate formation.

REFFERENCES

Allison, E. (2008). Methane Hydrate. In T. M. Letcher (Ed.), *Future Energy: Improved, Sustainable and Clean Options for our Planet* (pp. 227-290). Netherlands: Elsevier.

Anderson, R., Chapoy, A., and Tohidi, B. (2007). Phase relations and binary clathrate hydrate formation in the system H2−THF−H2O. Langmuir, 23(6), 3440-3444.

Babu, P., Kumar, R., and Linga, P. (2013). Pre-combustion capture of carbon dioxide in a fixed bed reactor using the clathrate hydrate process. Energy, 50, 364-373.

Bimbo, N., Physick, A. J., Noguera-Díaz, A., Pugsley, A., Holyfield, L. T., Ting, V. P., and Mays, T. J. (2015). High volumetric and energy densities of methane stored in nanoporous materials at ambient temperatures and moderate pressures. Chemical Engineering Journal, 272, 38-47.

Carroll, J. (2014). *Natural gas hydrates: A guide for engineers* (3 ed.). USA: Gulf Professional Publishing.

Cha, S. B., Ouar, H., Wildeman, T. R., and Sloan, E. D. (1988). A third-surface effect on hydrate formation. The Journal of Physical Chemistry, 92(23), 6492-6494.

Chari, V. D., Prasad, P. S. R., and Murthy, S. R. (2015). Hollow silica: A novel material for methane storage. Oil & Gas Science and Technology, 70(6), 1125-1132.

Chaturvedi, E., Prasad, N., and Mandal, A. (2018). Enhanced formation of methane hydrate using a novel synthesized anionic surfactant for application in storage and transportation of natural gas. Journal of Natural Gas Science and Engineering, 56, 246-257.

Chen, H., Yan, Z., Li, B., Li, Y., and Wu, Q.-H. (2013). Manipulation of mesoporous silica hollow spheres by control of silica precursors. Materials Letters, 112, 78-80.

Collett, T. S. (2002). Energy resource potential of natural gas hydrates. AAPG Bulletin, 86(11), 1971-1992.

Curran, S. J., Wagner, R. M., Graves, R. L., Keller, M., and Green, J. B. (2014). Well-to-wheel analysis of direct and indirect use of natural gas in passenger vehicles. Energy, 75, 194-203.

De, S., Malik, S., Ghosh, A., Saha, R., and Saha, B. (2015). A review on natural surfactants. RSC Advances, 5(81), 65757-65767.

Demirbas, A. (2010a). Methane hydrates as potential energy resource: Part 1 – Importance, resource and recovery facilities. Energy Conversion and Management, 51(7), 1547-1561.

Demirbas, A. (2010b). Natural Gas. In A. Demirbas (Ed.), *Mathane Hydrate* (pp. 57-76). London, England: Springer-Verlag London.

EIA. (2016). Annual Energy Outlook 2016. 152.

EIA. (2019). Annual Energy Outlook 2019. 152.

Englezos, P. (1993). Clathrate hydrates. Industrial & Engineering Chemistry Research, 32(7), 1251-1274.

Florusse, L. J., Peters, C. J., Schoonman, J., Hester, K. C., Koh, C. A., Dec, S. F., Marsh, K. N., and Sloan, E. D. (2004). Stable low-pressure hydrogen clusters stored in a binary clathrate hydrate. Science 306(5695), 469-471.

Fukumoto, K., Tobe, J.-i., Ohmura, R., and Mori, Y. H. (2001). Hydrate formation using water spraying in a hydrophobic gas: A preliminary study. AlChE Journal, 47(8), 1899-1904.

Ganji, H., Manteghian, M., Sadaghiani zadeh, K., Omidkhah, M. R., and Rahimi Mofrad, H. (2007). Effect of different surfactants on methane hydrate formation rate, stability and storage capacity. Fuel, 86(3), 434-441.

Giavarini, C., Maccioni, F., Politi, M., and Santarelli, M. L. (2007). CO2 hydrate: formation and dissociation compared to methane hydrate. Energy & Fuels, 21(6), 3284-3291.

Gudmundsson, J. S., Parlaktuna, M., and Khokhar, A. A. (1994). Storage of natural gas as frozen hydrate. SPE Production & Facilities, 9(01), 69-73.

Haligva, C., Linga, P., Ripmeester, J. A., and Englezos, P. (2010). Recovery of methane from a variable-volume bed of silica sand/hydrate by depressurization. Energy & Fuels, 24(5), 2947-2955.

Iwasaki, T., Katoh, Y., Nagamori, S., Takahashi, S., and Oya, N. (2005). *Continuous natural gas hydrate pellet production (NGHP) by process development unit (PDU)*: Tapir forlag, Trondheim (Norway).

Javanmardi, J., Nasrifar, K., Najibi, S. H., and Moshfeghian, M. (2005). Economic evaluation of natural gas hydrate as an alternative for natural gas transportation. Applied Thermal Engineering, 25(11), 1708-1723.

Khamehchi, E., Yousefi, S., and Sanaei, A. (2013). Selection of the Best Efficient Method for Natural Gas Storage at High Capacities Using TOPSIS Method. Gas Processing Journal, 1, 9-18.

Khan, M. I., Yasmin, T., and Shakoor, A. (2015). Technical overview of compressed natural gas (CNG) as a transportation fuel. Renewable and Sustainable Energy Reviews, 51, 785-797.

Koh, C. A., Sloan, E. D., Sum, A. K., and Wu, D. T. (2011). Fundamentals and applications of gas hydrates. Annu Rev Chem Biomol Eng, 2, 237-257.

Kumar, A., Daraboina, N., Kumar, R., and Linga, P. (2016). Experimental investigation to elucidate why tetrahydrofuran rapidly promotes methane hydrate formation kinetics: Applicable to energy storage. The Journal of Physical Chemistry C, 120(51), 29062-29068.

Kumar, A., Veluswamy, H. P., Linga, P., and Kumar, R. (2019). Molecular level investigations and stability analysis of mixed methane-tetrahydrofuran hydrates: Implications to energy storage. Fuel, 236, 1505-1511.

Kvamme, B., Graue, A., Buanes, T., Kuznetsova, T., and Ersland, G. (2007). Storage of CO2 in natural gas hydrate reservoirs and the effect of hydrate as an extra sealing in cold aquifers. International Journal of Greenhouse Gas Control, 1(2), 236-246.

Kvenvolden, K. A. (1993). Gas hydrates—geological perspective and global change. 31(2), 173-187.

Kvenvolden, K. A. (1999). Potential effects of gas hydrate on human welfare. 96(7), 3420-3426.

Lee, H., Lee, J.-w., Kim, D. Y., Park, J., Seo, Y.-T., Zeng, H., Moudrakovski, I. L., Ratcliffe, C. I., and Ripmeester, J. A. (2005). Tuning clathrate hydrates for hydrogen storage. Nature, 434, 743.

Lee, Y.-J., Kawamura, T., Yamamoto, Y., and Yoon, J.-H. (2012). Phase equilibrium studies of tetrahydrofuran (THF) + CH4, THF + CO2, CH4 + CO2, and THF + CO2 + CH4 hydrates. Journal of Chemical & Engineering Data, 57(12), 3543-3548.

Lin, W., Chen, G. J., Sun, C. Y., Guo, X. Q., Wu, Z. K., Liang, M. Y., Chen, L. T., and Yang, L. Y. (2004). Effect of surfactant on the formation and dissociation kinetic behavior of methane hydrate. Chemical Engineering Science, 59(21), 4449-4455.

Linga, P., Kumar, R., and Englezos, P. (2007). The clathrate hydrate process for post and pre-combustion capture of carbon dioxide. J Hazard Mater, 149(3), 625-629.

Lozano-Castelló, D., Alcañiz-Monge, J., de la Casa-Lillo, M. A., Cazorla-Amorós, D., and Linares-Solano, A. (2002). Advances in the study of methane storage in porous carbonaceous materials. Fuel, 81(14), 1777-1803.

Luo, Y. T., Zhu, J. H., Fan, S. S., and Chen, G. J. (2007). Study on the kinetics of hydrate formation in a bubble column. Chemical Engineering Science, 62(4), 1000-1009.

Mandal, A., and Laik, S. (2008). Effect of the promoter on gas hydrate formation and dissociation. Energy & Fuels, 22(4), 2527-2532.

Milkov, A. V. (2004). Global estimates of hydrate-bound gas in marine sediments: how much is really out there? Earth-Science Reviews, 66(3), 183-197.

Nam, S. C., Linga, P., Haligva, C., Ripmeester, J. A., and Englezos, P. (2008). *Kinetics of hydrate fromation and decomposition methane in silica sand.* Paper presented at the the 6th International Conference on Gas Hydrate (ICGH2008), British Columbia, Canada.

Okutani, K., Kuwabara, Y., and Mori, Y. H. (2008). Surfactant effects on hydrate formation in an unstirred gas/liquid system: An experimental study using methane and sodium alkyl sulfates. Chemical Engineering Science, 63(1), 183-194.

Partoon, B., and Javanmardi, J. (2013). Effect of mixed thermodynamic and kinetic hydrate promoters on methane hydrate phase boundary and formation kinetics. Journal of Chemical & Engineering Data, 58(3), 501-509.

Perrin, A., Musa, O. M., and Steed, J. W. (2013). The chemistry of low dosage clathrate hydrate inhibitors. Chemical Society Reviews, 42(5), 1996-2015.

Prasad, P. S. R., Sowjanya, Y., and Dhanunjana Chari, V. (2014). Enhancement in methane storage capacity in gas hydrates formed in hollow silica. The Journal of Physical Chemistry C, 118(15), 7759-7764.

Prasad, P. S. R., Sowjanya, Y., and Shiva Prasad, K. (2009). Micro-Raman investigations of mixed gas hydrates. Vibrational Spectroscopy, 50(2), 319-323.

Rios, R. B., Stragliotto, F. M., Peixoto, H. R., Torres, A. E. B., Bastos-Neto, M., Azevedo, D. C. S., and Cavalcante Jr, C. L. (2013). Studies on the adsorption behavior of CO2-CH4 mixtures using activated carbon. Brazilian Journal of Chemical Engineering, 30, 939-951.

Ripmeester, J. A., Tse, J. S., Ratcliffe, C. I., and Powell, B. M. (1987). A new clathrate hydrate structure. Nature, 325(6100), 135-136.

Rogers, R. E., Kothapalli, C., Lee, M. S., and Woolsey, J. R. (2003). Catalysis of Gas Hydrates by Biosurfactants in Seawater-Saturated Sand/Clay. The Canadian Journal of Chemical Engineering, 81(5), 973-980.

Roosta, H., Khosharay, S., and Varaminian, F. (2013). Experimental study of methane hydrate formation kinetics with or without additives and modeling based on chemical affinity. Energy Conversion and Management, 76, 499-505.

Sapag, K., Vallone, A., Blanco, A. G., and Solar, C. (2010). Adsorption of Methane in Porous Materials as the Basis for the Storage of Natural Gas. In P. Potocnik (Ed.), *Natural Gas* (pp. 205-244). New York: IntechOpen.

Saw, V. K., Gudala, M., Udayabhanu, G., Mandal, A., and Laik, S. (2014). Kinetics of methane hydrate formation and its dissociation in presence of non-ionic surfactant Tergitol. Journal of Unconventional Oil and Gas Resources, 6, 54-59.

Seo, Y. T., Kang, S. P., and Lee, H. (2001). Experimental determination and thermodynamic modeling of methane and nitrogen hydrates in the presence of THF, propylene oxide, 1,4-dioxane and acetone. Fluid Phase Equilibria, 189(1), 99-110.

Sharma, D. V. S. G. K., Sowjanya, Y., Chari, V. D., and Prasad, P. S. R. (2014). Methane storage in mixed hydrates with tetrahydrofuran. Indian Journal of Chemical Technology, 21, 114-119.

Siangsai, A., Rangsunvigit, P., Kitiyanan, B., Kulprathipanja, S., and Linga, P. (2015). Investigation on the roles of activated carbon particle sizes on methane hydrate formation and dissociation. Chemical Engineering Science, 126, 383-389.

Sloan, E. D., and Koh, C. A. (2008). *Clathrate Hydrates of Natural Gases*. New York: CRC Press.

Smith, J. M., Van Ness, H. C., and Abbott, M. M. (2005). *Introduction to Chemical Engineering Thermodynamics*. Singapore: McGraw-Hill.

Stern, L. A., Circone, S., Kirby, S. H., and Durham, W. B. (2001). Preservation of methane hydrate at 1 atm. Energy & Fuels, 15(2), 499-501.

Sun, C., Li, W., Yang, X., Li, F., Yuan, Q., Mu, L., Chen, J., Liu, B., and Chen, G. (2011). Progress in research of gas hydrate. Chinese Journal of Chemical Engineering, 19(1), 151-162.

Sun, Z., Wang, R., Ma, R., Guo, K., and Fan, S. (2003). Natural gas storage in hydrates with the presence of promoters. Energy Conversion and Management, 44(17), 2733-2742.

Takahashi, M., Oonari, H., and Yamamoto, Y. (2002). *A novel manufacturing method of gas hydrate using the micro-bubble technology.* Paper presented at the The 4th International Conference on Natural Gas Hydrates, Yohama, Japan.

Veluswamy, H. P., Kumar, A., Seo, Y., Lee, J. D., and Linga, P. (2018). A review of solidified natural gas (SNG) technology for gas storage via clathrate hydrates. Applied Energy, 216, 262-285.

Veluswamy, H. P., Kumar, S., Kumar, R., Rangsunvigit, P., and Linga, P. (2016a). Enhanced clathrate hydrate formation kinetics at near ambient temperatures and moderate pressures: Application to natural gas storage. Fuel, 182, 907-919.

Veluswamy, H. P., and Linga, P. (2013). Macroscopic kinetics of hydrate formation of mixed hydrates of hydrogen/tetrahydrofuran for hydrogen storage. International Journal of Hydrogen Energy, 38(11), 4587-4596.

Veluswamy, H. P., Prasad, P. S. R., and Linga, P. (2016b). Mechanism of methane hydrate formation in the presence of hollow silica. Korean Journal of Chemical Engineering, 33(7), 2050-2062.

Veluswamy, H. P., Wong, A. J. H., Babu, P., Kumar, R., Kulprathipanja, S., Rangsunvigit, P., and Linga, P. (2016c). Rapid methane hydrate formation to develop a cost effective large scale energy storage system. Chemical Engineering Journal, 290, 161-173.

Wang, W., Huang, Z., Chen, H., Tan, Z., Chen, C., and Sun, L. (2012). Methane hydrates with a high capacity and a high formation rate promoted by biosurfactants. Chemical Communications, 48(95), 11638-11640.

Wang, X., French, J., Kandadai, S., and Chua, H. T. (2010). Adsorption measurements of methane on activated carbon in the temperature range (281 to 343) K and pressures to 1.2 MPa. Journal of Chemical & Engineering Data, 55(8), 2700-2706.

Xiong, L., Li, X., Wang, Y., and Xu, C. (2012). Experimental study on methane hydrate dissociation by depressurization in porous sediments. Energies 5(2), 13.

Zakaria, Z., and George, T. (2011). The performance of commercial activated carbon absorbent for adsorbed natural gas storage. International Journal of Recent Research and Applied Studies, 9(2), 6.

Zhang, J. S., Lee, S., and Lee, J. W. (2007a). Does SDS micellize under methane hydrate-forming conditions below the normal Krafft point? Journal of Colloid and Interface Science, 315(1), 313-318.

Zhang, J. S., Lee, S., and Lee, J. W. (2007b). Kinetics of methane hydrate formation from SDS solution. Industrial & Engineering Chemistry Research, 46(19), 6353-6359.

Zhang, T., Walawender, W. P., and Fan, L. T. (2010). Grain-based activated carbons for natural gas storage. Bioresource Technology, 101(6), 1983-1991.

Zhong, D.-L., Daraboina, N., and Englezos, P. (2013). Coal mine methane gas recovery by hydrate formation in a fixed bed of silica sand particles. Energy & Fuels, 27(8), 4581-4588.

CURRICULUM VITAE

Name: Mr. Katipot Inkong
Date of Birth: June 30, 1990
Nationality: Thai

University Education:

2009–2013 Bachelor Degree of Engineering (1st honor), Petrochemical and Polymeric Materials Engineering, Faculty of Engineering and Industrial Technology, Silpakorn University, Nakhon Pathom, Thailand.

Work Experience:

April-June 2012	Position:	Internship Student
	Company Name:	Thatawan Industry PLC. Thailand
June-August 2015	Position:	Internship Student
	Company Name:	UOP, A Honeywell Company, USA
Jane-May 2019	Position	Exchange Student
	University:	National University of Singapore, Singapore

Publications:

1. Inkong, K., Rangsunvigit, R., Chaisuwan, T., and Kulprathipanja, S. (2016) CO_2 adsorption on polybenzoxazine grafted activated carbon: Effects of amine precursor. Chemical Engineering Transactions. 52, 103-108.
2. Siangsai, A., Inkong, K. Kulprathipanja, S., Kitiyanan, B., Rangsunvigit, P. (2018) Roles of sodium dodecyl sulfate on tetrahydrofuran-assisted methane hydrate formation, Journal of Oleo Science, 67, 707-717.
3. Inkong, K., Rangsunvigit, P., Kulprathipanja, S., Linga, P. (2019) Effects of temperature and pressure on the methane hydrate formation with the presence of tetrahydrofuran (THF) as a promoter in an unstirred tank reactor, Fuel, 255, 115705.
4. Inkong, K., Veluswamy, H. P., Rangsunvigit, P., Kulprathipanja, S., and Linga, P. (2019). Investigation on the kinetics of methane hydrate formation in the presence

of methyl ester sulfonate. Journal of Natural Gas Science and Engineering, 71, 102999.

5. Inkong, K., Veluswamy, H. P., Rangsunvigit, P., Kulprathipanja, S., and Linga, P. (2019). Innovative approach to enhance the methane hydrate formation at near ambient temperature and moderate pressure for gas storage applications. Industrial & Engineering Chemistry Research, 58(49), 22178-22192

Proceedings:

1. Inkong, K., Rangsunvigit, R., Chaisuwan, T., and Kulprathipanja, S. (21 April, 2015) Effect of Grafting Polybenzoxazine on Activated Carbon to Enhance CO_2 Adsorption. Proceedings of The 6th Research Symposium on Petrochemical and Material Technology and The 21nd PPC Symposium on Petroleum, Petrochemicals, and Polymers, Bangkok, Thailand.

Presentations:

1. Inkong, K., Rangsunvigit, R., Chaisuwan, T., and Kulprathipanja, S. (20-22, May, 2015) Roles of Polybenzoxazine Functionalization on CO_2 Adsorption. Poster Presentation at Energy, Science and Technology Conference and Exhibition EST 2015, Karlsruhe, Germany.
2. Inkong, K., Rangsunvigit, R., Chaisuwan, T., and Kulprathipanja, S. (2016, August 27 - 31) CO_2 adsorption on polybenzoxazine grafted activated carbon: Effects of amine precursor. Poster Presentation at PRES 2016 - the 19th Conference on Process Integration, Modelling and Optimisation for Energy Saving and Pollution Reduction, Prague, Czech Republic.
3. Inkong, K., Rangsunvigit, R., and Kulprathipanja, S. (2016, August 27 - 31) Effects of Mixed Surfactants on Methane Hydrate Formation and Dissociation. Poster Presentation at PRES 2016 - the 19th Conference on Process Integration, Modelling and Optimisation for Energy Saving and Pollution Reduction, Prague, Czech Republic.
4. Inkong, K., Rangsunvigit, R., and Kulprathipanja, S. (2017, June 25-30) Pressure and Temperature Effects on Methane Hydrate Formation and Dissociation with the

Presence of Tetrahydrofuran (THF) Promoters. Poster Presentation at 9th International Conference on Gas Hydrates (ICGH 9th), Coronado, USA.

5. Inkong, K., Rangsunvigit, R., and Kulprathipanja, S. (2017, August 8-11) Enhancement of Hydrate Formation and Dissociation Kinetics at High Temperature and Low Pressure. Poster Presentation at 7th Asian Conference Colloid & Interface Science 2017 (ACCIS 2017), Kula lumper, Malaysia.
6. Inkong, K., Rangsunvigit, R., and Kulprathipanja, S. (2018, September 9-14) Methane Hydrate Formation Enhancement at Lower Diving Force: Effect of THF Concentration. Oral Presentation at the 8th IUPAC International Conference on Green Chemistry - 8th ICGC. Bangkok, Thailand.
7. Inkong, K., Rangsunvigit, R., and Kulprathipanja, S. (2018, November 8-9) Role of surfactants on methane hydrate formation and dissociation: effects of different anionic surfactants. Oral Presentation at the 8th International Thai Institute of Chemical Engineering and Applied Chemistry Conference (ITIChE 2018). Chonburi, Thailand.
8. Inkong, K., Rangsunvigit, R., and Kulprathipanja, S. (2018, December 10-14) Roles of THF Concentration on Methane Hydrate Formation at Lower Diving Force. Poster Presentation at the 8th C&F symposium, Bangkok, Thailand.
9. Inkong, K., Rangsunvigit, R., Kulprathipanja, S. and Linga, P., (2019, August 8-9) Effects of temperature and pressure on the methane hydrate formation with the presence of tetrahydrofuran (THF) as a promoter in an unstirred tank reactor. Oral Presentation at TSRI Congress 2019, Bangkok, Thailand.
10. Inkong, K., Veluswamy, H. P., Rangsunvigit, P., Kulprathipanja, S., and Linga, P. (2019, November 3-8) Double Promoter Enhanced Mixed Methane-THF Hydrate Formation at Higher Temperature and Low Pressure. Oral Presentation at Okinawa Colloids 2019, Okinawa, Japan.